國立交通大學

電子物理學系

碩 士 論 文

在共平面磁場中與 Rashba 及 Dresselhaus 自旋軌道交互作用之窄通道的量子傳輸

Quantum transport of narrow-channels in in-plane magnetic fields with Rashba and Dresselhaus spin-orbit interactions

研 究 生：張書瑜

指導教授：鄭舜仁　教授

中 華 民 國 一百 年 六 月

在共平面磁場中與 Rashba 及 Dresselhaus 自旋 軌道交互作用之窄通道的量子傳輸

Quantum transport of narrow-channels in in-plane magnetic fields with Rashba and Dresselhaus spin-orbit interactions

研 究 生：張書瑜　　Student：Shu-Yu Chang

指導教授：鄭舜仁 教授　　Advisor：Prof. Shun-Jen Chen

國 立 交 通 大 學
電 子 物 理 學 系
碩 士 論 文

A Thesis
Submitted to Department of Electrophysics
College of Science
National Chiao Tung University
in partial Fulfillment of the Requirements
for the Degree of
Master
in

Electrophysics

Nov. 2010

Hsinchu, Taiwan, Republic of China

中華民國一百年六月

在共平面磁場與 Rashba 及 Dresselhaus 自旋軌道交互作用之窄通道的量子傳輸

學生：張書瑜　　指導教授：鄭舜仁 教授

國立交通大學電子物理研究所碩士班

摘要

我們研究考慮共平面磁場與 Rashba 及 Dresselhaus 自旋軌道交互作用之窄通道的同調量子傳輸。因為 Rashba 及 Dresselhaus 自旋軌道交互作用造成能帶水平方向的仳裂，而外加共平面磁場則造成能帶垂直方向的仳裂。首先，當我們同時考慮 Rashba 自旋軌道交互作用及共平面磁場時，能帶中，會出現虛能隙。在調變磁場大小的過程中，我們觀察電子自旋方向的改變。傳輸特性上，我們發現了似電子和似電洞的準束縛態。而當我們同時考慮共平面磁場與 Rashba 及 Dresselhaus 自旋軌道交互作用時，能帶開始變得不對稱。在傳輸特性上，除了發現似電子和似電洞的準束縛態之外，我們發現了 Fano 效應。因此，在考慮 Rashba 自旋軌道交互作用及共平面磁場時，Dresselhaus 效應對傳輸特性有重大的影響。

Quantum transport of narrow-channels in in-plane magnetic fields with Rashba and Dresselhaus spin-orbit interactions

Student：Shu-Yu Chang **Advisor：Shun-Jen Cheng**

Department of Electrophysics
National Chiao Tung University

ABSTRACT

We investigate coherent electronic quantum transport in a narrow channel with Rashba and Dresselhaus spin-orbit interaction in the presence of an external in-plane magnetic field that is applied along the channel direction. The spin-split energy spectrum is horizontally shifted respectively by the Rashba and the Dresselhaus effects and is vertically shifted by the applied magnetic field. First, we consider the Rashba spin-orbit interaction and the in-plane magnetic field in the narrow channel, there is a pseudo-gap in the energy spectrum. With the increasing magnetic field, we investigate the variation of the spin orientation. Furthermore, we find the hole-like quasi bound state and electron-like quasi-bound state features in conductance. When we consider the Rashba, Dresselhaus and Zeeman effects simultaneously, energy spectrum becomes asymmetry. In some specific cases, except for the quasi-bound state feature, we find the Fano effect in transport properties. Hence, in the presence of the Rashba spin-orbit interaction and the in-plane magnetic field, the Dresselhaus effect significantly affects coherent magneto-quantum transport properties.

致謝

很開心可以從交大畢業了，兩年的碩士生活過的很充實。特別感謝唐志雄老師，總是擁有許多的耐心，不厭其煩的和我解釋相同的物理觀念。在每個禮拜五的討論時間，總是讓我獲益良多。老師也很願意和我們打成一片，分享生活中的許多樂趣。感謝鄭舜仁老師的細心指導，從老師身上學習到做事情以及處理事情的嚴謹態度，這將讓我往後的人生道路上受用無窮。也感謝口試委員，朱仲夏老師以及關肇正老師給的寶貴意見，使我了解到自己的研究還有哪些細節需要注意。

碩班生活中，有時快樂、也有時低落，很感謝有以理、毓謙的陪伴。謝謝你們在我忙碌的時候，陪我一起在研究室待到很晚。在我口試前，陪我一起奔波，甚至在口試當天，都比我還緊張了。很開心能夠認識你們，在兩年的研究生活中，彼此互相扶持著，很令人感到溫暖。感謝我的家人的默默陪伴，因為知道你們是無比的支持我，使我的內心能夠更強大，無後顧之憂的專注在課業研究上，謝謝你們，真的很愛你們。感謝博文、俊弦、志榮，很關心我也很鼓勵我，使我能夠更勇敢的面對生活中的挑戰。感謝可愛的安頡，每個禮拜四看到你，聽你的童言童語，是我最放鬆快樂的時候。以及可愛的 Happy，雖然你看不懂我的論文，但我還是很愛你很謝謝你的陪伴，晚上在實驗室做研究時，你都會乖乖的趴在旁邊陪我。

最後，感謝實驗室的夥伴們，以及陳煜璋老師的學生們，很開心能夠認識你們，讓我的碩班生活更增添色彩，謝謝你們的相伴。

Contents

Abstract in Chinese ii

Abstract in English iii

1 Introduction to charge transport in semiconductors 1

1.1 Introduction to semiconductors……1

1.2 Low dimensional semiconductor systems……1

1.2.1 Introduction to heterostructure semiconductors…….....1

1.2.2 Modeling the low dimensional semiconductor systems……..3

1.3 Quantum transport in quasi-one-dimensional quantum systems.....4

1.3.1 Introduction to quantum transport……...4

1.3.2 Quasi-one-dimensional quantum systems……...5

1.3.3 Analytical approach……6

1.3.4 Numerical approach……8

2 Spin-resolved quantum transport 9

2.1 Introduction to spintronics……9

2.2 The spin-orbit interactions and the Zeeman effect……10

3 Quantum transport in the presence of the Rashba spin-orbit interaction with in-plane magnetic field 12

3.1 Theory……12

3.1.1 System and Formulation……..12

3.1.2 The Rashba effect……18

3.1.3 The Zeeman effect……...20

3.1.4 Spin orientation……...21

3.1.5 Complex energy dispersion……23

3.2 Transport theory……..25

3.3 Numerical results……29

3.3.1 Ideal conductance with the tunable Rashba effects……...29

3.3.2 Transport properties with the Rashba effects in the presence of in-plane magnetic field……..31

4 Quantum transport in the presence of Rashba and Dresselhaus spin-orbit interactions with in-plane magnetic field 35

4.1 Theory……...35

4.1.1 System and Formulation……..35

4.1.2 The Dresselhaus effects……...38

4.1.3 The Rashba and Dresselhaus effects……42

4.1.4 The Zeeman effects……..44

4.1.5 Complex energy dispersion……48

4.2 Spin-resolved transport theory……..49

4.3 Numerical results……..52

4.3.1 Ideal conductance with tunable the Dresselhaus effects…52

4.3.2 Ideal conductance with the tunable Rashba and Dresselhaus effects…….54

4.3.3 The Dresselhaus effects in the presence of the Rashba spin-orbit interaction and in-plane magnetic field……..56

4.3.4 Transport properties with the Rashba-Dresselhaus effects in the presence of an in-plane magnetic field……60

5 Conclusion and future work 65

Bibliography 66

Appendix 68

List of Figures

1.2.1.1. The bandage profile of semiconductor heterostructures……2

1.2.1.2. The conduction-band edge across a graded AlGaAs-GaAs heterojunction in thermal equilibrium……..3

1.2.2.1. The GaAs/AlGaAs high electron mobility transistor……4

1.3.2.1. System figuration……...5

1.3.3.1. System picture……...6

1.3.4.1. Conductance (in units of $2e^2/h$) versus kinetic energy in a quantum channel with tunable potential strength V_0……8

3.1.1.1. System picture……..…13

3.1.1.2. (a) For the case $2\alpha^2 > gB$, energy spectrum with labeling local energy extreme values and corresponding wavevectors. (b) For the case $2\alpha^2 \leq gB$, energy spectrum with labeling local energy extreme values and corresponding wavevectors……15

3.1.1.3. For the case of considering the Rashba effect and turning off the magnetic field $B = 0$, energy spectrum with labeling local energy extreme values and corresponding wavevectors……16

3.1.1.4. For the case of considering only the in-plane magnetic field and the Rashba coefficient $\alpha = 0$, energy spectrum with labeling local energy extreme values and corresponding wavevectors....17

3.1.2.1. Energy spectrum versus wave number with magnetic field strength $gB = 0.02$ for different values of α: (a) $\alpha = 0.0$ (b) $\alpha = 0.05$, (c) $\alpha = 0.1$, and (d) $\alpha = 0.2$ (the Rashba-Zeeman effect). The Fermi energy $E_F = 66$ meV and the Fermi wave vector

$k_F = 2\times10^6$ cm^{-1}. The magnetic field strength is approximately 3T when $gB = 0.02$ ($g_s = -15$ for InAs). The black and red curves indicate the plus ($\sigma = +$) and minus ($\sigma = -$) spin branches, respectively. The black dot and the red dot correspond to the local minima of plus and minus branches at the subband bottoms, denoted by P_{b+} and P_{b-}. The red circle stands for the local maxima of the minus branch at the subband top, denoted by P_{t-}……18

3.1.3.1 Energy spectrum versus wave number with different magnetic field strength gB and the fixed Rashba strength α: (a) $gB = 0$, $\alpha = 0.2$; (b) $gB = 0.04$, $\alpha = 0.2$; (c) $gB = 0.08$, $\alpha = 0.2$ (d) $gB = 0.12$, $\alpha = 0.2$. The Fermi energy $E_F = 66$ meV and the Fermi wave vector $k_F = 2\times10^6$ cm^{-1}. The magnetic field strength is approximately 6T when $gB = 0.04$ ($g_s = -15$ for InAs). The black and red curves indicate the plus ($\sigma = +$) and minus ($\sigma = -$) spin branches, respectively. The black dot and the red dot correspond to the local minima of plus and minus branches at the subband bottoms, denoted by P_{b+} and P_{b-}. The red circle stands for the local maxima of the minus branch at the subband top, denoted by P_{t-}……20

3.1.4.1. Energy dispersion with spin orientation illustrated by the arrows with the different Zeeman effects and the fixed Rashba strength α. (a) $gB = 0$, $\alpha = 0.2$; (b) $gB = 0.04$, $\alpha = 0.2$; (c) $gB = 0.08$, $\alpha = 0.2$

(d) gB = 0.12, α = 0.2. The magnetic field strength is approximately 6T when gB = 0.04 (g_s = –15 for InAs)……22

3.1.5.1. 3D Energy dispersion in the presence of the Rashba spin-orbit interaction and in-plane magnetic field (α = 0.2, gB = 0.02). k_R and k_I represent, respectively, the real part and the imaginary part of the wave number ($k = k_R + k_I$). The black solid line represents the propagating modes and the red solid line represents the evanescent modes. The Fermi energy E_F = 66 meV and the Fermi wave vector $k_F = 2\times10^6$ cm^{-1}……24

3.2.1. Energy spectrum with labeling modes. k_1, q_1 indicate the outer right-going and left-going modes. k_2, q_2 in this energy regime are evanescent modes……..….26

3.2.2. Scattering process in the high energy regime……...……...28

3.3.1.1. Conductance (in units of $G_0 = e^2/h$) versus kinetic energy without the scattering potential in the presence of in-plane magnetic field with different Rashba coefficients: (a) α = 0, gB = 0.02; (b) α = 0.05, gB = 0.02; (c) α = 0.1, gB = 0.02; (d) α = 0.2, gB = 0.02. The Fermi energy E_F = 66 meV and the Fermi wave vector k_F = 2 $\times10^6$ cm^{-1}. The magnetic field strength is approximately 3T when gB = 0.02 (g_s = –15 for InAs)……29

3.3.2.1. Conductance (in units of $G_0 = e^2/h$) versus kinetic energy with the attractive scattering potential in the presence of in-plane magnetic field with different Rashba coefficients: (a) α = 0.0, gB = 0.02 ($2\alpha^2 < gB$) (b) α = 0.05, gB = 0.02 ($2\alpha^2 < gB$) (c) α = 0.1, gB = 0.02 ($2\alpha^2 = gB$) (d) α = 0.2, gB = 0.02 ($2\alpha^2 > gB$). The Fermi

energy E_F = 66 meV and the Fermi wave vector k_F = 2×10^6 cm^{-1}. The magnetic field strength is approximately 3T when gB = 0.02 (g_s = −15 for InAs)……31

3.3.2.2. Conductance (in units of $G_0 = e^2/h$) versus kinetic energy with the repulsive scattering potential in the presence of in-plane magnetic field with different Rashba coefficients: (a) α = 0.0, gB = 0.02 ($2\alpha^2 < gB$) (b) α = 0.05, gB = 0.02 ($2\alpha^2 < gB$) (c) α = 0.1, gB = 0.02 ($2\alpha^2 = gB$) (d) α = 0.2, gB = 0.02 ($2\alpha^2 > gB$). The Fermi energy E_F = 66 meV and the Fermi wave vector k_F = 2×10^6 cm^{-1}. The magnetic field strength is approximately 3T when gB = 0.02 (g_s = −15 for InAs)……33

4.1.1.1. System picture……36

4.1.2.1. Energy spectrum versus wave number in the presence of the Rashba spin-orbit interaction and in-plane magnetic field with different Dresselhaus coefficients: (a) α = 0.2, β = 0.0, gB = 0.02 (b) α = 0.2, β = 0.1, gB = 0.02 (c) α = 0.2, β = 0.2, gB = 0.02 (d) α = 0.2, β = 0.3, gB = 0.02. The Fermi energy E_F = 66 meV and the Fermi eave vector k_F = 2×10^6 cm^{-1}. The magnetic field strength is approximately 3T when gB = 0.02 (g_s = −15 for InAs). The black and red curves indicate the plus (σ = +) and minus (σ = –) spin branches, respectively. The black dot and the red dot correspond to the local minima of plus and minus branches at the subband bottoms, denoted by P_{b+} and P_{b-}. The red circle stands for the local maxima of the minus branch at the subband top,

denoted by P_{t-}……..38

4.1.2.2. Energy spectrum versus wave number in the presence of the Rashba, the Dresselhaus and the Zeeman effects with different Dresselhaus strength. (a) α = 0.2, β = 0.0, gB = 0.0 (b) α = 0.2, β = 0.1, gB = 0.0 (c) α = 0.2, β = 0.2, gB = 0.0 (a) α = 0.2, β = 0.3, gB = 0.0. The Fermi energy E_F = 66 meV and the Fermi eave vector k_F = 2×10^6 cm^{-1}. The black and red curves indicate the plus (σ = +) and minus (σ = –) spin branches, respectively……..40

4.1.3.1. Energy spectrum versus wave number in the presence of in-plane magnetic field with different Rashba and Dresselhaus coefficients. (a) $\alpha = \beta$ = 0.01, gB = 0.02 (b) $\alpha = \beta = gB$ = 0.02 (c) $\alpha = \beta$ = 0.1, gB = 0.02 (d) $\alpha = \beta$ = 0.2, gB = 0.02. The Fermi energy E_F = 66 meV and the Fermi eave vector k_F = 2×10^6 cm^{-1}. The magnetic field strength is approximately 3T when gB = 0.02 (g_s = –15 for InAs). The black and red curves indicate the plus (σ = +) and minus (σ = –) spin branches, respectively. The black dot and the red dot correspond to the local minima of plus and minus branches at the subband bottoms, denoted by P_{b+} and P_{b-}. The red circle stands for the local maxima of the minus branch at the subband top, denoted by P_{t-}……..……...42

4.1.4.1. Energy spectrum versus wave number in the presence of the Rashba, the Dresselhaus and the Zeeman effects with different Dresselhaus strength. (a) $\alpha = \beta$ = 0.2, gB = 0.0 (b) $\alpha = \beta$ = 0.2,

gB = 0.1 (c) $\alpha = \beta$ = 0.2, gB = 0.2 (d) $\alpha = \beta$ = 0.2, gB = 0.3. The Fermi energy E_F = 66 meV and the Fermi eave vector $k_F = 2\times10^6$ cm^{-1}. The magnetic field strength is approximately 15T when gB = 0.1 (g_s = –15 for InAs). The black and red curves indicate the plus (σ = +) and minus (σ = –) spin branches, respectively. The black dot and the red dot correspond to the local minima of plus and minus branches at the subband bottoms, denoted by P_{b+} and P_{b-}…….44

4.1.4.2. Energy dispersion with spin orientation illustrated by the arrows in the presence of the fixed Rashba and Dresselhaus spin-orbit interactions with different Zeeman coefficients. (a) $\alpha = \beta$ = 0.2, gB = 0.0 (b) $\alpha = \beta$ = 0.2, gB = 0.1 (c) $\alpha = \beta$ = 0.2, gB = 0.2 (d) $\alpha = \beta$ = 0.2, gB = 0.3. The magnetic field strength is approximately 15T when gB = 0.1 (g_s = –15 for InAs)…….46

4.1.5.1. 3D Energy dispersion in the presence of the spin-orbit interactions and in-plane magnetic field ($\alpha = \beta$ = 0.2, gB = 0.02). k_R and k_I represent, respectively, the real part and the imaginary part of the wave number ($k = k_R + k_I$). The black solid line represents the propagating modes and the red solid line represents the evanescent modes. The Fermi energy E_F = 66 meV and the Fermi eave vector $k_F = 2\times10^6$ cm^{-1}…….48

4.2.1. The scattering process in the high energy regime……..51

4.3.1.1. Conductance (in units of $G_0 = e^2/h$) versus kinetic energy without the scattering potential in the presence of the Rashba spin-orbit

interaction and in-plane magnetic field with different Dresselhaus coefficients: (a) $\alpha = 0.2$, $\beta = 0.0$, $gB = 0.02$; (b) $\alpha = 0$, $\beta = 0.1$, $gB = 0.02$; (c) $\alpha = 0.2$, $\beta = 0.2$, $gB = 0.02$; (d) $\alpha = 0$, $\beta = 0.3$, $gB = 0.02$. The Fermi energy $E_F = 66$ meV. The magnetic field strength is approximately 3T when $gB = 0.02$ ($g_s = -15$ for InAs)……...52

4.3.2.1. Conductance (in units of $G_0 = e^2/h$) versus kinetic energy without the scattering potential in the presence of in-plane magnetic field with different Rashba and Dresselhaus coefficients: (a) $\alpha = \beta = 0.01$, $gB = 0.02$ (b) $\alpha = \beta = gB = 0.02$ (c) $\alpha = \beta = 0.1$, $gB = 0.02$ (d) $\alpha = \beta = 0.2$, $gB = 0.02$. The Fermi energy $E_F = 66$ meV. The magnetic field strength is approximately 3T when $gB = 0.02$ ($g_s = -15$ for InAs)……...……54

4.3.3.1. Conductance (in units of $G_0 = e^2/h$) versus kinetic energy with the attractive scattering potential in the presence of the Rashba spin-orbit interaction and in-plane magnetic field with different Dresselhaus coefficients: (a) $\alpha = 0.2$, $\beta = 0.0$, $gB = 0.02$ (b) $\alpha = 0.2$, $\beta = 0.1$, $gB = 0.02$ (c) $\alpha = 0.2$, $\beta = 0.2$, $gB = 0.02$ (d) $\alpha = 0.2$, $\beta = 0.3$, $gB = 0.02$. The Fermi energy $E_F = 66$ meV. The magnetic field strength is approximately 3T when $gB = 0.02$ ($g_s = -15$ for InAs)……..….56

4.3.3.2. Scattering process in the presence of the true bound state……..57

4.3.3.3. Conductance (in units of $G_0 = e^2/h$) versus kinetic energy with the repulsive scattering potential in the presence of the Rashba spin-orbit interaction and in-plane magnetic field with different Dresselhaus coefficients: (a) $\alpha = 0.2$, $\beta = 0.0$, $gB = 0.02$ (b) $\alpha =$

0.2, β = 0.1, gB = 0.02 (c) α = 0.2, β = 0.2, gB = 0.02 (d) α = 0.2, β = 0.3, gB = 0.02. The Fermi energy E_F = 66 meV. The magnetic field strength is approximately 3T when gB = 0.02 (g_s = –15 for InAs)…….59

4.3.4.1. Conductance (in units of $G_0 = e^2/h$) versus kinetic energy with the attractive scattering potential in the presence of in-plane magnetic field with different Rashba and Dresselhaus coefficients: (a) $\alpha = \beta$ = 0.01, gB = 0.02 (b) $\alpha = \beta = gB$ = 0.02 (c) $\alpha = \beta$ = 0.1, gB = 0.02 (d) $\alpha = \beta$ = 0.2, gB = 0.02. The Fermi energy E_F = 66 meV. The magnetic field strength is approximately 3T when gB = 0.02 (g_s = –15 for InAs)……..60

4.3.4.2. Scattering process in the presence of the true bound state……..61

4.3.4.3. Scattering process in the presence of the true bound state……..62

4.3.4.4. Conductance (in units of $G_0 = e^2/h$) versus kinetic energy with the repulsive scattering potential in the presence of in-plane magnetic field with different Rashba and Dresselhaus coefficients: (a) $\alpha = \beta$ = 0.01, gB = 0.02 (b) $\alpha = \beta = gB$ = 0.02 (c) $\alpha = \beta$ = 0.1, gB = 0.02 (d) $\alpha = \beta$ = 0.2, gB = 0.02. The Fermi energy E_F = 66 meV. The magnetic field strength is approximately 3T when gB = 0.02 (g_s = –15 for InAs)……...…….63

Chapter 1 Introduction to charge transport in semiconductors

1.1 Introduction to semiconductors

The term “semiconductor” represents a certain class of solid materials. It suggests that the electrical conductivity is intermediate in magnitude between a conductor and an insulator. Semiconductor materials are numerous and versatile. We can distinguish it into elementary semiconductors and compound semiconductors.

Elementary semiconductors are Silicon (Si) and germanium (Ge), phosphorous (P), sulfur (S), selenium (Se), and tellurium (Te). Compound semiconductors are categorized following by the group of their constituents in the periodic table of elements. Such as gallium arsenide (GaAs), aluminium arsenide (AlAs), indium arsenide (InAs), indium antimonide (InSb), gallium antimonide (GaSb), gallium phosphide (GaP), gallium nitride (GaN), aluminium antimonide (AlSb), and indium phosphide (InP) are all belong to the so-called III-V semiconductors. There are also II-VI semiconductors, such as zinc sulfide (ZnS), zinc selenide (ZnSe) and cadmium telluride (CdTe), III-VI compounds, such as gallium sulfide (GaS) and indium selenide (InSe), as well as IV-VI compounds, such as lead sulfide (PbS), lead telluride (PbTe), lead selenide (PbSe), germanium telluride (GeTe), tin selenide (SnSe), and tin telluride (SnTe).

For compound semiconductors, there are two chemical constituents are called binary compounds. Additionally, there are compound semiconductors with three constituents, such as $Al_xGa_{1-x}As$ (aluminium gallium arsenide), $In_xGa_{1-x}As$ (indium gallium arsenide), and also $In_xGa_{1-x}P$ (indium gallium phosphide). In this situation, it is called about ternary semiconductors or semiconductor alloys.

$$H(x,y,z) = H_x + H_y + H_z \tag{1.1.1}$$

1.2 Low dimensional semiconductor systems

1.2.1 Introduction to heterostructure semiconductors

For heterostructure, since the two different materials will have two different energy bandgaps, the energy band will have a discontinuity at the junction interface. We may have an abrupt junction in which the semiconductor changes abruptly from a narrow bandgap material to a wide-band gap material. In Fig. 1.2.1.1 shows the energy-band diagram of a GaAs-AlGaAs heterojunction in thermal equilibrium. The

AlGaAs is moderately to heavily doped n type, while the GaAs is more lightly doped or even intrinsic. In order to achieve thermal equilibrium, electrons flow from the wide-bandgap AlGaAs into the GaAs, forming an accumulation layer of electrons in the potential well adjacent to the interface. The electrons contained in a potential well are quantized. The two-dimensional electron gas refers to the condition in which the electrons have quantized energy levels in one spatial direction (perpendicular to the interface), but are free to move in the other two spatial directions.

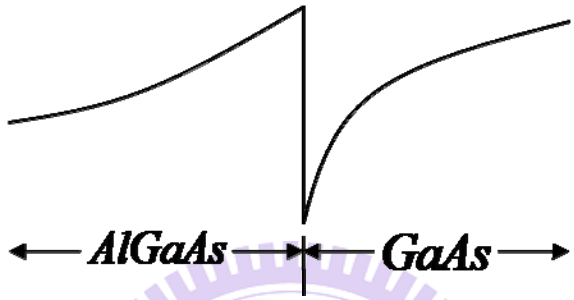

Fig. 1.2.1.1. The bandage profile of semiconductor heterostructures.

Since the GaAs is lightly doped or intrinsic, the two-dimensional electron gas is in a region of low impurity doping so that impurity scattering effects are minimized. The electron mobility will be much larger than if the electrons were in the same region with the ionized donors. The movement of the electrons parallel to the interface will still be influenced by the coulomb attraction of the ionized impurities in the AlGaAs. The effect of these forces can be further reduced by using a graded AlGaAs-GaAs heterojunction. The graded layer is $Al_xGa_{1-x}As$ in which the fraction x varies with distance. In this situation, an intrinsic layer of graded AlGaAs can be sandwiched between the N-type AlGaAs and the intrinsic GaAs. Fig. 1.2.1.2 shows the conduction-band edge across a graded AlGaAs-GaAs heterojunction in thermal equilibrium. The electrons in the potential well are further separated from the ionized impurities so that the electron mobility is increased above that in an abrupt heterojunction.

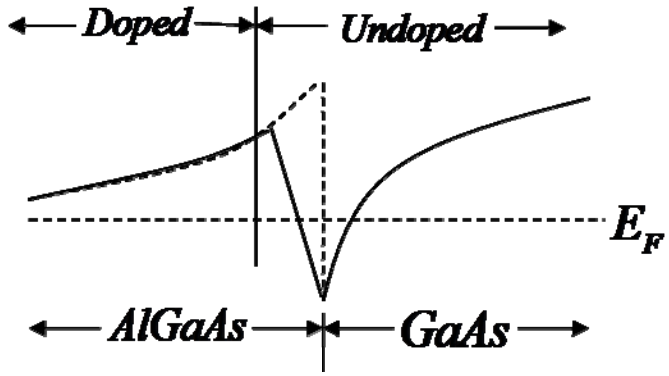

Fig. 1.2.1.2. the conduction-band edge across a graded AlGaAs-GaAs heterojunction in thermal equilibrium.

The two-dimensional electron gas (2DEG) trapped at a doped heterostructure is the most important low-dimensional system for electronic transport. It forms the kernel of a field-effect transistor. The high electron mobility transistor has many acronyms including modulation-doped field-effect transistor (MODFET) and high electron mobility transistor (HEMT).

1.2.2 Modeling the low dimensional semiconductor systems

Fig. 1.2.2.1 is the GaAs/AlGaAs high electron mobility transistor. The cap layer in the transistor can prevent the n-type AlGaAs from oxidizing. Above the cap layer, we use two metal gates to define a quasi-one dimensional quantum channel. The Hamiltonian of a semiconductor with heterostructure can be written separately in the vertical and lateral parts of form

$$H(x,y,z) = H_{\|} + H_z , \tag{1.2.2.1}$$

where

$$H_{\|} = \frac{\hbar^2}{2m^*}\left(k_x^2 + k_y^2\right) + V(x,y) \tag{1.2.2.2}$$

and

$$H_z = \frac{\hbar^2 k_z^2}{2m^*} + V_c(z) . \tag{1.2.2.3}$$

$V_c(z)$ is the quantum well at the interface of the heterostructure. The electrons underneath the gate oxide are confined to the heterostructure interface, and thus occupy well defined energy levels. Nearly always, only the lowest level is occupied, and so the motion of the electrons perpendicular to the interface can be ignored. While, the electron can be free to move in the other two spatial directions. Hence, we can ignore the z-part Hamiltonian and emphasize the x, y dependant Hamiltonian (Eq. 1.2.2.2).

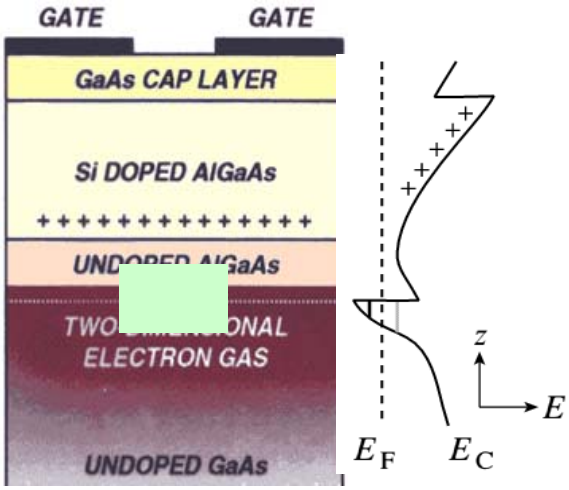

Fig. 1.2.2.1. The GaAs/AlGaAs high electron mobility transistor.

1.3 Quantum transport in quasi-one-dimensional quantum systems

1.3.1 Introduction to quantum transport

In macroscopic systems, the conductance obeys an ohmic scaling law:

$$G = \frac{\sigma W}{L}. \tag{1.3.1.1}$$

As the dimensions become smaller, there are two corrections to this law. Firstly there is an interface resistance independent of the length L of the sample. Secondly the conductance does not decrease linearly with the width W anymore. Instead it depends on the number of transverse modes in the quantum channel. The Landauer-Buttiker formula incorporates both of these features [1, 2]:

$$G = \frac{2e^2}{h} NT. \tag{1.3.1.2}$$

The factor T is the average probability that an electron incident from the source will transmit to the drain, the factor 2 is for the spin and N is the number of propagating modes with positive group velocity due to transverse confinement. The Landauer-Buttiker formalism only applies to coherent transport. In this paper, we assume that the phase-coherent length is larger than the sample of linear size L, in which $l_\phi > L$ and the elastic mean free path is larger than the sample size $l_e > L$. Namely, our system is in the coherent quantum transport regime.

1.3.2 Quasi-one-dimensional quantum systems

To form a quasi-one-dimensional quantum system (Fig. 1.2.2.1), we use two split top gates above the HEMT. We can rewrite the Eq. 1.2.2.2 in the following form:

$$H_{\parallel}(x,y)=\frac{\hbar^2}{2m^*}\left(k_x^2+k_y^2\right)+V_c(y)+V_s(x,y)\,. \tag{1.3.2.1}$$

Since the two split top gates are quite near each another, electrons will be confined in the quantum channel and can only propagate along the x direction. Hence, the single particle Hamiltonian in the narrow channel can be described by.

$$H=\frac{\hbar^2k^2}{2m^*}+V(x,y)\,. \tag{1.3.2.2}$$

This Hamiltonian can be separated into two parts:

$$H_y=\frac{\hbar^2k_y^2}{2m^*}+V_c(y)\,. \tag{1.3.2.3}$$

$$H_x=\frac{\hbar^2k_x^2}{2m^*}+V(x) \tag{1.3.2.4}$$

$V_C(y)$ indicates the confining potential in the transverse direction. The corresponding eigenvalue of H_y is the sub-band energy. In the narrow channel, the electron propagates along x direction whose kinetic energy will be the total energy of an incident electron subtracting the subband energy $E_k = E_{tot} - \varepsilon_n$, ε_n depends on which subband the electron occupying. $V(x)$ exhibits the x dependant potential which can be the spin orbit interaction or the scattering potential in longitudinal direction. In this chapter, we consider the system is only with the static scattering potential along x direction without spin orbit interaction. In the following chapters, we will discuss the spin-resolved transport properties including both the static scattering potential and spin orbit interaction.

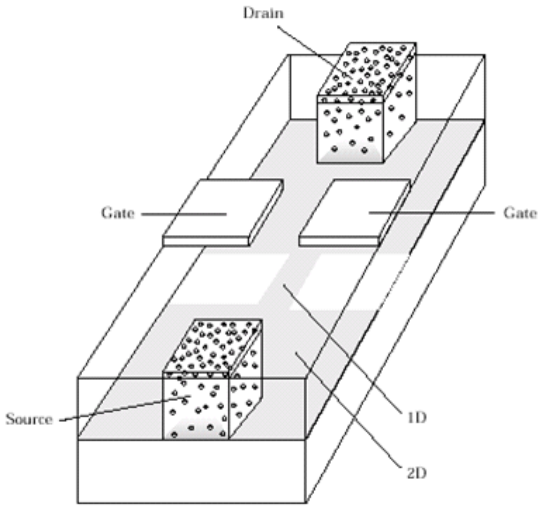

Fig. 1.3.2.1. System figuration.

1.3.3 Analytical approach

The system figuration is shown in Fig. 1.3.2.1. A static finger gate is in the middle of the narrow channel. The system under investigation can be described by the Hamiltonian:

$$H = \frac{p^2}{2m^*} + V_c(y) + V_0\delta(x)\,,\quad V_c(y) = \frac{1}{2}m\omega_y^2 y^2 \tag{1.3.3.1}$$

In order to simplify the calculation, the dimensionless Hamiltonian is introduced by choosing appropriate physical units: the length unit $l^* = \frac{1}{k_F}$, the energy unit $E^* = \frac{\hbar^2 k_F^2}{2m^*}$, and the unit of the parameter ω_y of the confining potential $\omega_y^* = \frac{2E^*}{\hbar}$.

Following performing standard dimensionless the Hamiltonian becomes:

$$H = k^2 + \omega_y^2 y^2 + V_0\delta(x)\,. \tag{1.3.3.2}$$

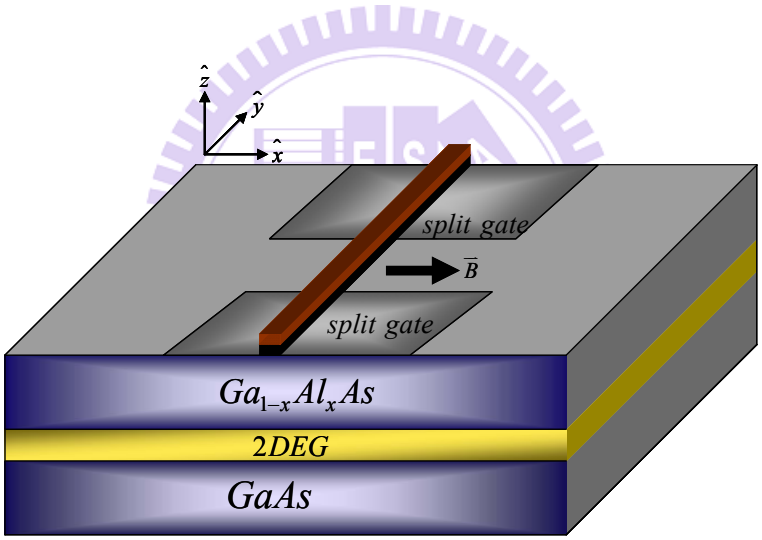

Fig. 1.3.3.1. System picture.

The wave function can factorize into functions of x and y, as follows:

$$\Psi(\mathbf{r}) = \psi(x)\varphi(y)\,. \tag{1.3.3.3}$$

Since the confining potential in the transverse direction is a parabolic potential, the wavefunction and the subband energy will be

$$\varepsilon_n = (2n+1)\omega_y\,. \tag{1.3.3.4}$$

and

$$\psi_n(x) = \frac{1}{\sqrt{\sqrt{\pi}\,2^n n!\,x_0}}\,e^{-x^2/2x_0^2}H_n\left(\frac{x}{x_0}\right). \tag{1.3.3.5}$$

The electrons incident from the left source will be scattered by the static delta potential in the middle of the quantum channel. The electrons may be back scattered or forward scattered. Therefore, the *x*-part wave functions can be written in the form:

$$x < 0, \psi(x) = e^{ikx} + re^{-ikx} \tag{1.3.3.6}$$

and

$$x > 0, \psi(x) = te^{ikx}, k = \sqrt{E - \varepsilon_n}\ . \tag{1.3.3.7}$$

r, *t* represent the reflected and transmitted coefficients. *E* is the total energy of the electron and ε_n is the subband energy. The wavefunctions should satisfy these boundary conditions:

$$\text{(i)}\ \psi(x = 0^-) = \psi(x = 0^+) \tag{1.3.3.8}$$

and

$$\text{(ii)}\ \psi'(x = 0^-) = \psi'(x = 0^+) - V_0\psi(x = 0^+)\,. \tag{1.3.3.9}$$

Substituting the x-part wave functions into these boundary conditions can obtain:

$$r = t - 1 \tag{1.3.3.10}$$

and

$$ik(1 - r) = ikt - V_0 t\,. \tag{1.3.3.11}$$

Combining these two equations and using linear algebra, the transmitted coefficient can be expressed as:

$$t = \frac{1}{1 - \frac{V_0}{2ik}}\,. \tag{1.3.3.12}$$

Once obtaining the transmitted coefficient, we can substitute it into the Landauer-Büttiker equation and acquire the conductance.

$$G = \frac{2e^2}{h}\sum_n |t_n|^2 = \frac{2e^2}{h}\sum_n \frac{1}{1 + \frac{V_0^2}{4k^2}}\,. \tag{1.3.3.13}$$

1.3.4 Numerical approach

In this section, we show the numerical results and discussion of the variation of conductance with the potential strength V_0. The numerical calculations presented below are carried out under the assumption that the electron effective mass $m^* = 0.067m_0$, which is appropriate to the GaAs-based semiconductors. The typical electron density is $n \sim 10^{11}$ cm^{-2}. Accordingly, the energy unit $E^* = 9\ meV$, the length unit $L^* = 7.96\ nm$, and the frequency unit $\omega^* = \frac{E^*}{\hbar} = 13.6$ THz [3].

In Fig. 1.3.4.1, we demonstrate the conductance at different scattering potential strength and the frequency remaining at ω_y = 13.6 THz. In the absence of scattering potential, the conductance is ideally quantized. The conductance regularly increases $2e^2/h$ as the energy raises $2E_F$, since the transverse modes will increase one mode whenever the energy raises $2E_F$ and we need to take account of another subband (the subband energy level spacing is $2E_F$.). As the magnitude of the scattering potential increases, the electrons may be reflected by the scattering potential and successfully transmitted. Then, the conductance can not transmit completely anymore. When the scattering potential strength changes into stronger, the probability for electrons to transmit is more difficult therefore the conductance is significantly suppressed and the degree of suppression will increase with the stronger of magnitude of the scattering potential.

(a) (b)

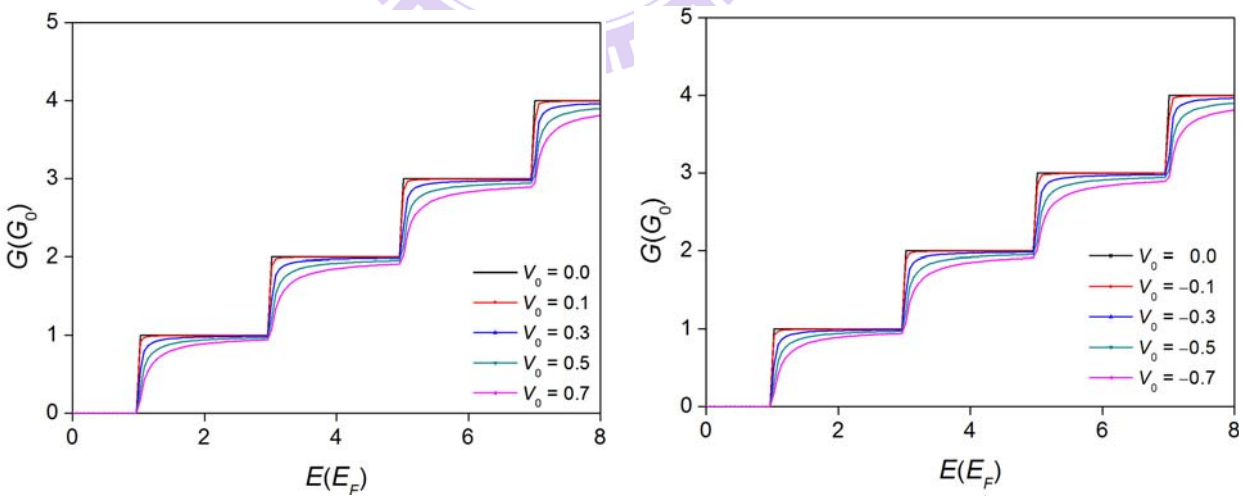

Fig. 1.3.4.1. Conductance (in units of $2e^2/h$) versus kinetic energy in a quantum channel with tunable potential strength V_0 (a) The potential is repulsive (b) The potential is attractive. The Fermi energy E_F = 9 meV

Chapter 2 Spin-resolved quantum transport

2.1 Introduction to spintronics

In the recent years, there has been growing interest in the emerging field of spin electronics or “spintronics”. Spintronics, where the spin of electrons is used to carry information, is a rapidly growing area of research [4–6]. There are several techniques for generating pure spin currents [7–9]; Spintronics involves exploration of the extra degrees of freedom provided by the electron spin, in addition to those due to electron charge, with a new view to realize the new functionalities in future electronic devices.

Spin-orbit interaction (SOI) is considered as an efficient manipulation via gate voltages, which is a relativistic effect that couples the electron spin, momentum, and electric field (or momentum dependant effective magnetic field in the electron frame.) The SOI has been utilized to devise various spintronics devices such as spin transistors, spin logic, and spin filters [10–13].

In 1990, Datta and Das proposed to control the strength of Rashba spin-orbit interaction using gate voltage as a spin-field transistor based on spin rotation, which can be a significant strong effect in narrow gap semiconductor heterostructures [14]. The gate control of the spin current employing the Aronov-Casher effect was considered. The electric dipole spin resonance controlled by the time-dependant gate was also studied. Furthermore, spin-orbit interaction is likely to be important in Einstein-Podolsky-Rosen type spin-dependant entangled electronic states for quantum information processing [15, 16]. Considering semiconductor systems, there are two main types of spin-orbit interaction. The Dresselhaus spin-orbit interaction [17] appears due to the asymmetry present in certain crystal lattices.

The Rashba spin-orbit interaction [18] arises due to the asymmetry associated with the confining potential of the heterostructure quantum well. The perpendicular electric fields inside heterostructure quantum wells are important for understanding spin-orbit coupling, which is sample-specific and adjustable. In narrow gap semiconducting quantum wells, a variation of about 50% of the spin-orbit coupling coefficient was observed experimentally by adjusting the voltage on adjacent gate electrodes, in which a quantum well is populated only by donor-layer electrons. Consequently, much interest has been attracted to the realization of spin polarized transistors, spin filter devices, and other devices based on electrical gate control to the spin-dependant transport.

2.2 The spin-orbit interactions and the Zeeman effect

To realize a spin device, it is important to utilize the spin-orbit interaction since it provides a way of controlling the spin degree of freedom electrically in semiconductor-based systems. Moreover, for a quasi-one-dimensional ballistic it is found that the SOI could significantly modify the band structure, thus additional subband extrema and energy gaps are produced. Effects of SOI and Zeeman splitting on the physical properties of quantum wires, e.g., photovoltaic effect [19] and shot noise [20] have been investigated in detail. Li et al [21]. have presented that the SOI and the Zeeman effect could result in significant variations of the conductance and the thermopower which are spin-dependent.

We will consider the transport properties in the presence of the SOI and the in-plane magnetic field. The spin-orbit interaction can be caused by structural inversion asymmetry (SIA), which can be artificially controlled by the applied gate voltages or by the specific design of the heterostructure, or by bulk inversion asymmetry (BIA), which is determined by the semiconductor material and the geometry of the sample. Both H_{BIA} and H_{SIA} lead to spin splitting of the conduction band linear in $\boldsymbol{k}$. The in-plane magnetic field will cause the energy splitting that is independent of $\boldsymbol{k}$.

The structural inversion asymmetry results in the Rashba spin-orbit interaction. The Rashba spin-orbit interaction depends on the gradient of the potential and is therefore more important the higher the nuclear charge of the element. In Ch. 1.2.1, we have mentioned that the electrons are confined at the heterostructure interface. For the purpose of confining electrons to nanostructure devices, potential well is necessary. The potential well at the interface results in the non-negligible Rashba spin–orbit interaction (SOI), especially in systems with structural inversion asymmetry (SIA) like e.g. semiconductor heterostructures. Heavy elements in the periodic table show stronger effects. This is also valid in crystals. For instance, in silicon the spin-orbit interaction is much weaker than in Ge or GaAs. It is even more important in InAs and InSb. In a two-dimensional electron gas (2DEG) obtained by a strong confinement in the z-direction (Fig. 1.3.3.1), the Rashba SOI is described by the Rashba term

$$H_R = \frac{\alpha}{\hbar}\left(p_y\sigma_x - p_x\sigma_y\right)_z . \tag{2.2.1}$$

The components of the electron momentum operator are denoted by p_{i}, the Pauli matrices are represented by σ_{i}, and α proportional to E_{z} is the SOI coupling coefficient set by the confining electric field or by the applied gate voltage.

In III-V or II-VI the heterostructure semiconductors, such as, the difference between cations and anions breaks the degeneracy of the band structure with respect to the spin degree of freedom, and is present in both bulk materials and semiconductor nanostructures. The electric fields resulting from the lack of an inversion centre lead to bulk inversion asymmetry (BIA) and to the Dresselhaus term in the Hamiltonian. In the conduction band, the spin splitting Hamiltonian is given by

$$H_{bulk,D} = \gamma_c \left[\sigma_x k_x \left(k_y^2 - k_z^2 \right) + \sigma_y k_y \left(k_z^2 - k_x^2 \right) + \sigma_z k_z \left(k_x^2 - k_y^2 \right) \right]. \tag{2.2.2}$$

To obtain the effective Hamiltonian of the two-dimensional quantum channel, we take the average of the above bulk Hamiltonian with respect to the ground state wave function along the vertical z direction.

$$H_D = \frac{\beta}{\hbar} \left(p_x \sigma_x - p_y \sigma_y \right). \tag{2.2.3}$$

The components of the electron momentum operator are denoted by p_i, the Pauli matrices are represented by σ_i, and β is the Dresselhaus spin-orbit interaction strength.

An external magnetic field lifts time inversion symmetry so that we can obtain a finite Zeeman energy splitting $\Delta E_Z = g^* \mu_B B$, where g^* is the effective g factor and μ_B the Bohr magneton of the electron or hole states. It was first shown by Roth et al. [22] that electrons can have an effective g factor g^* that differs substantially from the free-electron value $g_0 = 2$. The effective g factor $g^* \neq 2$ results from the spin–orbit interaction, which couples the orbital motion with the spin degree of freedom. Because of without SOI, the motion of spin-up electrons would be completely decoupled from the motion of spin-down electrons, and there would be identical Hamiltonians for spin-up and spin-down electrons except for the trivial Zeeman term $\pm(g_0/2)\mu_B B$, so that in this case Zeeman splitting would be controlled by the g factor, in which $g_0 = 2$ of free electrons. Recently, calculations and experiments have shown that g^* can have different values for B applied in the direction normal to the plane of the 2D system and for B in the plane of the quantum wire [23–26].

In Ch3 and Ch4, we will analyze the transport properties in a quantum channel in the presence of the spin-orbit interactions and in-plane magnetic field.

Chapter 3 Quantum transport in the presence of the Rashba spin-orbit interaction with in-plane magnetic field

In this chapter, we will use the analytical approach to investigate how the Rashba spin-orbit interaction and an in-plane magnetic field affect the electron transport. We will introduce the system Hamiltonian and analyze the energy spectrum and the wavefunction in the first section. In the second section we will use the Landauer-Buttiker formula by the matching method to calculate the conductance. At last, we will demonstrate the numerical results under different strengths of the Rashba spin-orbit interaction, the magnetic field and the gate voltage.

3.1 Theory

In this section, we use the numerical approach to calculate the energy spectrum and the spinor states of the system considering both the Rashba and the Dresselhaus spin-orbit coupling and an in-plane magnetic field.

3.1.1 System and Formulation

In this paragraph, we use the analytical approach to derive the energy spectrum and the spinor states of the system considering the Rashba spin-orbit coupling and an in-plane magnetic field [27].

We use a transverse hard wall potential to simulate the confinement potential along ***y*** direction. The transverse potential is a narrow constriction therefore we can neglect the momentum p_y along y direction. Then, the Rashba term can be reduced from Eq.(2.2.1) to

$$H_R = -\frac{\alpha}{\hbar} p_x \sigma_y . \tag{3.1.1.1}$$

The Hamiltonian for the quantum channel in the presence of the Rashba spin-orbit interaction and the Zeeman effect which is due to an applied magnetic field along x direction has the form

$$H_0 = \frac{p^2}{2m^*} - \frac{\alpha}{\hbar} p_x \sigma_y + \frac{1}{2} g_s \mu_B B \sigma_x + V_c(y), \tag{3.1.1.2}$$

where α is the Rashba strength, B is the magnetic field strength and V_c is the confining potential. In the middle of the quantum channel there is a scattering potential in forms of delta potential. Then the total single particle Hamiltonian is

$$H = H_0 + V_s(x), \;\; V_s(x) = V_0 \delta(x) . \tag{3.1.1.3}$$

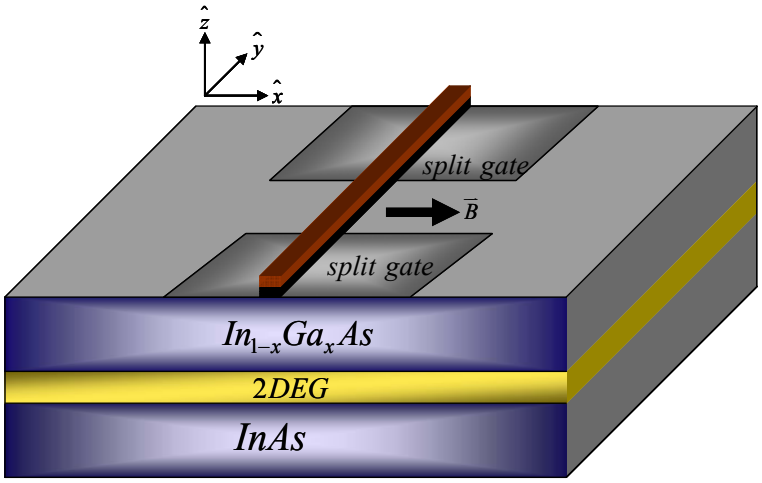

Fig. 3.1.1.1. System picture

For convenience, we choose the following units: length unit $l^* \equiv \frac{1}{k_F}$, energy unit $E^* \equiv \frac{\hbar^2 k_F^2}{2m^*}$, magnetic field unit $B^* \equiv \frac{E^*}{\mu_B}$, the Rashba coefficient unit $\alpha^* = \frac{\hbar^2 k_F}{m^*}$, the confinement potential in units of Fermi energy $V_c(y) = V(y)E^*$ and defining $g \equiv \frac{1}{2} g_s$. In the following way, we can obtain the dimensionless unperturbed Hamiltonian:

$$H_0 = k^2 - 2\alpha k_x \sigma_y + gB\sigma_x + V(y). \tag{3.1.1.4}$$

Separating the unperturbed Hamiltonian into the *x*-dependant and *y*-dependant parts can get:

$$H_0 = H_x^0 + H_y^0 \tag{3.1.1.5}$$

with

$$H_x^0 = k_x^2 - 2\alpha k_x \sigma_y + gB\sigma_x \tag{3.1.1.6}$$

and

$$H_y^0 = k_y^2 + V(y), \tag{3.1.1.7}$$

where

$$V(y) = \begin{cases} 0, & |y| < \frac{d}{2} \\ \infty, & \text{otherwise} \end{cases} \tag{3.1.1.8}$$

is a potential that confines the electron in the transverse direction and we suppose that the confining potential with only the lowest occupied subband.

The wavefunction of the unperturbed Hamiltonian can be expanded by the spatial wavefunction and spinor state,

$$\Psi(x,y)=\phi_n(y)e^{ik_x x}\chi\,. \tag{3.1.1.9}$$

Since the transverse confinement potential is the hard wall potential, the transverse wavefunction will be

$$\phi_n(y)=\sqrt{\frac{\pi}{d}}\sin\left(\frac{n\pi}{d}y\right), \tag{3.1.1.10}$$

and the subband energy will be

$$\varepsilon_n=\left(\frac{n\pi}{d}\right)^2. \tag{3.1.1.11}$$

Here, we only consider the lowest occupied subband. That is n is equal to 1. Then, substituting the transverse wavefunction and the subband energy into Eq. (3.1.1.4) and Eq. (3.1.1.9) obtain

$$(-2\alpha k_x\sigma_y+gB\sigma_x)\chi=(E-\varepsilon_n-k_x^{\,2})\chi\,. \tag{3.1.1.12}$$

Expanding the above equation by the Pauli matrices:

$$\begin{pmatrix}0 & gB+i2\alpha k_x\\ gB-i2\alpha k_x & 0\end{pmatrix}\chi=(E-\varepsilon_n-k_x^2)\chi\,. \tag{3.1.1.13}$$

The spinor state and the eigen-energy can be obtained by solving the above eigenvalue problem. The spinor state is

$$\chi_\sigma=\frac{1}{\sqrt{2}}\begin{bmatrix}1\\ \sigma e^{i\theta(kx)}\end{bmatrix};\sigma=\pm, \tag{3.1.1.14}$$

where

$$\theta(k)\equiv\tan^{-1}\left(\frac{2\alpha k_x}{|gB|}\right), \tag{3.1.1.15}$$

and the energy is

$$E_n^{\pm}=\varepsilon_n+k_x^2+\sigma\sqrt{(gB)^2+(2\alpha k_x)^2}\quad, \tag{3.1.1.16}$$

where k_x can only be real and $\sigma=\pm$ indicating the spin branches for a given subband n. For an ideal wire without scattering potential, it is convenient to use Eq. (3.1.1.16) to obtain energy spectrum as a function of wave vector for propagating modes, as shown

in Secs. 3.1.2 and 3.1.3.

In general, there are four extreme values in the energy dispersion. For convenience, we define $P_{b\sigma} = (k_{b\sigma}, E_{b\sigma})$ and $P_{t\sigma} = (k_{t\sigma}, E_{t\sigma})$ to denote the extreme values of the energy dispersion at the subband bottom (b) and subband top (t), respectively. We also define ΔE_Z to represent the pseudo-gap or the branch level spacing for a given subband, respectively. In addition, $\sigma = +, -$ represents the upper branch and lower branch, respectively.

To analyze the energy spectrum and find the local minimum and local maximum in the energy dispersion for the case involving both the Rashba and the Zeeman effects, it is convenient to define the group velocity, given by

$$\upsilon_g = \frac{dE_{\mathrm{n}}^{\sigma}}{dk_{\mathrm{x}}} = 2k_{\mathrm{x}} + \sigma \frac{4\alpha^2 k_{\mathrm{x}}}{\sqrt{g^2B^2 + 4\alpha^2 k_{\mathrm{x}}^2}}, \tag{3.1.1.17}$$

where the subscript $\sigma = \pm$ indicating the spin branches. As the group velocity is identical to zero for specific wavevectors, there will be local minimum or local maximum in the energy spectrum (Fig. 3.1.1.2).

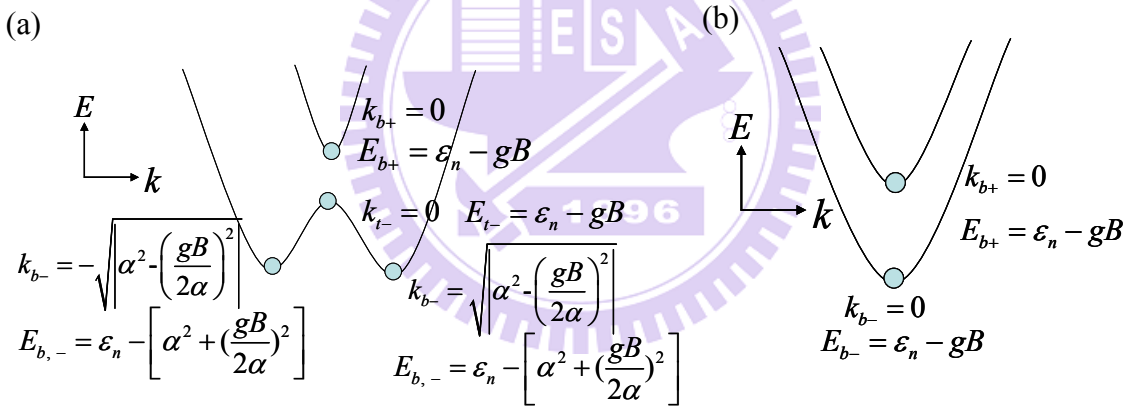

Fig. 3.1.1.2. (a) For the case $2\alpha^2 > gB$, energy spectrum with labeling local energy extreme values and corresponding wavevectors. (b) For the case $2\alpha^2 \leq gB$, energy spectrum with labeling local energy extreme values and corresponding wavevectors.

These local extreme values occur at

$$P_{t-} = (k_{t-}, E_{t-}) = (0, \varepsilon_n - gB), \tag{3.1.1.18}$$

$$P_{b+} = (k_{b+}, E_{b+}) = (0, \varepsilon_n + gB), \tag{3.1.1.19}$$

and

$$P_{b-} = (k_{b-}, t_{b-}) = (\pm\sqrt{\left|\alpha^2 - \left(\frac{gB}{2\alpha}\right)^2\right|}, E_{b,-} = \varepsilon_n - \left[\alpha^2 + (\frac{gB}{2\alpha})^2\right]). \tag{3.1.1.20}$$

It is noteworthy that this extreme value (Eq. 3.1.1.20) only exists as $2\alpha^2 > gB$ otherwise the value in the square root will be negative. Namely, this extreme value only occurs when the Rashba is significantly stronger than the Zeeman effects (Fig. 3.1.1.2 (a)). The gap between the upper branch and the lower branch would be

$$\Delta E_Z = 2gB. \tag{3.1.1.21}$$

If the Rashba coefficient is not strong enough, the energy spectrum will be vertical splitting (Fig. 3.1.1.2(b)). The energy spacing between the upper branch and the lower branch is

$$\Delta E_Z = 2gB. \tag{3.1.1.22}$$

For the specific cases, we consider only the Rashba effect, and then the energy dispersion (Eq. 3.1.1.16) becomes

$$E_n^{\pm} = \varepsilon_n + k_x^2 + \sigma 2\alpha k_x \,. \tag{3.1.1.23}$$

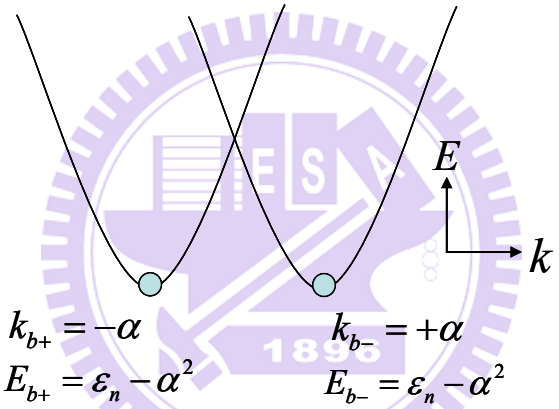

Fig. 3.1.1.3. For the case of considering the Rashba effect and turning off the magnetic field $B = 0$, energy spectrum with labeling local energy extreme values and corresponding wavevectors.

The energy dispersion is lateral splitting. The local extreme values which can be solved from the group velocity (Eq. 3.1.1.17) are at

$$P_{b+} = (k_{b+}, E_{b+}) = (-\alpha, \varepsilon_n - \alpha^2), \tag{3.1.1.24}$$

and

$$P_{b-} = (k_{b-}, E_{b-}) = (\alpha, \varepsilon_n - \alpha^2). \tag{3.1.1.25}$$

If we consider only the Zeeman effect, the energy dispersion (Eq. 3.1.16) becomes

$$E_n^{\pm} = \varepsilon_n + k_x^2 + \sigma g B \,. \tag{3.1.1.26}$$

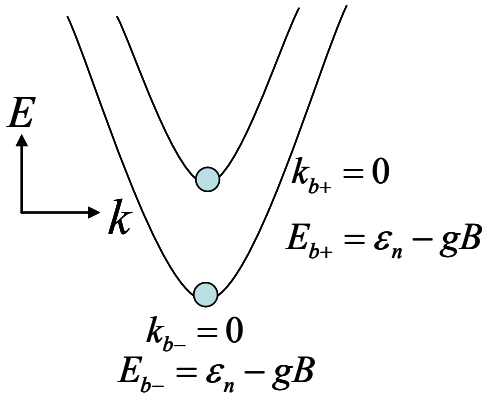

Fig. 3.1.1.4. For the case of considering only the in-plane magnetic field and the Rashba coefficient = 0, energy spectrum with labeling local energy extreme values and corresponding wavevectors.

The energy dispersion is vertical splitting. The local extrema are at

$$P_{b+} = (k_{b+}, E_{b+}) = (0, \varepsilon_n + gB)\,, \tag{3.1.1.27}$$

and

$$P_{b-} = (k_{b-}, E_{b-}) = (0, \varepsilon_n - gB)\,, \tag{3.1.1.28}$$

which can be solved from the group velocity (Eq. 3.1.1.17). Then, the energy spacing between the upper branch and the lower branch is

$$\Delta E_Z = 2gB\,. \tag{3.1.1.29}$$

3.1.2 The Rashba effect

In this section, we investigate the energy spectrum with the different Rashba effect in the presence of the in-plane magnetic field ($gB = 0.02$). There are four cases: $\alpha = 0.0(2\alpha^2 < gB)$, $0.05(2\alpha^2 < gB)$, $0.1(2\alpha^2 = gB)$, and $0.2(2\alpha^2 > gB)$, as shown in Fig. 3.1.2.1. The magnetic field strength is approximately 3T when $gB = 0.02$ ($g_s = -15$ for InAs)

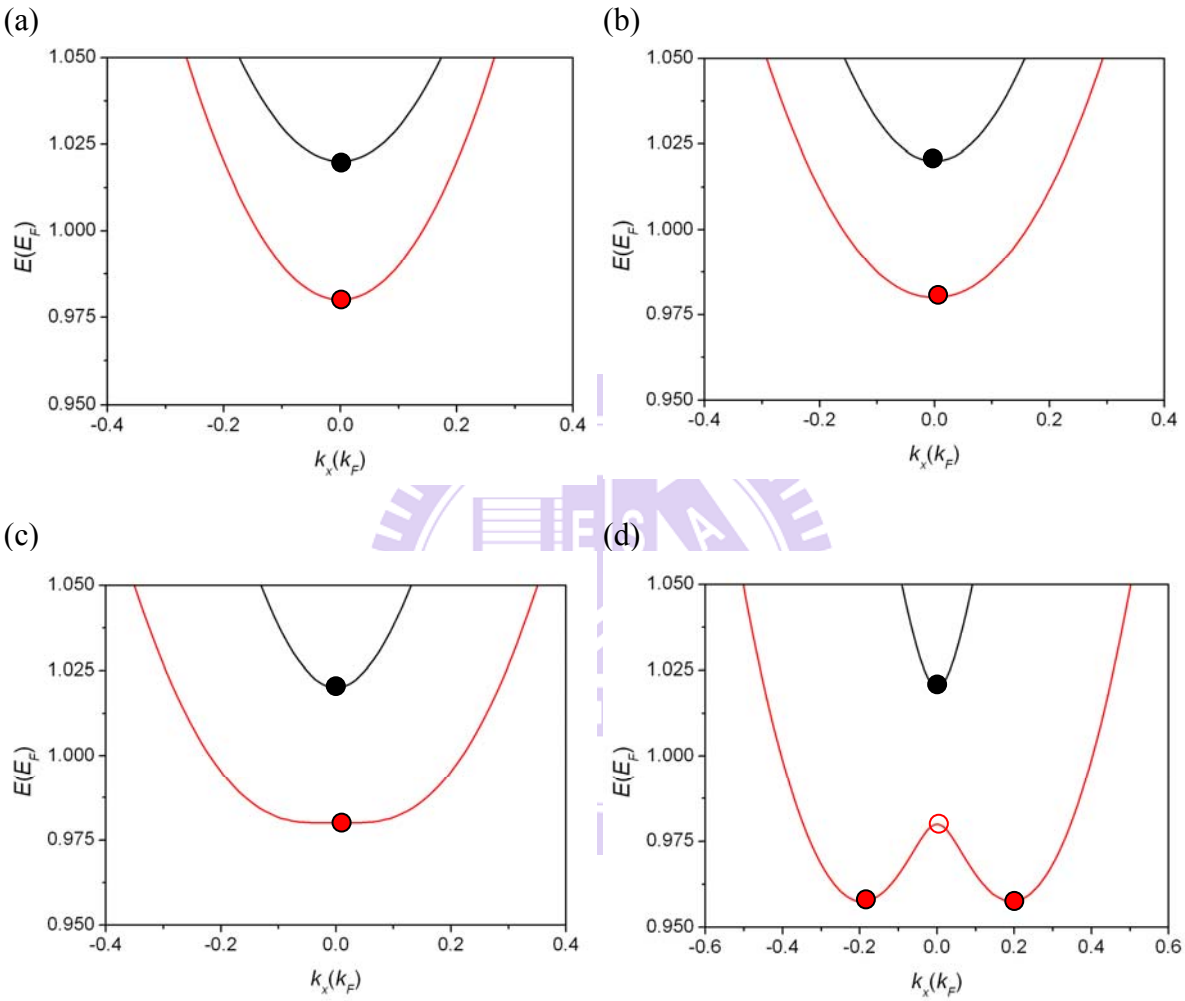

Fig. 3.1.2.1. Energy spectrum versus wave number with magnetic field strength $gB = 0.02$ for different values of α: (a) $\alpha = 0.0$ (b) $\alpha = 0.05$, (c) $\alpha = 0.1$, and (d) $\alpha = 0.2$ (the Rashba-Zeeman effect). The Fermi energy $E_F = 66$ meV and the Fermi wave vector $k_F = 2\times 10^6$ cm^{-1}. The magnetic field strength is approximately 3T when $gB = 0.02$ ($g_s = -15$ for InAs). The black and red curves indicate the plus ($\sigma = +$) and minus ($\sigma = -$) spin branches, respectively. The black dot and the red dot correspond to the local minima of plus and minus branches at the subband bottoms, denoted by P_{b+} and P_{b-}. The red circle stands for the local maxima of the minus branch at the subband top, denoted by P_{t-}.

In Fig. 3.1.2.1(a), we consider only the Zeeman effect. In the presence of the in-plane magnetic field, the energy spectrum is vertical splitting. The local minima are

at $P_{b-} = (k_{b-}, E_{b-}) = (0.0, \varepsilon_n - gB) = (0.0, 0.98)$, $P_{b+} = (k_{b+}, E_{b+}) = (0.0, \varepsilon_n + gB) = (0.0, 1.02)$ and the branch level spacing for a given subband is $\Delta E_Z = 2gB = 0.04$ as we mentioned in (Eq. 3.1.28). In the second case, the Rashba effect is week and not strong enough to form a pseudo-gap, that is, $2\alpha^2 < gB$, therefore the energy spectrum is vertical splitting (Fig. 3.1.2.1(b)) and the local minima are $P_{b+} = (k_{b+}, E_{b+}) = (0.0, \varepsilon_n + gB) = (0.0, 1.02)$ and $P_{b-} = (k_{b-}, E_{b-}) = (0.0, \varepsilon_n - gB) = (0.0, 0.98)$. The branch level spacing for a given subband is still $\Delta E_Z = 2gB = 0.04$. When the Rashba effect satisfy $2\alpha^2 = gB$, the energy spectrum is still vertical splitting and the local minima are the same as the first two cases. When the Rashba effect is strong enough to from a pseudo-gap, that is, $2\alpha^2 > gB$, there is a magneto-spin-orbit pseudo-gap in the energy spectrum (Fig. 3.1.2.1(d)). The local minimum at the upper branch is $P_{b+} = (k_{b+}, E_{b+}) = (0.0, \varepsilon_n + gB) = (0.0, 1.02)$ (Eq. 3.1.19) and the local extreme values at the lower branch are $P_{t-} = (k_{t-}, E_{t-}) = (0.0, \varepsilon_n - gB) = (0.0, 0.98)$, $P_{b-,1} = (k_{b-,1}, E_{b-,1}) = (0.1952, 0.9575)$ and $P_{b-,2} = (k_{b-,2}, E_{b-,2}) = (0.1952, 0.9575)$ (Eq. 3.1.18 and 3.1.20). The pseudo-gap is $\Delta E_Z = 2gB = 0.04$.

3.1.3 The Zeeman effect

For comprehending how the Zeeman effect would affect the energy spectrum, we fix the Rashba effect ($\alpha = 0.2$) and tune the Zeeman effect from weak to strong. Below, there are five cases: $gB = 0 (2\alpha^2 > gB)$, $gB = 0.02 (2\alpha^2 > gB)$, $gB = 0.08$ $(2\alpha^2 = gB)$, $gB = 0.1$ $(2\alpha^2 < gB)$.

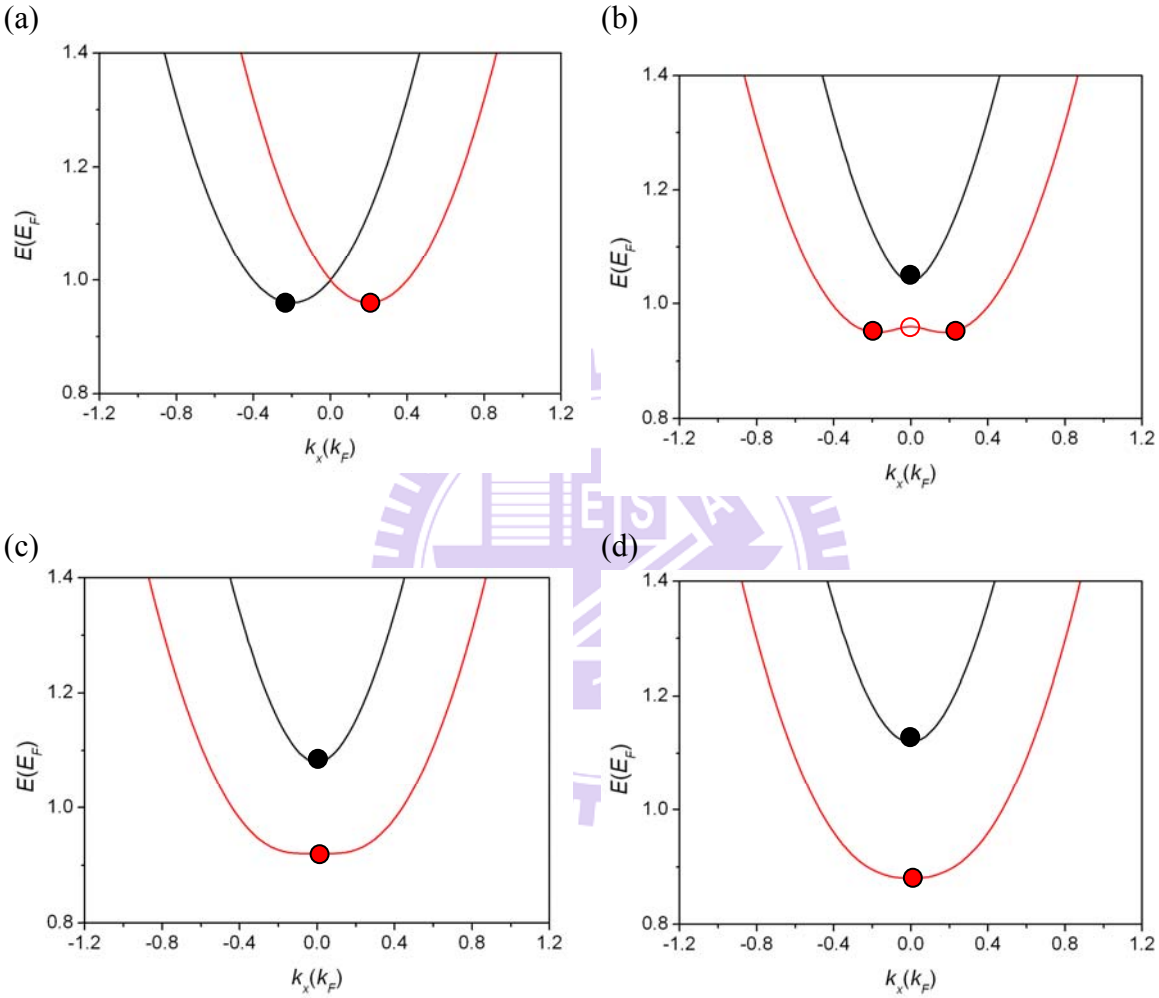

Fig. 3.1.3.1 Energy spectrum versus wave number with different magnetic field strength gB and the fixed Rashba strength α: (a) $gB = 0$, $\alpha = 0.2$; (b) $gB = 0.04$, $\alpha = 0.2$; (c) $gB = 0.08$, $\alpha = 0.2$ (d) $gB = 0.12$, $\alpha = 0.2$. The Fermi energy $E_F = 66$ meV and the Fermi wave vector $k_F = 2\times 10^6$ cm^{-1}. The magnetic field strength is approximately 6T when $gB = 0.04$ ($g_s = -15$ for InAs). The black and red curves indicate the plus ($\sigma = +$) and minus ($\sigma = -$) spin branches, respectively. The black dot and the red dot correspond to the local minima of plus and minus branches at the subband bottoms, denoted by P_{b+} and P_{b-}. The red circle stands for the local maxima of the minus branch at the subband top, denoted by P_{t-}.

In Fig. 3.1.3.1(a), we show the energy dispersion in the presence of the Rashba

spin-orbit interaction. The energy dispersion is lateral splitting. The local minimum at the plus branch is $P_{b+} = (k_{b+}, E_{b+}) = (-0.2, 0.96)$ and at the minus branch is $P_{b-} = (k_{b-}, E_{b-}) = (0.2, 0.96)$ (Eq. 3.1.24 and 3.1.25). In Fig. 3.1.3.1(b), when the Zeeman effect $gB = 0.04$ and $2\alpha^2 > gB$, there is a pseudo-gap in the energy spectrum. The local extreme value at the upper branch is $P_{b+} = (k_{b+}, E_{b+}) = (0.0, 1.04)$. The local extreme values at the lower branch are $P_{b-} = (k_{b-,1}, E_{b-,1}) = (-0.17, 0.95)$, $P_{b-,2} = (k_{b-,2}, E_{b-,2}) = (0.17, 0.95)$ and $P_{t,-} = (k_{t,-}, E_{t,-}) = (0.0, 1.04)$ (Eq. 3.1.18 and 3.1.20). As the magnetic field increases and $gB = 0.08$ and $2\alpha^2 = gB$, the energy dispersion is vertical splitting (Fig. 3.1.3.1(c)) and the branch level spacing for a given subband is $\Delta E_Z = 2gB = 0.16$. As the Zeeman coefficient increases ($gB = 0.12$) and satisfies $2\alpha^2 < gB$, the branch level spacing compare to Fig. 3.1.3.1(c) increases $\Delta E_Z = 2gB = 0.24$ since the in-plane magnetic field increases.

3.1.4 Spin orientation

In order to investigate the spin orientation in the presence of the Rashba spin-orbit interaction and the in-plane magnetic field, we calculate the effective magnetic field for these spin-orbit interactions and the Zeeman effect [28]. The dimensionless Hamiltonian for an electron in the presence of the magnetic field can be expressed as:

$$H = \vec{\sigma} \cdot \vec{B}, \tag{3.1.4.1}$$

where B is dimensionless ($B^* = E^*/\mu_B$). Hence, when the above equation is identical to the Rashba term,

$$-2\alpha k_x \sigma_y = \vec{\sigma} \cdot \vec{B} = B_y \sigma_y, \tag{3.1.4.2}$$

we can obtain the effective magnetic field for the Rashba spin-orbit interaction:

$$\vec{B_R} = -2\alpha k_x \hat{y}. \tag{3.1.4.3}$$

In the same way, we can obtain the effective magnetic field for the Zeeman effect:

$$\vec{B_Z} = gB\hat{x}. \tag{3.1.4.4}$$

Then, the effective magnetic field of the system can be expressed as:

$$\vec{B_{eff}} = B_Z \hat{x} + B_R \hat{y} = gB\hat{x} - 2\alpha k_x \hat{y}. \tag{3.1.4.5}$$

In order to achieve equilibrium, the spin orientation of the electron in the presence of the magnetic field tends to be opposite to the direction of the magnetic field. Therefore, the spin orientation of the electron at the plus branch is aligned in the direction of the effective magnetic field. However, the spin orientation of the electron

at the minus branch will be opposite to the direction of the effective magnetic field. We can express the spin orientation for the electrons at the plus branch as:

$$\overrightarrow{S_\sigma} = \frac{gB}{\sqrt{(gB)^2 + (2\alpha k_x)^2}}\hat{x} - \frac{2\alpha k_x}{\sqrt{(gB)^2 + (2\alpha k_x)^2}}\hat{y}, \quad \sigma = +. \tag{3.1.4.6}$$

and the spin orientation for the electrons at the minus branch is:

$$\overrightarrow{S_\sigma} = -\frac{gB}{\sqrt{(gB)^2 + (2\alpha k_x)^2}}\hat{x} + \frac{2\alpha k_x}{\sqrt{(gB)^2 + (2\alpha k_x)^2}}\hat{y}, \quad \sigma = -. \tag{3.1.4.7}$$

Below, we show the energy spectrum with the spin orientation in the presence of the Rashba spin-orbit interaction with different Zeeman effects.

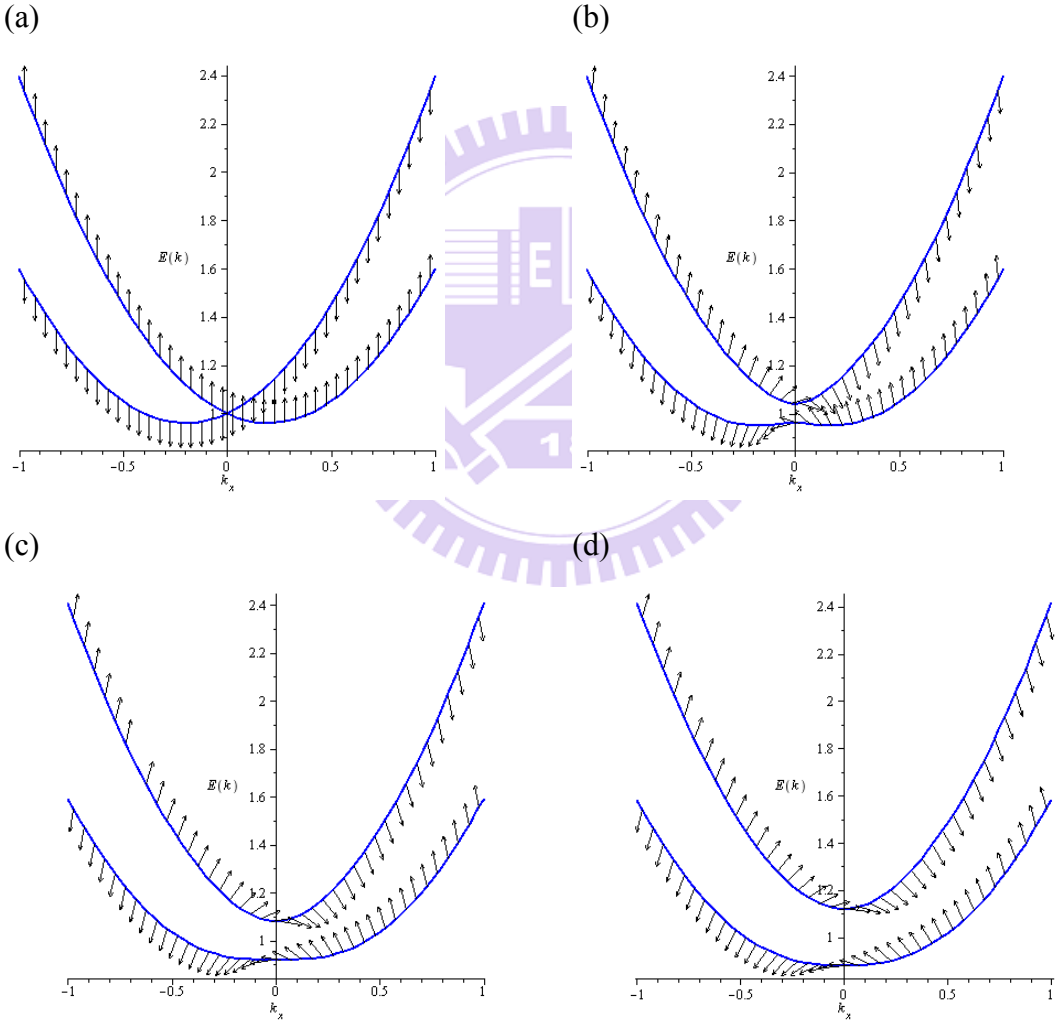

Fig. 3.1.4.1. Energy dispersion with spin orientation illustrated by the arrows with the different Zeeman effects and the fixed Rashba strength α. (a) $gB = 0$, $\alpha = 0.2$; (b) $gB = 0.04$, $\alpha = 0.2$; (c) $gB = 0.08$, $\alpha = 0.2$ (d) $gB = 0.12$, $\alpha = 0.2$. The magnetic field strength is approximately 6T when $gB = 0.04$ ($g_s = -15$ for InAs)

In Fig. 3.1.4.1 (a), we turn off the magnetic field and only consider the Rashba spin-orbit interaction. The spin orientation is along the **y** direction. When the in-plane magnetic field increases, the spin orientation is inclined to along the ***x*** direction. Therefore, the spin orientation is at the angle between the ***x*** axis and the ***y*** axis. When the Zeeman effect increases from gB = 0.04 to 0.12, the angle between the spin orientation and the ***x*** axis decreases. Since the effective magnetic field of the Rashba spin-orbit interaction is dependant of the linear k_x, at k_x = 0 the spin orientation is always along the ***x*** direction.

3.1.5 Complex energy dispersion

It is interesting to note since the Rashba and the Zeeman effects result in the spin-splitting energy dispersion, there is a gap appearing in the energy regime (see Fig. 3.1.2.1(d)). The channel number must be conservative, and therefore there are two evanescent modes in this gap regime [29]. For finding these evanescent modes, we rearrange (3.1.16) into this following form

$$k_x^2 = (E + 2\alpha^2 - \varepsilon_n) \mp \sqrt{(E + 2\alpha^2 - \varepsilon_n)^2 + (gB)^2 - (E - \varepsilon_n)^2} \quad (3.1.5.1)$$

From this degree 4 polynomial we find that for a given energy there are four corresponding modes. Namely, for a given energy we can find the corresponding wave vectors from the above equation. The above polynomial problem can be solved by calling the DZPOCC subroutine from the IMSL library. For a given energy, this subroutine can find the corresponding four complex roots k_x. In Fig. 3.1.5.1, we demonstrate a three dimensional energy dispersion considering both the Rashba and the Zeeman effects ($2\alpha^2 > gB$). In this picture, the x axis represents the real part of k, the y axis represents the imaginary part of k and the z axis stands for energy. We can see below the lower band bottom, there are four evanescent modes which represents by the red line. At the gap energy regime there are two propagating modes and two evanescent modes. The evanescent modes in the gap are in form of a bubble. These evanescent modes won't contribute to the current since the electron at these modes would decay with distance and they can not successfully transmit to the drain. However, during the scattering process it might be scattered into these evanescent modes, thus we still need to know the wavevectors and spinor states about the evanescent modes for calculating transport.

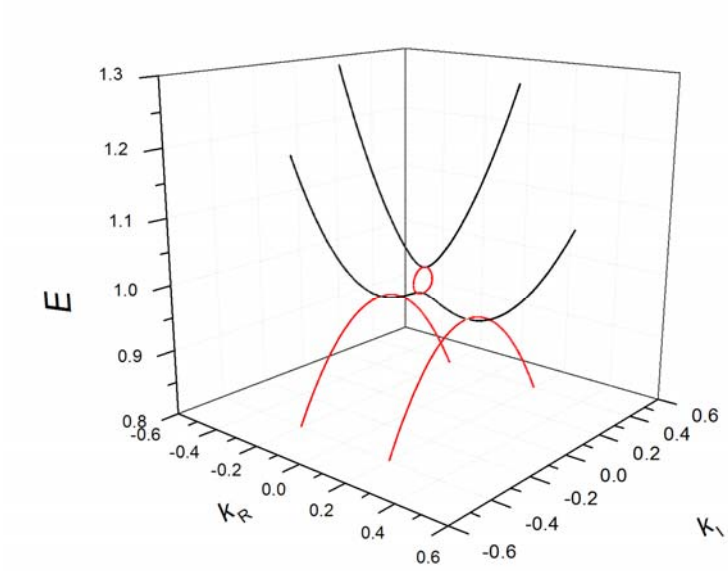

Fig. 3.1.5.1. 3D Energy dispersion in the presence of the Rashba spin-orbit interaction and in-plane magnetic field (α = 0.2, gB = 0.02). k_R and k_I represent, respectively, the real part and the imaginary part of the wave number ($k = k_R + k_I$). The black solid line represents the propagating modes and the red solid line represents the evanescent modes. The Fermi energy E_F = 66 meV and the Fermi wave vector $k_F = 2\times10^6$ cm^{-1}.

The evanescent modes in the bubble are pure imaginary since the local minimum $P_{b,+}$ at the upper branch and the local maximum $P_{t,-}$ at the lower branch are at $k_x = 0$. We substitute $k_x = i\kappa$ into Eq. (3.1.16) and obtain

$$E = \varepsilon_n + \kappa^2 \pm \sqrt{g^2B^2 - 4\alpha^2\kappa^2} \quad . \tag{3.1.5.2}$$

The spinor state for the evanescent modes is

$$\chi = \left[\frac{(gB+2\alpha\kappa)^2}{(gB+2\alpha\kappa)^2 + \left|g^2B^2 - 4\alpha^2\kappa^2\right|}\right]^{\frac{1}{2}} \begin{bmatrix} 1 \\ \pm\dfrac{\sqrt{g^2B^2 - 4\alpha^2\kappa^2}}{gB+2\alpha\kappa} \end{bmatrix}, \tag{3.1.5.3}$$

which can be solved by substituting $k_x = i\kappa$ into Eq. (3.1.13). Then, we can write down the general spinor state for propagating modes and evanescent modes

$$\chi = \sqrt{\frac{\left|gB - i2\alpha k_x\right|^2}{\left|gB - i2\alpha k_x\right|^2 + \left|g^2B^2 - 4\alpha^2k_x^2\right|}} \begin{bmatrix} 1 \\ \pm\dfrac{\sqrt{g^2B^2 + 4\alpha^2k_x^2}}{gB - i2\alpha k_x} \end{bmatrix}. \tag{3.1.5.4}$$

3.2 Transport theory

In this section, we derive the analysis wavefunction and transport formulation of the system.

$$H = H_0 + V_s(x), \tag{3.2.1}$$

where

$$H_0 = \frac{p^2}{2m^*} - \alpha p_x \sigma_y + \frac{1}{2} g_s \mu_B B \sigma_x + V_c(y), \tag{3.2.2}$$

For the electron incident along $\boldsymbol{x}$ at a given energy, we use k_σ (q_σ) to denote the wavevector of right-going (left-going) modes at the spin branch σ, where the dummy index σ could be the outer or the inner modes, denoted by 1 or 2, as shown in Fig. 3.2.1. Then, the scattering wavefunction is of the form

$$\psi(x) = e^{ik_\sigma x}\chi(k_\sigma) + \sum_\sigma r_\sigma e^{iq_\sigma x}\chi(q_\sigma), x < 0, \tag{3.2.3}$$

and

$$\psi(x) = \sum_\sigma t_\sigma e^{ik_\sigma x}\chi(k_\sigma), x > 0, \tag{3.2.4}$$

where σ representing that the electron is at which mode and the spinor state $\chi(k_\sigma)$ is in the form of

$$\chi_\sigma = \sqrt{\frac{\left|gB - i2\alpha k_x\right|^2}{\left|gB - i2\alpha k_x\right|^2 + \left|g^2B^2 - 4\alpha^2 k_x^2\right|}} \begin{bmatrix} 1 \\ \sigma \dfrac{\sqrt{g^2B^2 + 4\alpha^2 k_x^2}}{gB - i2\alpha k_x} \end{bmatrix}; \sigma = \pm, \tag{3.2.5}$$

where the sign of σ depends on which mode the electron is at, spin up or spin down.

At the nano-scale, the coherent quantum transport at zero temperature is

$$G = \sum_{\sigma_L,\sigma_R} G_{\sigma_L,\sigma_R} = \sum_{\sigma_L,\sigma_R} \left[\frac{e^2}{h} \left| t_{\sigma_R,\sigma_L} \right|^2 \frac{\upsilon_{\sigma_R}}{\upsilon_{\sigma_L}} \right]. \tag{3.2.6}$$

To solve the reflection and transmission coefficients, we use the property that the wavefunctions must satisfy the boundary conditions. The boundary conditions for $\psi(x)$ is continuous at $x = 0$

$$\psi\left(x = 0^-\right) = \psi\left(x = 0^+\right) \tag{3.2.7}$$

and for the derivative of $\psi(x)$ is given by

$$\psi'\left(x = 0^-\right) = \psi'\left(x = 0^+\right) - V_0\psi\left(x = 0^+\right). \tag{3.2.8}$$

After some algebra, we get the four equations relating to the reflection coefficients and the transmission coefficients.

We take the energy regime $\varepsilon_n - gB < E < \varepsilon_n + gB$ for example (Fig. 3.2.1). The wavefunction is expressed as in the form:

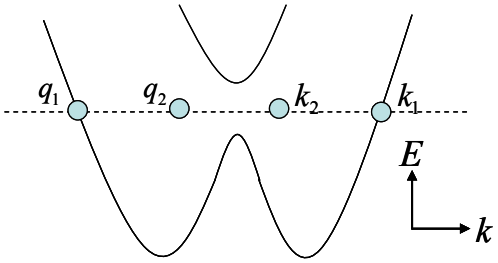

Fig. 3.2.1. Energy spectrum with labeling modes. k_1, q_1 indicate the outer right-going and left-going modes. k_2, q_2 in this energy regime are evanescent modes.

$$\psi(x) = e^{ik_\sigma x}\chi(k_\sigma) + \sum_\sigma r_\sigma e^{iq_\sigma x}\chi(q_\sigma), x < 0 \tag{3.2.9}$$

and

$$\psi(x) = \sum_\sigma t_\sigma e^{ik_\sigma x}\chi(k_\sigma), x > 0\,. \tag{3.2.10}$$

Expanding the wavefunction, the wavefunction is in the form:

$$\psi(x) \equiv e^{ik_\sigma x}\begin{bmatrix} a_\sigma \\ b_\sigma \end{bmatrix} + r_\sigma e^{iq_\sigma x}\begin{bmatrix} c_\sigma \\ d_\sigma \end{bmatrix} + r_{\bar\sigma} e^{iq_{\bar\sigma} x}\begin{bmatrix} c_{\bar\sigma} \\ d_{\bar\sigma} \end{bmatrix}, \quad x < 0 \tag{3.2.11}$$

and

$$\psi(x) \equiv t_\sigma \cdot e^{ik_\sigma x}\begin{bmatrix} a_\sigma \\ b_\sigma \end{bmatrix} + t_{\bar\sigma} e^{ik_{\bar\sigma} x}\begin{bmatrix} a_{\bar\sigma} \\ b_{\bar\sigma} \end{bmatrix}, \quad x > 0\,, \tag{3.2.12}$$

where

$$a_\sigma = \frac{1}{\sqrt{2}} \quad , \tag{3.2.13}$$

$$b_\sigma = -\frac{1}{\sqrt{2}} e^{i\theta(k_\sigma)}\,, \tag{3.2.14}$$

$$\theta(k_\sigma) = \tan^{-1}\left(\frac{2\alpha k_\sigma}{gB}\right), \tag{3.2.15}$$

$$c_\sigma = \frac{1}{\sqrt{2}}, \tag{3.2.16}$$

$$d_\sigma = -\frac{1}{\sqrt{2}} e^{i\theta(q_\sigma)}, \tag{3.2.17}$$

and

$$\theta(q_\sigma) = \tan^{-1}\left(\frac{2\alpha q_\sigma}{gB}\right), \tag{3.2.18}$$

$$a_{\bar{\sigma}} = \left\{\frac{(gB+2\alpha\kappa_{\bar{\sigma}})^2}{(gB+2\alpha\kappa_{\bar{\sigma}})^2 + \left|g^2B^2 - 4\alpha^2\kappa_{\bar{\sigma}}^2\right|}\right\}^{1/2}, \tag{3.2.19}$$

$$b_{\bar{\sigma}} = a_{\bar{\sigma}} \cdot \frac{\sqrt{g^2B^2 - 4\alpha^2\kappa_{\bar{\sigma}}^2}}{gB+2\alpha\kappa_{\bar{\sigma}}}, \tag{3.2.20}$$

$$c_{\bar{\sigma}} = \left\{\frac{(gB+2\alpha Q_{\bar{\sigma}})^2}{(gB+2\alpha Q_{\bar{\sigma}})^2 + \left|g^2B^2 - 4\alpha^2 Q_{\bar{\sigma}}^2\right|}\right\}^{1/2}, \tag{3.2.21}$$

$$d_{\bar{\sigma}} = c_{\bar{\sigma}} \cdot \frac{\sqrt{g^2B^2 - 4\alpha^2 Q_{\bar{\sigma}}^2}}{gB+2\alpha Q_{\bar{\sigma}}}. \tag{3.2.22}$$

Matching the wavefunction at the boundary conditions of the scattering potential:

$$\psi\left(x=0^-\right) = \psi\left(x=0^+\right). \tag{3.2.23}$$

$$\psi'\left(x=0^-\right) = \psi'\left(x=0^+\right) - V_0\psi\left(x=0^+\right). \tag{3.2.24}$$

We can get four simultaneous equations.

1. $a_\sigma + r_\sigma c_\sigma + r_{\bar{\sigma}} c_{\bar{\sigma}} = t_\sigma a_\sigma + t_{\bar{\sigma}} a_{\bar{\sigma}}$ (3.2.25)
2. $b_\sigma + r_\sigma d_\sigma + r_{\bar{\sigma}} d_{\bar{\sigma}} = t_\sigma b_\sigma + t_{\bar{\sigma}} b_{\bar{\sigma}}$ (3.2.26)
3. $k_\sigma a_\sigma + r_\sigma q_\sigma c_\sigma + r_{\bar{\sigma}} q_{\bar{\sigma}} c_{\bar{\sigma}} = t_\sigma(k_\sigma + iV_0)a_\sigma + t_{\bar{\sigma}}(k_{\bar{\sigma}} + iV_0)a_{\bar{\sigma}}$ (3.2.27)
4. $k_\sigma b_\sigma + r_\sigma q_\sigma d_\sigma + r_{\bar{\sigma}} q_{\bar{\sigma}} d_{\bar{\sigma}} = t_\sigma(k_\sigma + iV_0)b_\sigma + t_{\bar{\sigma}}(k_{\bar{\sigma}} + iV_0)b_{\bar{\sigma}}$ (3.2.28)

Rearranging the four simultaneous equations into a matrix form, it becomes

$$\begin{bmatrix} -c_\sigma & -c_{\bar{\sigma}} & a_\sigma & a_{\bar{\sigma}} \\ -d_\sigma & -d_{\bar{\sigma}} & b_\sigma & b_{\bar{\sigma}} \\ -q_\sigma c_\sigma & -q_{\bar{\sigma}} c_{\bar{\sigma}} & (k_\sigma + iV_0)a_\sigma & (k_{\bar{\sigma}} + iV_0)a_{\bar{\sigma}} \\ -q_\sigma d_\sigma & -q_{\bar{\sigma}} d_{\bar{\sigma}} & (k_\sigma + iV_0)b_\sigma & (k_{\bar{\sigma}} + iV_0)b_{\bar{\sigma}} \end{bmatrix} \begin{bmatrix} r_\sigma \\ r_{\bar{\sigma}} \\ t_\sigma \\ t_{\bar{\sigma}} \end{bmatrix} = \begin{bmatrix} a_\sigma \\ b_\sigma \\ k_\sigma a_\sigma \\ k_\sigma b_\sigma \end{bmatrix} \quad (\mathbf{AX}=\mathbf{B}). \tag{3.2.29}$$

For a given energy, there are four modes and four corresponding spinor states. Substituting the wave vectors and the spinor states into these elements in the matrix, solving the inverse matrix of **A** and operating it on matrix **B** can get the transmission coefficients t_σ, $t_{\bar{\sigma}}$. At the zero temperature, the conductance is given by

$$G = \sum_{\sigma_L,\sigma_R} \left[\frac{e^2}{h} \left| t_{\sigma_L,\sigma_R} \right|^2 \frac{\upsilon_{\sigma_R}}{\upsilon_{\sigma_L}} \right], \tag{3.2.30}$$

where σ_R, σ_L denote the branch index, and υ_{σ_R}, υ_{σ_L} represent the group velocity at the corresponding mode. In the scattering process, the electrons may be incident from a right-going mode k_σ but transmitted at another right-going mode $k_{\bar{\sigma}}$ or transmitted at the same mode k_σ (Fig. 3.2.2). The total transmission in this energy regime is

$$T = \sum_{\sigma_L,\sigma_R} \left| t_{\sigma_L,\sigma_R} \right|^2 = \left| t_{-,-} \right|^2 + \left| t_{-,+} \right|^2 + \left| t_{+,+} \right|^2 + \left| t_{+,-} \right|^2. \tag{3.2.31}$$

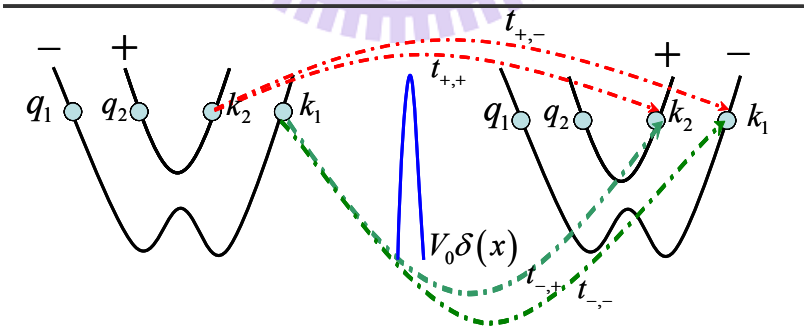

Fig. 3.2.2.Scattering process in the high energy regime.

3.3 Numerical results

The numerical calculation presented below are carried out under the assumption that the electron effective mass $m^* = 0.023\ m_0$, which is appropriate to the InAs-based semiconductors. The typical electron density is n ~ 10^{12} cm^{-2}. Accordingly, the length unit is $L^* = 5.0$ nm, the transverse width unit of the quantum channel is $w^* = \pi L^* = 15.7$ nm, the energy unit is $E^* = 66$ meV and the spin-orbit coupling parameter is in units of $\alpha^* = \frac{\hbar^2 k_F}{m^*} = 3.317\times10^{-10}$ eV m [30]. All the physical units are shown in Appendix.

3.3.1 Ideal conductance with the tunable Rashba effects

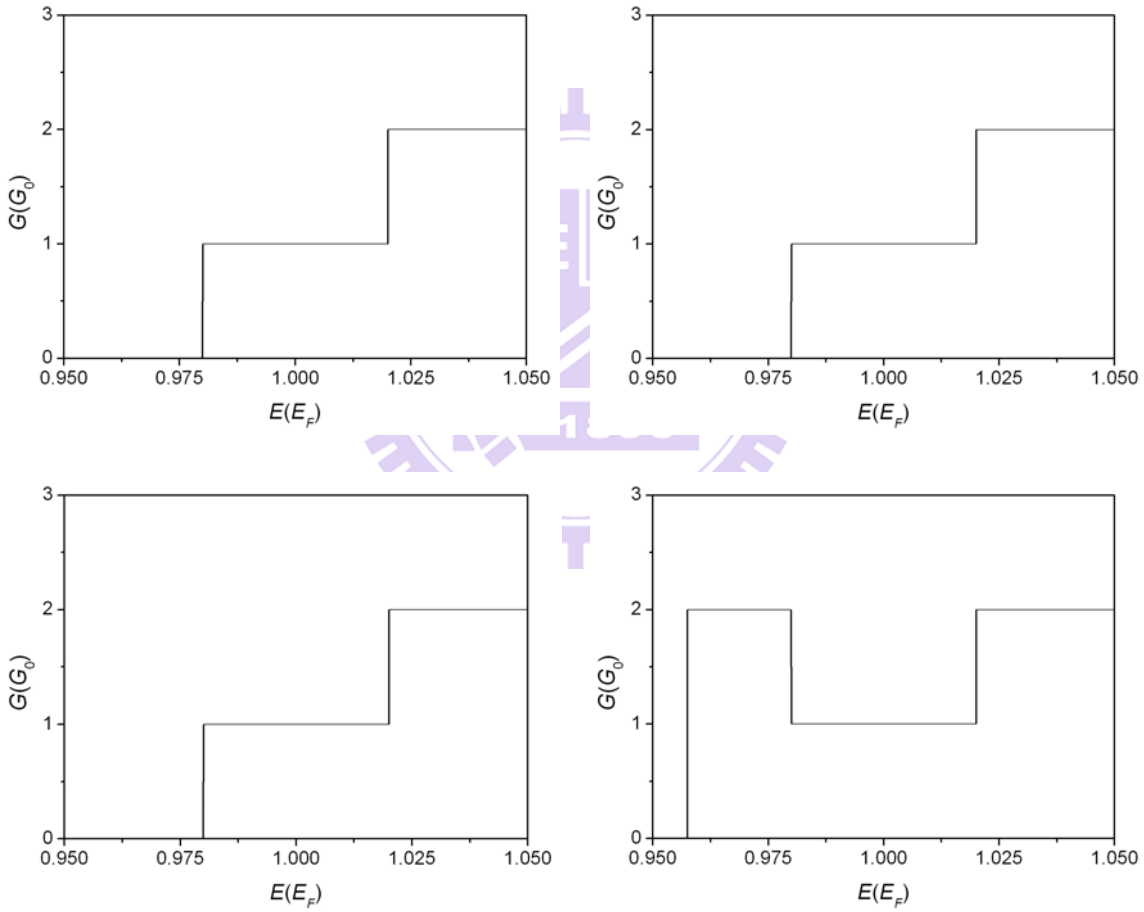

Fig. 3.3.1.1. Conductance (in units of $G_0 = e^2/h$) versus kinetic energy without the scattering potential in the presence of in-plane magnetic field with different Rashba coefficients: (a) $\alpha = 0$, $gB = 0.02$; (b) $\alpha = 0.05$, $gB = 0.02$; (c) $\alpha = 0.1$, $gB = 0.02$; (d) $\alpha = 0.2$, $gB = 0.02$. The Fermi energy $E_F = 66$ meV and the Fermi wave vector $k_F = 2\times10^6$ cm^{-1}. The magnetic field strength is approximately 3T when $gB = 0.02$ ($g_s = -15$ for InAs).

In Fig. 3.3.1.1, we investigate the ideal conductance [31] in the presence of in-plane magnetic field with different Rashba coefficients. Since there is no scattering potential, the electron can be totally transmitted through the quantum channel without reflection. It is shown in Fig. 3.3.1.1(a) when we only consider in-plane magnetic field in the system, the conductance will be identical to G_0 with $G_0 = e^2/h$ above the subband bottom of the energy. There is only one propagating mode contributing to the conductance for the energy regime above the subband bottom (Fig. 3.1.2.1(a)). In the higher energy regime, namely the electron energy is higher than the bottom of the upper subband, there are four propagating modes (two left and two right going modes) and the conductance is increasing to $2G_0$. In Fig. 3.3.1.1(b) and (c), the Rashba coefficient increases from 0.0 to 0.05 and 0.1. However, the Rashba effect is not strong enough ($2\alpha^2 \leqq gB$) to form a pseudo-gap in the energy spectrum, that is, the corresponding energy spectrum is still vertical splitting (Fig. 3.1.2.1(b) and (c)). Therefore, the conductance in Fig. 3.3.1.1(b) and (c) will be identical to G_0 in lower energy regime and identical to $2G_0$ in higher energy regime. In Fig. 3.3.1.1(d), the Rashba coefficient $\alpha = 0.2$ satisfying $2\alpha^2 > gB$, therefore there are a pseudo-gap in the energy spectrum (Fig. 3.1.2.1 (d)). In low energy regime, there are two inner modes (left and right going modes with low momentum) and two outer modes (left and right going modes with high momentum), and hence the transported electrons contribute to conductance $2G_0$. In mediate energy regime, that is the magneto-spin-orbit pseudo-gap energy regime, there are two outer propagating modes (left and right going modes), and the two inner modes belong to evanescent modes. Hence, the conductance reduces to G_0. For the high energy regime, namely the electron energy is higher than the bottom of the upper subband, there are four propagating modes (two right-going modes and two left-going modes) and the conductance is increasing to $2G_0$.

3.3.2 Transport properties with the Rashba effects in the presence of in-plane magnetic field

(I) The attractive scattering potentials

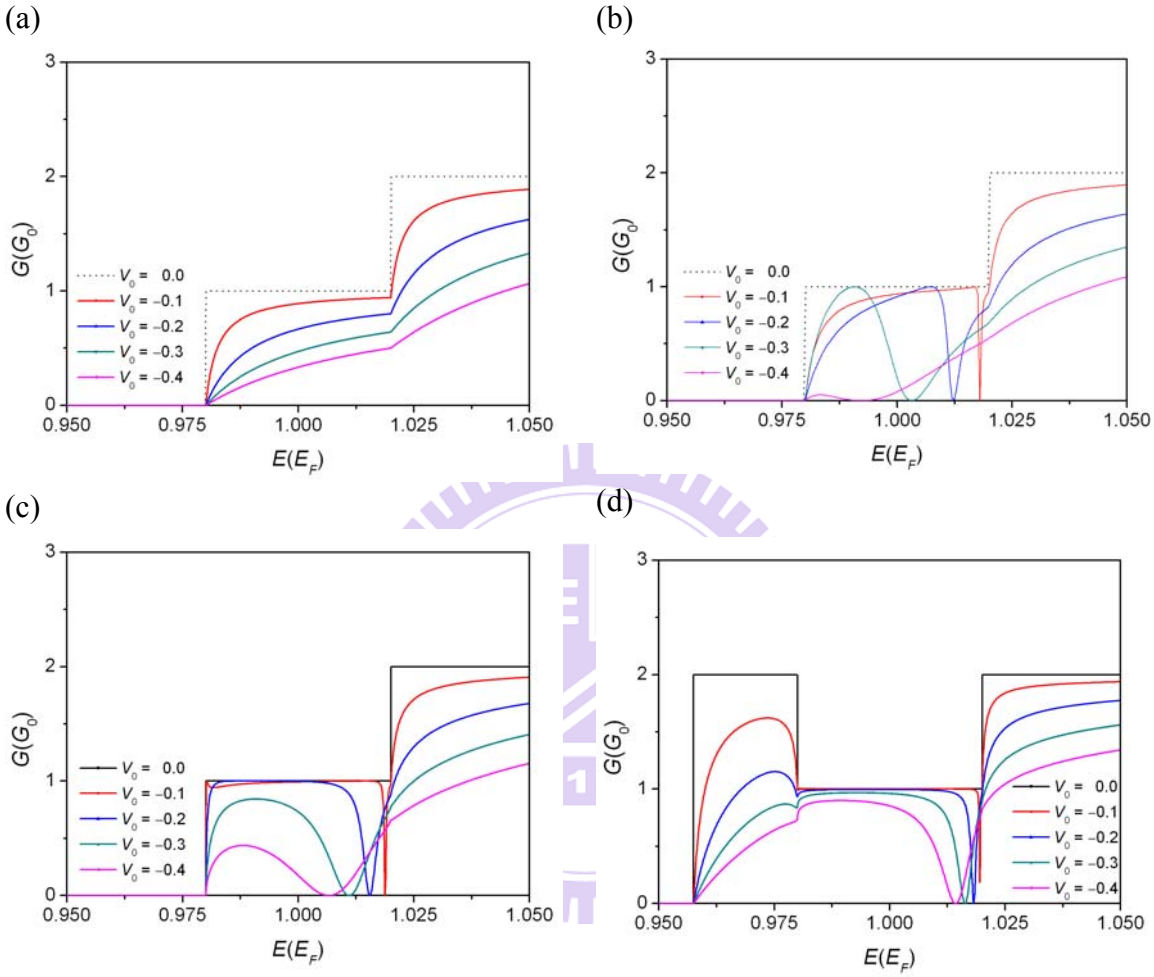

Fig. 3.3.2.1. Conductance (in units of $G_0 = e^2/h$) versus kinetic energy with the attractive scattering potential in the presence of in-plane magnetic field with different Rashba coefficients: (a) $\alpha = 0.0$, $gB = 0.02$ ($2\alpha^2 < gB$) (b) $\alpha = 0.05$, $gB = 0.02$ ($2\alpha^2 < gB$) (c) $\alpha = 0.1$, $gB = 0.02$ ($2\alpha^2 = gB$) (d) $\alpha = 0.2$, $gB = 0.02$ ($2\alpha^2 > gB$). The Fermi energy $E_F = 66$ meV and the Fermi wave vector $k_F = 2\times10^6$ cm^{-1}. The magnetic field strength is approximately 3T when $gB = 0.02$ ($g_s = -15$ for InAs).

In the presence of the scattering potential, the conductance is not ideally quantized anymore since the electron may be back scattered and has no contribution to the conductance. In Fig. 3.3.2.1 we show the transport properties in the presence of in-plane magnetic field with different Rashba coefficients. We find that the increasing of the strength of the scattering potential will cause the more suppressive of conductance.

In Fig. 3.3.2.1(a), we investigate the transport properties in the presence of the in-plane magnetic field (gB = 0.02) with applying the attractive scattering potential. The conductance is suppressed with the increasing strength of the potential. When the Rashba coefficient α = 0.05 with the in-plane magnetic field (gB = 0.02), there is a dip structure in the conductance (Fig. 3.3.2.1(b)). The dip structure occurs at electron-like quasi-bound state which is at the bottom of the upper branch. As the potential strength increases, the dip structure shifts along the direction of the low energy regime. Namely, the corresponding energy of the electron-like quasi-bound state decreases when the potential strength increases. In addition, the width of the dip structure increases as the potential strength increases. Since the life time is defined as the reciprocal of the width of the dip structure, the life time for the electron staying at the quasi-bound state becomes shorter when the potential strength increases.

When the Rashba coefficient increases to α = 0.1 with the in-plane magnetic field (gB = 0.02), there is the dip structure in the conductance (Fig. 3.3.2.1(c)). However, when the Rashba coefficient is identical to α = 0.1, the dip structure shifts along the low energy direction with the increasing potential strength less than the dip structure shifts with the increasing potential strength along as the Rashba coefficient α = 0.05 (Fig. 3.3.2.1(b)). In Fig. 3.3.2.1(d), the transport properties are with the Rashba coefficient α = 0.2 in the presence of the magnetic field gB = 0.02. The shift along the low energy direction for the dip structure with the increasing potential strength is less and the width of the dip structure in the conductance is narrower. That is, the life time for the electron staying at the quasi-bound state becomes longer. Therefore, we can deduce that except the potential strength, the life time for the electron staying at the quasi-bound state is also affected by the Rashba effect.

(II) The repulsive scattering potentials

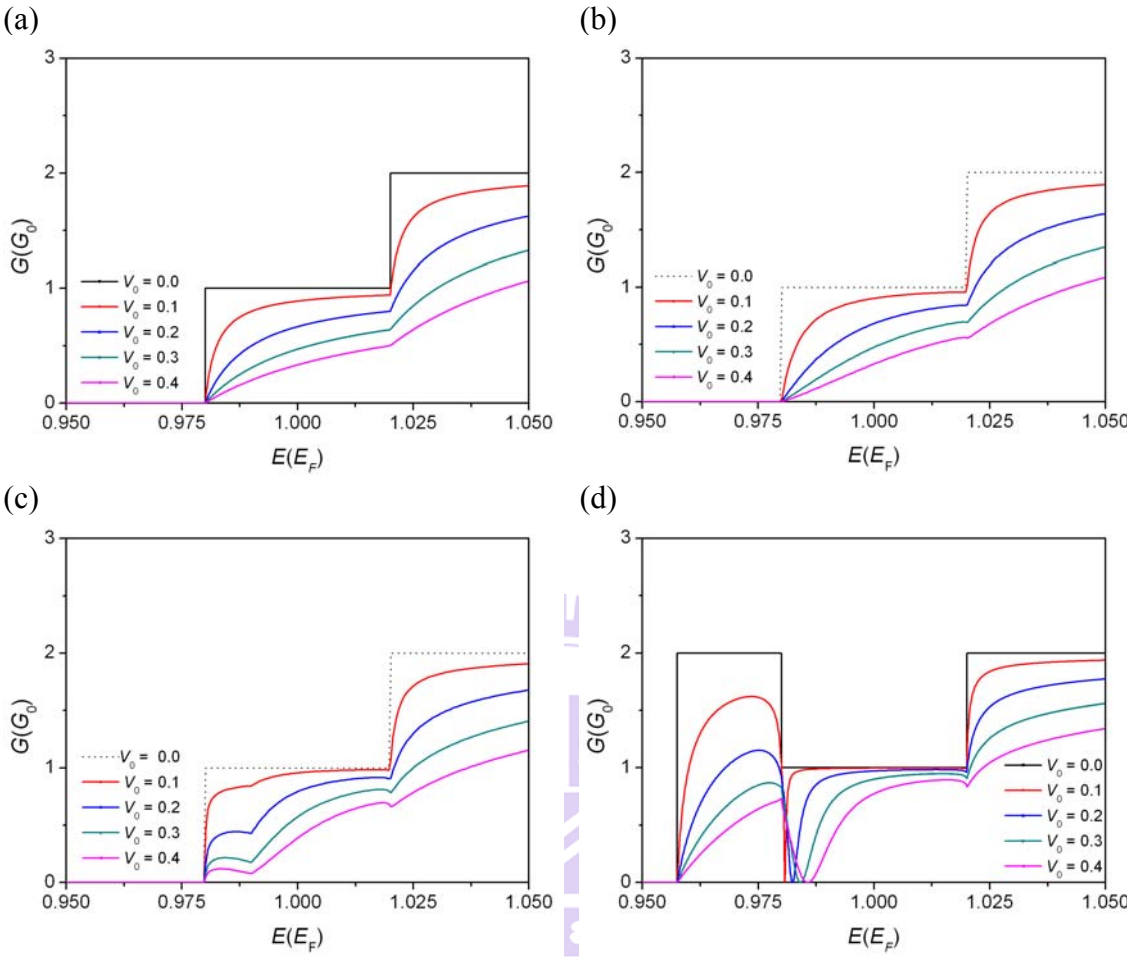

Fig. 3.3.2.2. Conductance (in units of $G_0 = e^2/h$) versus kinetic energy with the repulsive scattering potential in the presence of in-plane magnetic field with different Rashba coefficients: (a) $\alpha = 0.0$, $gB = 0.02$ ($2\alpha^2 < gB$) (b) $\alpha = 0.05$, $gB = 0.02$ ($2\alpha^2 < gB$) (c) $\alpha = 0.1$, $gB = 0.02$ ($2\alpha^2 = gB$) (d) $\alpha = 0.2$, $gB = 0.02$ ($2\alpha^2 > gB$). The Fermi energy $E_F = 66$ meV and the Fermi wave vector $k_F = 2\times10^6$ cm^{-1}. The magnetic field strength is approximately 3T when $gB = 0.02$ ($g_s = -15$ for InAs).

In Fig. 3.3.2.2(a) and (b), we investigate the transport properties in the presence of the in-plane magnetic field ($gB = 0.02$) with applying the repulsive scattering potential. The conductance is suppressed with the increasing strength of the potential. As the Rashba coefficient ($\alpha = 0.1$) satisfies $2\alpha^2 = gB$, the energy dispersion is at the critical point to form a pseudogap and the energy dispersion is vertical splitting (Fig. 3.1.2.1(c)). Hence, in this case, the hole-like quasi-bound state is not well defined. The dip structure in the conductance is not obvious (Fig. 3.3.2.2(c)).

In Fig. 3.3.2.2(d), we show the transport properties in the presence of the in-plane magnetic field $gB = 0.02$ with the Rashba coefficient $\alpha = 0.2$. A dip structure

appears at the hole-like quasi-bound state. The corresponding energy for the hole-like quasi-bound state is above the subband top of the lower branch. Since the repulsive scattering potential will enhance the hole-like quasi-bound state, the dip structure at the hole-like quasi-bound state with the applying repulsive potential is obvious.

Chapter 4 Quantum transport in the presence of Rashba and Dresselhaus spin-orbit interactions with in-plane magnetic field

In this chapter, we use the numerical approach different from the way used in Chapter 3 to investigate how the Rashba spin-orbit interaction, the Dresselhaus spin-orbit interaction an in-plane magnetic field affect the electron transport. We will introduce the system Hamiltonian and analyze the energy spectrum and the wavefunction in the first section. In the second section we will use the Landauer-Buttiker formula by the matching method to calculate the conductance. At last, we will demonstrate the numerical results under different strengths of the spin-orbit interaction and the magnetic field and the gate voltage.

4.1 Theory

In this section, we use the numerical approach to calculate the energy spectrum and the spinor states of the system considering both the Rashba and the Dresselhaus spin-orbit coupling and an in-plane magnetic field.

4.1.1 System and Formulation

The confinement potential defined by the two closed split gates is a transverse hard wall potential, as shown in Fig. 4.1.1.1. The transverse potential is a narrow constriction hence we can neglect the momentum p_y along y direction. Then, the Dresselhaus term Eq. (2.2.3) can be reduced to

$$H_D = \frac{\beta}{\hbar} p_x \sigma_x . \tag{4.1.1.1}$$

Also, the Rashba term can be reduced as mentioned in Ch3. The Hamiltonian of the quantum channel in the presence of the Rashba and the Dresselhaus spin-orbit interaction and the Zeeman effect which is due to an applied magnetic field along x direction is

$$H_0 = \frac{p^2}{2m^*} - \frac{\alpha}{\hbar} p_x \sigma_y + \frac{\beta}{\hbar} p_x \sigma_x + \frac{1}{2} g_s \mu_B B \sigma_x + V_c(y), \tag{4.1.1.2}$$

where α is the Rashba strength, β is the Dresselhaus strength, B is the magnetic field strength and V_c is the confining potential [32]. In the middle of the quantum channel there is a finger gate in forms of delta potential. The total single particle Hamiltonian is

$$H = H_0 + V_s(x), \;\; V_s(x) = V_0 \delta(x) . \tag{4.1.1.3}$$

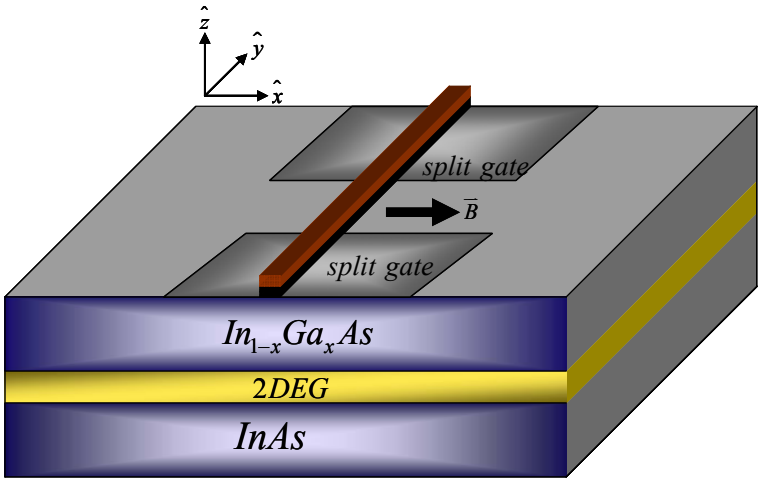

Fig. 4.1.1.1. System picture

For the sake of convenience, the physical quantities that appear in the following equations are dimensionless: length unit $l^* \equiv \frac{1}{k_F}$, energy unit $E^* \equiv \frac{\hbar^2 k_F^2}{2m^*}$, magnetic field unit $B^* \equiv \frac{E^*}{\mu_B}$, the Rashba coefficient unit $\alpha^* = \frac{\hbar^2 k_F}{m^*}$, the Dresselhaus coefficient unit $\beta^* = \frac{\hbar^2 k_F}{m^*}$, the confinement potential in units of Fermi energy $V_c(y) = V(y)E^*$ and defining $g \equiv \frac{1}{2} g_s$. Then, the dimensionless unperturbed Hamiltonian is:

$$H_0 = k^2 - 2\alpha k_x \sigma_y + 2\beta k_x \sigma_x + gB\sigma_x + V_c(y). \tag{4.1.1.4}$$

The unperturbed Hamiltonian can be separated into two different parts:

$$H_0 = H_x^0 + H_y^0 \tag{4.1.1.5}$$

with

$$H_x^0 = k_x^2 - 2\alpha k_x \sigma_y + 2\beta k_x \sigma_x + gB\sigma_x \tag{4.1.1.6}$$

and

$$H_y^0 = k_y^2 + V(y), \tag{4.1.1.7}$$

where

$$V(y) = \begin{cases} 0, & |y| < \frac{d}{2} \\ \infty, & \text{otherwise} \end{cases} \tag{4.1.1.8}$$

is a potential confining the electron in the transverse direction. We suppose that the confining potential with only the lowest occupied subband. The wavefunction of the unperturbed Hamiltonian can be expanded by the spatial wavefunction and spinor state,

$$\Psi(x,y)=\phi_n(y)e^{ik_x x}\chi\,. \tag{4.1.1.9}$$

Since the transverse confining potential is a hard wall potential, the transverse wavefunction will be

$$\phi_n(y)=\sqrt{\frac{\pi}{d}}\sin\left(\frac{n\pi}{d}y\right), \tag{4.1.1.10}$$

the subband energy will be

$$\varepsilon_n=\left(\frac{n\pi}{d}\right)^2. \tag{4.1.1.11}$$

Here, we only consider the lowest occupied subband. Namely, n is equal to 1. Substituting the transverse wavefunction and the subband energy into (4.1.1.5) and (4.1.1.9) obtain:

$$\varepsilon_n\Psi+\left(k_x{}^2-2\alpha k_x\sigma_y+2\beta k_x\sigma_x+gB\sigma_x\right)\Psi=E\Psi\,. \tag{4.1.1.12}$$

Expanding Eq. (4.1.1.12) with the Pauli matrices obtains

$$\begin{pmatrix} k_x^2 & gB+2\beta k_x+i2\alpha k_x \\ gB+2\beta k_x-i2\alpha k_x & k_x^2 \end{pmatrix}\chi=(E-\varepsilon_n)\chi\,. \tag{4.1.1.13}$$

The eigen-energy can be obtained by solving the above eigen-value problem. The energy is

$$E_n^{\pm}=\varepsilon_n+k_x^2\pm\sqrt{(2\beta k_x+gB)^2+(2\alpha k_x)^2}\,. \tag{4.1.1.14}$$

For an ideal wire without scattering potential, it is convenient to use Eq. (4.1.1.14) to obtain energy spectrum as a function of the real wave vector for propagating modes.

4.1.2 The Dresselhaus effects

(I) With Rashba spin-orbit interaction and in-plane magnetic field

For understanding how the Dresselhaus effect would affect the energy spectrum, in the presence of the Rashba spin-orbit interaction and in-plane magnetic field. Below, we fix the Rashba coefficient α = 0.2 and the Zeeman parameter gB = 0.02, and then we tune the Dresselhaus coefficient β from weak to strong: We shall consider four cases: β = 0.0, 0.1 ($\beta<\alpha$), 0.2 ($\alpha=\beta$), and 0.3 ($\beta>\alpha$), as shown in Fig. 4.1.2.1.

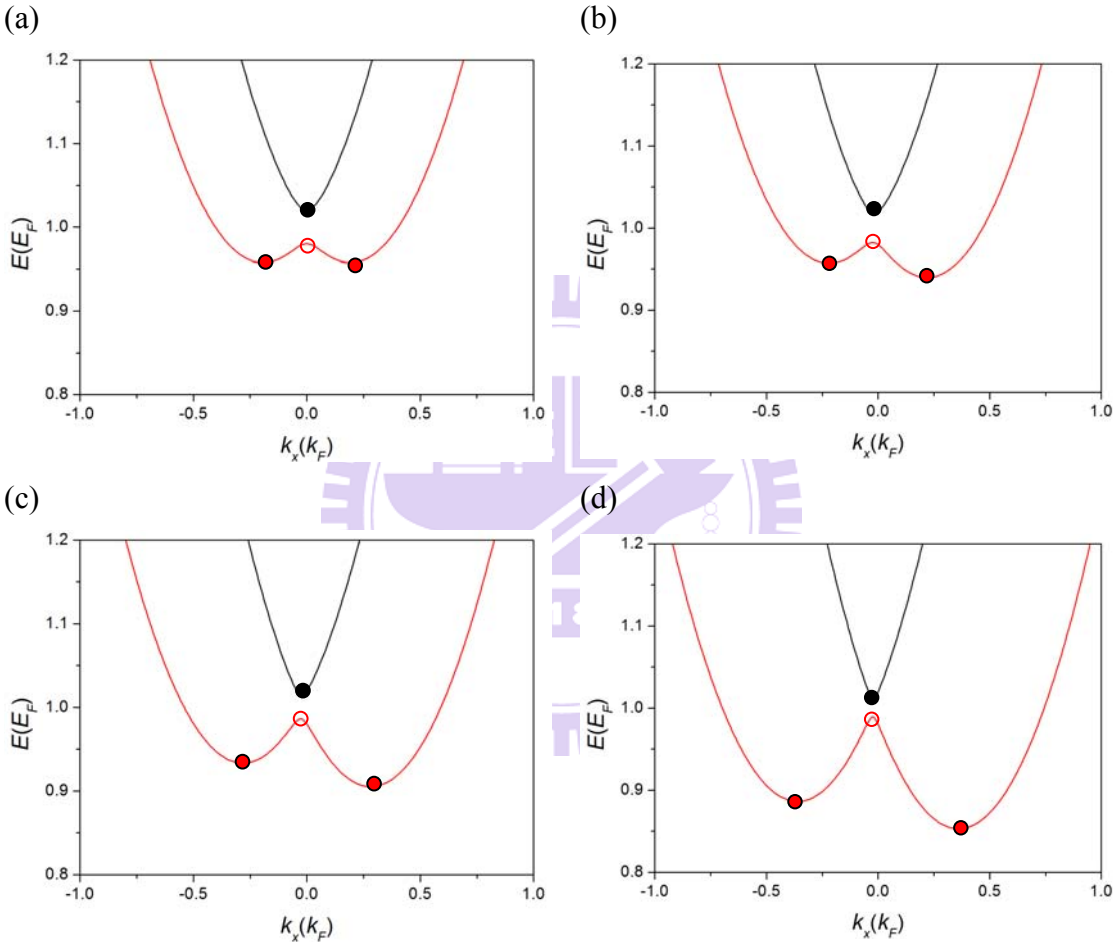

Fig. 4.1.2.1. Energy spectrum versus wave number in the presence of the Rashba spin-orbit interaction and in-plane magnetic field with different Dresselhaus coefficients: (a) α = 0.2, β = 0.0, gB = 0.02 (b) α = 0.2, β = 0.1, gB = 0.02 (c) α = 0.2, β = 0.2, gB = 0.02 (d) α = 0.2, β = 0.3, gB = 0.02. The Fermi energy E_F = 66 meV and the Fermi eave vector $k_F = 2\times10^6$ cm^{-1}. The magnetic field strength is approximately 3T when gB = 0.02 (g_s = −15 for InAs). The black and red curves indicate the plus (σ = +) and minus (σ = −) spin branches, respectively. The black dot and the red dot correspond to the local minima of plus and minus branches at the subband bottoms, denoted by P_{b+} and P_{b-}. The red circle stands for the local maxima of the minus branch at the subband top, denoted by P_{t-}.

In general, there are four extreme values in the energy dispersion. For convenience, we define $P_{b\sigma} = (k_{b\sigma}, E_{b\sigma})$ and $P_{t\sigma} = (k_{t\sigma}, E_{t\sigma})$ to denote the extreme values of the energy dispersion at the subband bottom (b) and subband top (t), respectively. We also define $\Delta E_g \equiv E_{b+} - E_{t-}$ and $\Delta E_b \equiv E_{b+} - E_{b-}$ to represent the pseudo-gap and the branch level spacing for a given subband, respectively. In addition, $\sigma = +, -$ represents the upper branch and lower branch, respectively. In Fig. 4.1.2.1 (a), we show the spin-splitting energy dispersion with the Rashba and the Zeeman effects but without the Dresselhaus effect. The energy dispersion we discussed before in Ch 3. We mentioned before that the pseudo-gap is identical to $\Delta E_Z = 2gB$, that is, $\Delta E_Z = 2gB = 0.04$. In the presence of the Dresselhaus effect ($\beta = 0.1$) (Fig. 4.1.2.1(b)), the local maximum at the lower branch is $P_{t-} = (k_{t-}, E_{t-}) = (-0.024, 0.9825)$ and the local minimum at the upper branch is $P_{b+} = (k_{b+}, E_{b+}) = (-0.02, 1.0183)$, that is, $\Delta E_g = 0.0358$. At the lower branch, there are two local minimums $P_{b-,1} = (k_{b-,1}, E_{b-,1}) = (-0.22, 0.9572)$ and $P_{b-,2} = (k_{b-,2}, E_{b-,2}) = (0.22, 0.9396)$. These two local energy minimums at the lower branch are in different energy values therefore the energy spectrum is asymmetry. As the strength of the Dresselhaus effect increases ($\beta = 0.2$) (Fig. 4.1.2.1(c)), these local extreme values are $P_{t-} = (k_{t-}, E_{t-}) = (-0.0281, 0.9865)$, $P_{b+} = (k_{b+}, E_{b+}) = (-0.02, 1.0148)$, $P_{b-,1} = (k_{b-,1}, E_{b-,1}) = (-0.28, 0.9335)$ and $P_{b-,2} = (k_{b-,2}, E_{b-,2}) = (0.28, 0.9053)$. In this case, $\Delta E_g = 0.0283$. In Fig. 4.1.2.1(d), the strength of the Dresselhaus effect is $\beta = 0.3$. The local energy minimum at the upper branch is at $P_{b+} = (k_{b+}, E_{b+}) = (-0.02, 1.0117)$. At the lower branch the local energy extreme values are at $P_{t-} = (k_{t-}, E_{t-}) = (-0.024, 0.9891)$, $P_{b-,1} = (k_{b-,1}, E_{b-,1}) = (-0.36, 0.8864)$ and $P_{b-,2} = (k_{b-,2}, E_{b-,2}) = (0.356, 0.8531)$ and $\Delta E_g = 0.0226$. Hence, when we consider the Dresselhaus effect in the presence of the Rashba and in-plane magnetic field, the pseudo-gap (ΔE_g) is smaller than ΔE_Z and the pseudo-gap ΔE_g decreases from 0.0358 to 0.0226 with the increasing Dresselhaus effect.

(I) Without in-plane magnetic field

For analyzing the energy dispersion, we have to calculate the group velocity, expressed as the analytical form

$$v_g = \frac{dE_n^{\pm}}{dk_x} = 2k_x \pm \frac{4\alpha^2 k_x + 2\beta\left(2\beta k_x + gB\right)}{\sqrt{\left(2\alpha k_x\right)^2 + \left(2\beta k_x + gB\right)^2}}. \qquad (4.1.2.1)$$

We have investigated how the Dresselhaus effect would influence the energy dispersion in the presence of the Rashba spin-orbit interaction and an applied in-plane magnetic field. Now, we turn off the in-plane magnetic field ($B = 0$) but still consider the Rashba spin-orbit interaction to see what affects the Dresselhaus effect would

bring about. In this case, we can take limit $B = 0$ from the group velocity. This yields the result

$$v_g\left(B=0\right)=\frac{dE_n^{\pm}}{dk_x}=2k_x\pm 2\sqrt{\alpha^2+\beta^2}\ . \tag{4.1.2.2}$$

As the group velocity equals to zero, we can obtain the analytical solutions about the local extreme values. These extreme values occurs at

$$k_x^{\sigma}\left(v_g=0\right)=\begin{cases}-\sqrt{\alpha^2+\beta^2}, & \sigma=+\\ +\sqrt{\alpha^2+\beta^2}, & \sigma=-\end{cases}. \tag{4.1.2.3}$$

When the Dresselhaus coefficient is equal to zero, then the extreme values are at

$$k_x^{\sigma}\left(v_g=0\right)=\begin{cases}-\alpha, & \sigma=+\\ +\alpha, & \sigma=-\end{cases}. \tag{4.1.2.4}$$

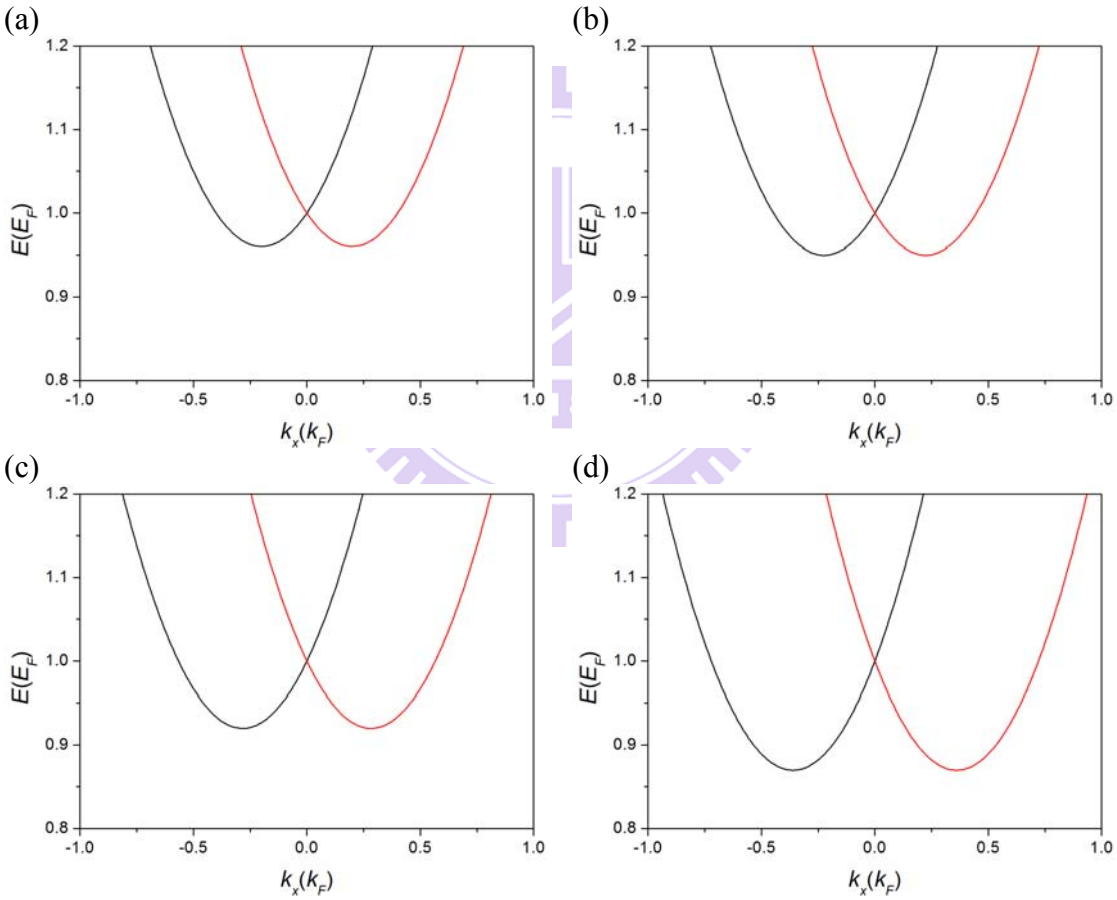

Fig. 4.1.2.2. Energy spectrum versus wave number in the presence of the Rashba, the Dresselhaus and the Zeeman effects with different Dresselhaus strength. (a) $\alpha = 0.2$, $\beta = 0.0$, $gB = 0.0$ (b) $\alpha = 0.2$, $\beta = 0.1$, $gB = 0.0$ (c) $\alpha = 0.2$, $\beta = 0.2$, $gB = 0.0$ (a) $\alpha = 0.2$, $\beta = 0.3$, $gB = 0.0$. The Fermi energy $E_F = 66$ meV and the Fermi eave vector $k_F = 2\times 10^6$ cm^{-1}. The black and red curves indicate the plus ($\sigma = +$) and minus ($\sigma = -$) spin branches, respectively.

In Fig. 4.1.2.2(a), in the presence of the Rashba spin-orbit interaction $\alpha = 0.2$ the energy spectrum is lateral spin-splitting and the local extreme values are at $k_x = -0.2$. 0.2 (Eq. 4.1.2.4) and the corresponding energy is $E = 0.96$. In Fig. 4.1.2.2(b), when we consider the Dresselhaus effect $\beta = 0.1$ in the presence of the Rashba spin-orbit interaction, the local extreme values are at $k_x = -0.2236$, 0.2236 (Eq. 4.1.2.3) and the corresponding energy is $E = 0.95$. As the Dresselhaus coefficient becomes $\beta = 0.2$, the local extreme values are at $k_x = -0.2828$, 0.2828 (Eq. 4.1.2.3) and the corresponding energy is $E = 0.92$, as shown in Fig. 4.1.2.2(c). In Fig. 4.1.2.2(d), the Dresselhaus coefficient increases to $\beta = 0.3$, the local extreme values are at $k_x = -0.3606$, 0.3606 (Eq. 4.1.2.3) and the corresponding energy is $E = 0.87$. From these figures, we find that as the Dresselhaus effect gradually increases, the energy spectrum is still lateral splitting and symmetry but the local extreme energy values decreases from 0.95 to 0.87.

4.1.3 The Rashba-Dresselhaus effects

After investigating how the Dresselhaus effect would influence the energy dispersion, we are going to tune the strength of the Rashba and the Dresselhaus effects and see how the spin-orbit interactions would affect the energy spectrum. The different ratio between the spin-orbit interactions and the Zeeman effect will result in different energy spectrums. We categorize them into three cases: (1) $\alpha = \beta < gB$, (2) $\alpha = \beta = gB$, (3) $\alpha = \beta > gB$.

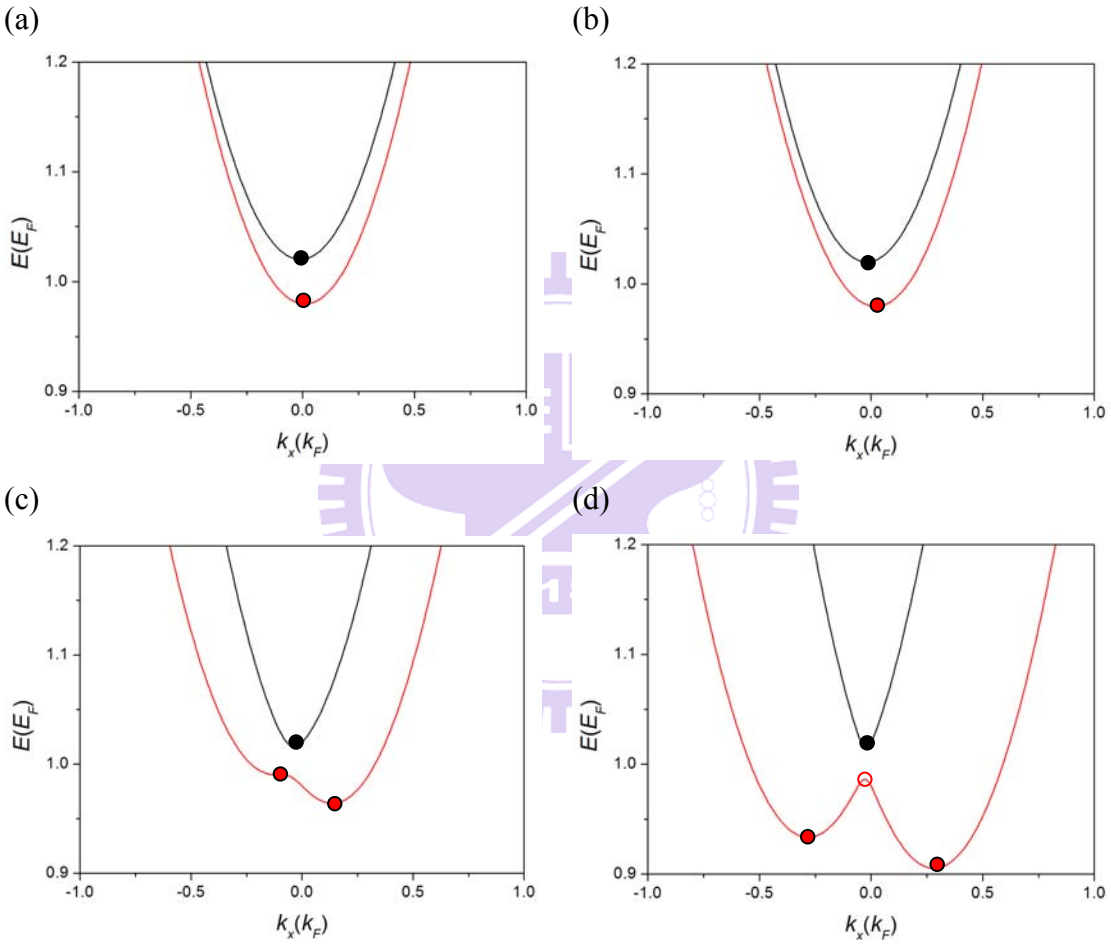

Fig. 4.1.3.1. Energy spectrum versus wave number in the presence of in-plane magnetic field with different Rashba and Dresselhaus coefficients. (a) $\alpha = \beta = 0.01$, $gB = 0.02$ (b) $\alpha = \beta = gB = 0.02$ (c) $\alpha = \beta = 0.1$, $gB = 0.02$ (d) $\alpha = \beta = 0.2$, $gB = 0.02$. The Fermi energy E_F = 66 meV and the Fermi eave vector $k_F = 2\times10^6$ cm^{-1}. The magnetic field strength is approximately 3T when $gB = 0.02$ ($g_s = -15$ for InAs). The black and red curves indicate the plus ($\sigma = +$) and minus ($\sigma = -$) spin branches, respectively. The black dot and the red dot correspond to the local minima of plus and minus branches at the subband bottoms, denoted by P_{b+} and P_{b-}. The red circle stands for the local maxima of the minus branch at the subband top, denoted by P_{t-}.

It is shown in Fig. 4.1.3.1(a), the Rashba is identical to the Dresselhaus but substantially less than the Zeeman effects. It breaks the spin degeneracy of the system and results in two vertically separated spin-splitting subbands. The energy extreme values are at $P_{b+}=(k_{b+}, E_{b+})=(-0.008, 1.0199)$ and $P_{b-}=(k_{b-}, E_{b-})=(0.008, 0.9799)$, that is, $\triangle E_b=0.04$. As the Rashba and the Dresselhaus are identical to the Zeeman effects (Fig. 4.1.3.1(b)), it is vertical spin-splitting. The energy extreme values are at $P_{b+,1}=(k_{b+,1}, E_{b+,1})=(-0.02, 1.0196)$ and $P_{b-,2}=(k_{b-,2}, E_{b-,2})=(0.02, 0.9796)$, that is, $\triangle E_b=0.04$. Therefore, we can deduce that when the Rashba and the Dresselhaus effects in the presence of in-plane magnetic field are small, there is no affect in the branch level spacing for a given subband $\triangle E_b=\triangle E_z=0.04$. In Fig. 4.1.3.1 (c) and (d), the spin-orbit interactions are larger than the Zeeman effect. As the Dresselhaus and the Rashba coefficients are identical to 0.1 ($\alpha=\beta=0.1$), there are two extreme values $P_{b-,1}=(k_{b-,1}, E_{b-,1})=(-0.1002, 0.99)$ and $P_{b-,2}=(k_{b-,2}, E_{b-,2})=(0.136, 0.964)$ at the lower branch. However when the Dresselhaus and the Rashba coefficients are identical to 0.2 ($\alpha=\beta=0.2$), there are three extreme values $P_{b-,1}=(k_{b+,1}, E_{b+,1})=(-0.28, 0.9335)$, $P_{b-,2}=(k_{b-,2}, E_{b-,2})=(0.28, 0.9053)$ and $P_{t-}=(k_{t-}, E_{t-})=(-0.02, 0.986)$ at the lower branch. Hence, we know that under the applying fixed in-plane magnetic field there is a critical value for the Rashba and Dresselhaus coefficients. When the Rashba and the Dresselhaus are smaller than the critical value ($\alpha=\beta<0.1$), there is only an extreme value at the lower band. However, if the Rashba and the Dresselhaus are larger than the critical value ($\alpha=\beta>0.1$), there are two local minimums and one local maximum at the lower branch. In Fig. 4.1.3.1 (c), the extreme value at the upper branch is $P_{b-}=(k_{b-}, E_{b-})=(-0.0361, 1.016)$. Therefore, the branch level spacing for a given subband is identical to 0.026 ($\triangle E_b=0.026$) and smaller than the pseudo-gap ($\triangle E_z=0.04$) considering the Rashba spin-orbit interaction an in-plane magnetic field. In Fig. 4.1.3.1 (d) the band bottom at the upper branch is at $P_{b-}=(k_{b-}, E_{b-})=(-0.02, 1.015)$. Hence, in mediate energy regime the pseudo-gap is identical to 0.029, $\triangle E_g=0.029$, and smaller than $\triangle E_z=0.04$.

From the above four cases, we know that the subband splitting depends on the ratio between the Rashba, Dresselhaus and the Zeeman effects. When the Rashba and the Dresselhaus coefficients are smaller than the critical value, the subbands are vertical splitting. However, as Rashba and the Dresselhaus coefficients are larger than the critical value, the magneto-spin-orbit pseudo-gap will exist.

4.1.4 The Zeeman effects

The strength of the in-plane magnetic field along ***x*** direction would influence the energy dispersion. The magnetic field strength is approximately 15T when $gB = 0.1$ ($g_s = -15$ for InAs).

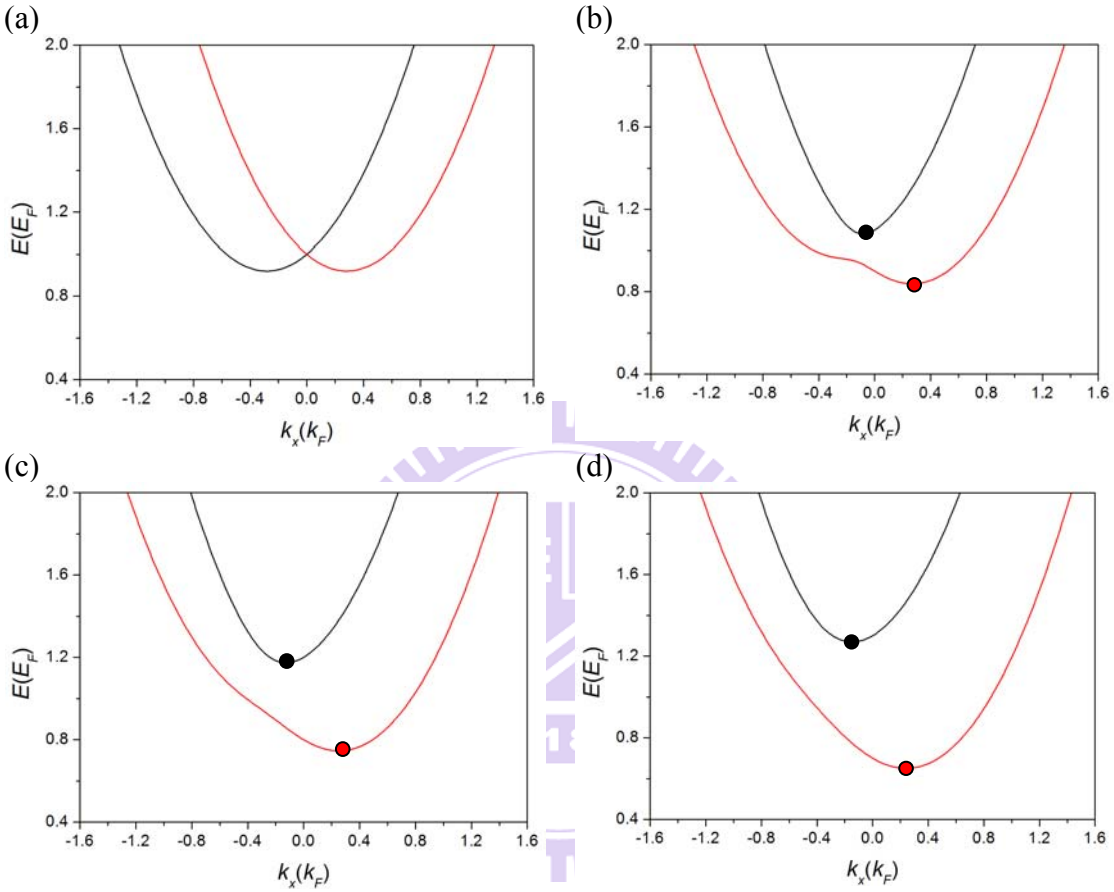

Fig. 4.1.4.1. Energy spectrum versus wave number in the presence of the Rashba, the Dresselhaus and the Zeeman effects with different Dresselhaus strength. (a) $\alpha = \beta = 0.2$, $gB = 0.0$ (b) $\alpha = \beta = 0.2$, $gB = 0.1$ (c) $\alpha = \beta = 0.2$, $gB = 0.2$ (d) $\alpha = \beta = 0.2$, $gB = 0.3$. The Fermi energy $E_F = 66$ meV and the Fermi wave vector $k_F = 2\times10^6$ cm^{-1}. The magnetic field strength is approximately 15T when $gB = 0.1$ ($g_s = -15$ for InAs). The black and red curves indicate the plus ($\sigma = +$) and minus ($\sigma = -$) spin branches, respectively. The black dot and the red dot correspond to the local minima of plus and minus branches at the subband bottoms, denoted by P_{b+} and P_{b-}.

In Fig. 4.1.4.1 we tune the in-plane magnetic field from weak to strong with the fixed Rashba and Dresselhaus spin-orbit interactions. In Fig. 4.1.4.1(a), we consider the Rashba and the Dresselhaus effects without the magnetic field, and then it causes lateral energy splitting as we mentioned before. When the magnetic field becomes stronger ($gB = 0.1$), the energy spectrum is vertical splitting (Fig. 4.1.4.1(b)). At the

lower branch the local minimum is at $P_{b-} = (k_{b-}, E_{b-}) = (0.008, 0.9799)$ and at the upper branch the local minimum is at $P_{b+} = (k_{b+}, E_{b+}) = (-0.008, 1.0199)$. Then, $\Delta E_b = 0.04$. As the Zeeman coefficient is identical to the Rashba and the Dresselhaus coefficients ($\alpha = \beta = gB = 0.2$), the energy spectrum is also vertical splitting (Fig. 4.1.4.1(c)). The extreme values are at $P_{b-} = (k_{b-}, E_{b-}) = (0.2525, 0.7463)$ and $P_{b+} = (k_{b+}, E_{b+}) = (-0.1242, 1.1737)$. The branch level spacing for a given subband is 0.4274, $\Delta E_b = 0.4274$. When the Zeeman effect is larger than the Rashba and the Dresselhaus spin-orbit interactions ($\alpha = \beta = 0.2 < gB = 0.3$) (Fig. 4.1.4.1(d)), the extreme values are at $P_{b-} = (k_{b-}, E_{b-}) = (0.2445, 0.6501)$, $P_{b+} = (k_{b+}, E_{b+}) = (-0.14, 1.2699)$ and the branch level spacing for a given subband is 0.6198, $\Delta E_b = 0.6198$. In conclusion, as the in-plane magnetic field gradually increases, the branch level spacing for a given subband ΔE_b increases from 0.04 to 0.6198.

Spin orientation

For investigating the spin orientation in the presence of the Rashba, Dresselhaus spin-orbit interactions and the in-plane magnetic field, we calculate the effective magnetic field for these spin-orbit interactions and the Zeeman effect. The dimensionless Hamiltonian for an electron in the presence of the magnetic field can be expressed as:

$$H = \vec{\sigma} \cdot \vec{B}, \tag{4.1.4.1}$$

where B is dimensionless ($B^* = E^*/\mu_B$). Hence, when the above equation is identical to the Rashba term,

$$-2\alpha k_x \sigma_y = \vec{\sigma} \cdot \vec{B} = B_y \sigma_y, \tag{4.1.4.2}$$

we can obtain the effective magnetic field for the Rashba spin-orbit interaction

$$\overrightarrow{B_R} = -2\alpha k_x \hat{y}. \tag{4.1.4.3}$$

In the same way, we can obtain the effective magnetic field for the Dresselhaus spin-orbit interaction and the Zeeman effect:

$$\overrightarrow{B_D} = 2\beta k_x \hat{x}, \text{ and} \tag{4.1.4.4}$$

$$\overrightarrow{B_Z} = gB\hat{x}. \tag{4.1.4.5}$$

Then, the effective magnetic field of the system can be expressed as:

$$\overrightarrow{B_{eff}} = \left(B_D + B_Z\right)\hat{x} + B_R\hat{y} = \left(2\beta k_x + gB\right)\hat{x} - 2\alpha k_x \hat{y}. \tag{4.1.4.6}$$

In order to achieve equilibrium, the spin orientation of the electron in the presence of the magnetic field tends to be opposite to the direction of the magnetic field.

Therefore, the spin orientation of the electron at the plus branch is aligned in the direction of the effective magnetic field. However, the spin orientation of the electron at the minus branch will be opposite to the direction of the effective magnetic field. We can express the spin orientation for the electrons at the plus branch as:

$$\overrightarrow{S_\sigma} = \frac{(2\beta k_x + gB)}{\sqrt{(2\beta k_x + gB)^2 + (2\alpha k_x)^2}}\hat{x} - \frac{2\alpha k_x}{\sqrt{(2\beta k_x + gB)^2 + (2\alpha k_x)^2}}\hat{y}, \quad \sigma = +. \tag{4.1.4.7}$$

and the spin orientation for the electrons at the minus branch is:

$$\overrightarrow{S_\sigma} = -\frac{(2\beta k_x + gB)}{\sqrt{(2\beta k_x + gB)^2 + (2\alpha k_x)^2}}\hat{x} + \frac{2\alpha k_x}{\sqrt{(2\beta k_x + gB)^2 + (2\alpha k_x)^2}}\hat{y}, \quad \sigma = -. \tag{4.1.4.8}$$

Below, we show the energy spectrum with the spin orientation in the presence of the Rashba and the Dresselhaus spin-orbit interactions with different Zeeman effects.

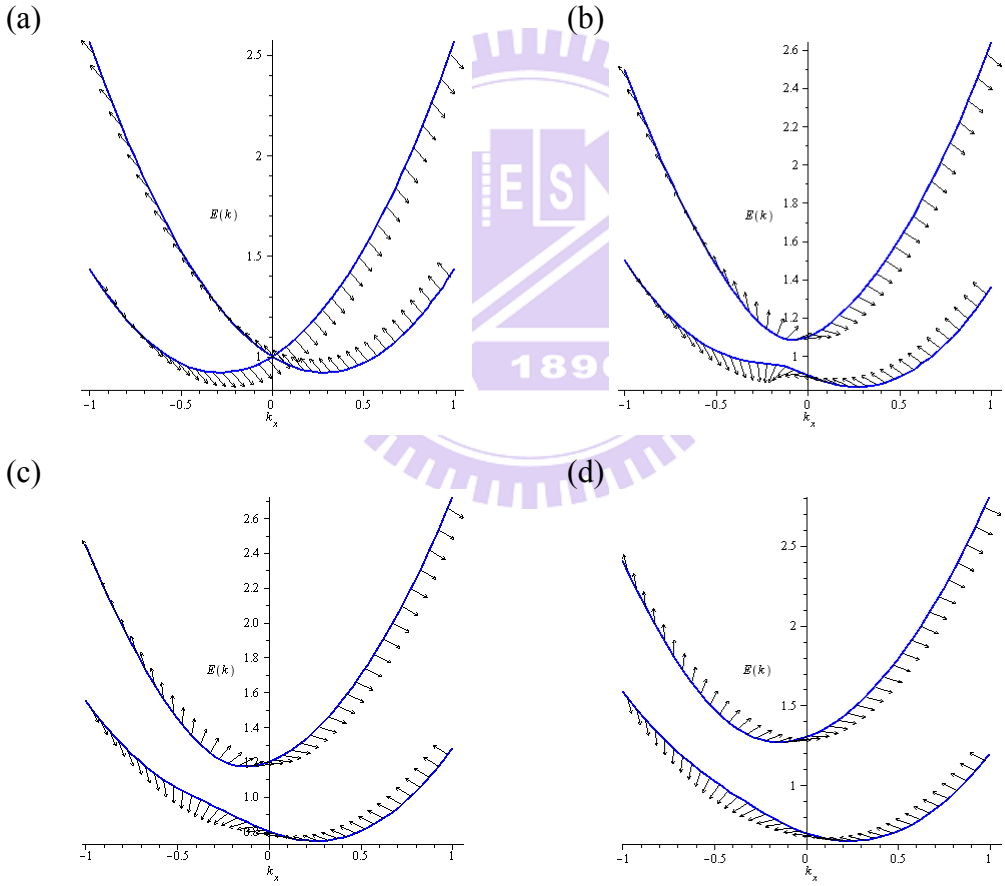

Fig. 4.1.4.2. Energy dispersion with spin orientation illustrated by the arrows in the presence of the fixed Rashba and Dresselhaus spin-orbit interactions with different Zeeman coefficients. (a) $\alpha = \beta = 0.2$, $gB = 0.0$ (b) $\alpha = \beta = 0.2$, $gB = 0.1$ (c) $\alpha = \beta = 0.2$, $gB = 0.2$ (d) $\alpha = \beta = 0.2$, $gB = 0.3$. The magnetic field strength is approximately 15T when $gB = 0.1$ ($g_s = -15$ for InAs).

In Fig. 4.1.4.2 (a), we turn off the magnetic field and only consider the Rashba and the Dresselhaus spin-orbit interactions. The spin orientation is at 45° between the ***x*** and ***y*** axes. When $\alpha = \beta$, spin is a good quantum number and D'yakonov-Perel' spin relaxation is absent [10] (Spin relaxation in disordered two-dimensional electron gas is dominated by the D'yakonov-Perel' mechanism.). Recently, in order to achieve $\alpha = \beta$ there has been much effort into this direction both the theoretically [10] with new device proposals and experimentally [33]. When the in-plane magnetic field increases, the angle between the ***x*** axis and the spin orientation is decreasing. Since the effective magnetic field of the Rashba and the Dresselhaus spin-orbit interactions are dependant of the linear k_x, at $k_x = 0$ the spin orientation is always along the ***x*** direction.

4.1.5 Complex energy dispersion

To perform numerical calculation for computing the spin-resolved conductance in the presence of arbitrary scattering potentials involving the coupling of propagating and evanescent modes [29], we start from rearranging the Eq. (4.1.1.14) into a polynomial equation

$$k_x^4 + \left[-2\left(E-\varepsilon_n\right)-(2\beta)^2-\left(2\alpha\right)^2\right]k_x^2 - 4\beta gBk_x + \left(E-\varepsilon_n\right)^2 - \left(gB\right)^2 = 0\,. \quad (4.1.5.1)$$

The polynomial problem can be solved by calling the DZPOCC subroutine from the IMSL library. For a given energy, this subroutine can find the corresponding four complex roots k_x. In this way, we can get the propagating modes and evanescent modes simultaneously, as shown in Fig. 4.1.5.1.

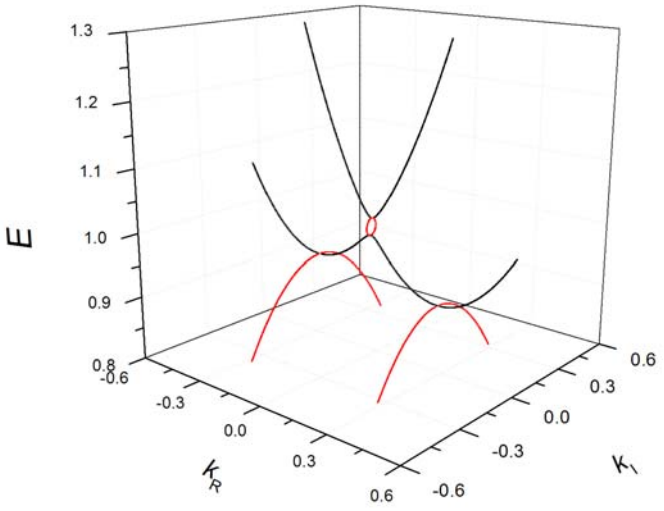

Fig. 4.1.5.1. 3D Energy dispersion in the presence of the spin-orbit interactions and in-plane magnetic field ($\alpha = \beta = 0.2$, $gB = 0.02$). k_R and k_I represent, respectively, the real part and the imaginary part of the wave number ($k = k_R + k_I$). The black solid line represents the propagating modes and the red solid line represents the evanescent modes. The Fermi energy E_F = 66 meV and the Fermi wave vector $k_F = 2\times10^6$ cm^{-1}.

4.2 Spin-resolved transport theory

In this section, we use the numerical method to calculate the wavefunction and derive the transport formulation. For the electron incident along ***x*** at a given energy, we use k_σ (q_σ) to denote the wavevector of right-going (left-going) modes at the spin branch σ, where the dummy index σ could be the outer or the inner modes, denoted by 1 or 2, as shown in Fig. 3.2.1. Then, the scattering wavefunction is of the form

$$\psi(x) = e^{ik_\sigma x}\chi(k_\sigma) + \sum_\sigma r_\sigma e^{iq_\sigma x}\chi(q_\sigma), x < 0\,, \tag{4.2.1}$$

and

$$\psi(x) = \sum_\sigma t_\sigma e^{ik_\sigma x}\chi(k_\sigma), x > 0\,, \tag{4.2.2}$$

where the $\chi(k_\sigma)$ is the spinor states. In section 4.1, we have already calculated the wave vectors for a given energy. In this section, we can substitute the corresponding wave vectors of the given energy into the eigen-value problem (Eq. 4.1.1.13) and use the DEVCCG subroutine in IMSL to solve this eigenvector problem. Solving the eigen-value problem can obtain two eigenvalues and two spinor states. We choose the one of eigenvalues close to the given energy and the corresponding spinor states. Namely, we have the spinor states and wave vectors for a given energy. The wavevectors and the spinor states can be classified by the group velocity. The Eq. (4.2.1) can be expressed explicitly in the form:

$$\psi(x) \equiv e^{ik_\sigma x}\begin{bmatrix} a_\sigma \\ b_\sigma \end{bmatrix} + r_\sigma e^{iq_\sigma x}\begin{bmatrix} c_\sigma \\ d_\sigma \end{bmatrix} + r_{\bar\sigma} e^{iq_{\bar\sigma} x}\begin{bmatrix} c_{\bar\sigma} \\ d_{\bar\sigma} \end{bmatrix}, \quad x < 0\,, \tag{4.2.3}$$

$$\psi(x) \equiv t_\sigma \cdot e^{ik_\sigma x}\begin{bmatrix} a_\sigma \\ b_\sigma \end{bmatrix} + t_{\bar\sigma} e^{ik_{\bar\sigma} x}\begin{bmatrix} a_{\bar\sigma} \\ b_{\bar\sigma} \end{bmatrix}, \quad x > 0\,. \tag{4.2.4}$$

Here k_σ and $k_{\bar\sigma}$ represent the right going mode, q_σ and $q_{\bar\sigma}$ denote the left going mode,

$$\begin{bmatrix} a_\sigma \\ b_\sigma \end{bmatrix} \text{ and } \begin{bmatrix} a_{\bar\sigma} \\ b_{\bar\sigma} \end{bmatrix} \tag{4.2.5}$$

denote the spinor states of the right-going modes and

$$\begin{bmatrix} c_\sigma \\ d_\sigma \end{bmatrix} \text{ and } \begin{bmatrix} c_{\bar\sigma} \\ d_{\bar\sigma} \end{bmatrix} \tag{4.2.6}$$

represent the spinor states of the left-going modes.

In order to calculate the conductance, we use the matching method to get the

transmission. The wavefunction $\psi(x)$ is continuous at $x = 0$

$$\psi\left(x=0^{-}\right)=\psi\left(x=0^{+}\right) \tag{4.2.7}$$

and the derivative of $\psi(x)$ satisfies

$$\psi'\left(x=0^{-}\right)=\psi'\left(x=0^{+}\right)-V_0\psi\left(x=0^{+}\right). \tag{4.2.8}$$

After the linear algebra, we can get the four equations relating the reflection coefficients r_σ, $r_{\bar{\sigma}}$ and the transmission coefficients t_σ, $t_{\bar{\sigma}}$.

1. $a_\sigma + r_\sigma c_\sigma + r_{\bar{\sigma}} c_{\bar{\sigma}} = t_\sigma a_\sigma + t_{\bar{\sigma}} a_{\bar{\sigma}}$, (4.2.9)
2. $b_\sigma + r_\sigma d_\sigma + r_{\bar{\sigma}} d_{\bar{\sigma}} = t_\sigma b_\sigma + t_{\bar{\sigma}} b_{\bar{\sigma}}$, (4.2.10)
3. $k_\sigma a_\sigma + r_\sigma q_\sigma c_\sigma + r_{\bar{\sigma}} q_{\bar{\sigma}} c_{\bar{\sigma}} = t_\sigma (k_\sigma + iV_0) a_\sigma + t_{\bar{\sigma}} (k_{\bar{\sigma}} + iV_0) a_{\bar{\sigma}}$, (4.2.11)
4. $k_\sigma b_\sigma + r_\sigma q_\sigma d_\sigma + r_{\bar{\sigma}} q_{\bar{\sigma}} d_{\bar{\sigma}} = t_\sigma (k_\sigma + iV_0) b_\sigma + t_{\bar{\sigma}} (k_{\bar{\sigma}} + iV_0) b_{\bar{\sigma}}$. (4.2.12)

Establishing a matrix form from the four simultaneous equations gets

$$\begin{bmatrix} -c_\sigma & -c_{\bar{\sigma}} & a_\sigma & a_{\bar{\sigma}} \\ -d_\sigma & -d_{\bar{\sigma}} & b_\sigma & b_{\bar{\sigma}} \\ -q_\sigma c_\sigma & -q_{\bar{\sigma}} c_{\bar{\sigma}} & (k_\sigma + iV_0) a_\sigma & (k_{\bar{\sigma}} + iV_0) a_{\bar{\sigma}} \\ -q_\sigma d_\sigma & -q_{\bar{\sigma}} d_{\bar{\sigma}} & (k_\sigma + iV_0) b_\sigma & (k_{\bar{\sigma}} + iV_0) b_{\bar{\sigma}} \end{bmatrix} \begin{bmatrix} r_\sigma \\ r_{\bar{\sigma}} \\ t_\sigma \\ t_{\bar{\sigma}} \end{bmatrix} = \begin{bmatrix} a_\sigma \\ b_\sigma \\ k_\sigma a_\sigma \\ k_\sigma b_\sigma \end{bmatrix} \quad (\mathbf{AX} = \mathbf{B}). \tag{4.2.13}$$

Substituting the modes and the corresponding spinor states into the matrix elements and calling the DLSACG subroutine in IMSL to obtain the inverse matrix of **A** and operate $\mathbf{A}^{-1}$ on matrix **B** will finally obtain the transmission coefficients t_σ, $t_{\bar{\sigma}}$. (The DLSACG subroutine can solve a complex general system of linear equations **AX** = **B** (**A**, **B** are already known).)

At the zero temperature, the conductance is given by

$$G = \sum_{\sigma_L, \sigma_R} \left[\frac{e^2}{h} \left| t_{\sigma_L, \sigma_R} \right|^2 \frac{\upsilon_{\sigma_R}}{\upsilon_{\sigma_L}} \right], \tag{4.2.14}$$

where σ_R, σ_L denote the branch index, and υ_{σ_R}, υ_{σ_L} represent the group velocity at the corresponding mode. As we mentioned before in Ch3, during the scattering process, the electrons may be incident from a right-going mode k_σ but transmitted at another right-going mode $k_{\bar{\sigma}}$ or transmitted at the same mode k_σ. In the high energy regime, the total transmission is

$$T = \sum_{\sigma_L, \sigma_R} \left| t_{\sigma_L, \sigma_R} \right|^2 = \left| t_{-,-} \right|^2 + \left| t_{-,+} \right|^2 + \left| t_{+,+} \right|^2 + \left| t_{+,-} \right|^2. \tag{4.2.16}$$

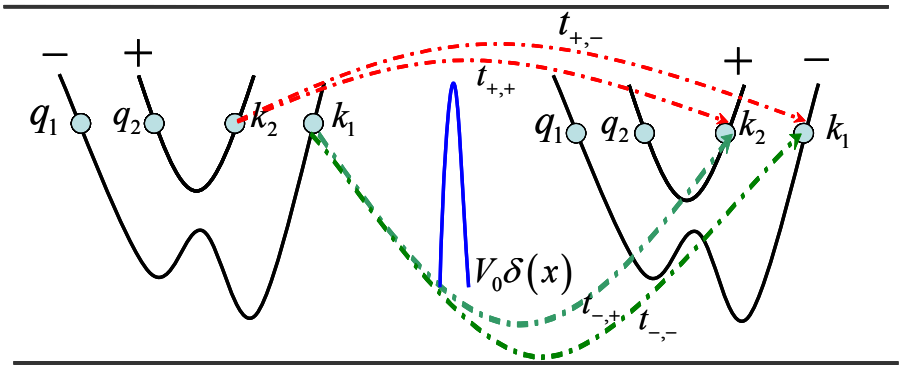

Fig. 4.2.1. The scattering process in the high energy regime.

4.3 Numerical results

The numerical calculation presented below are carried out under the assumption that the electron effective mass $m^* = 0.023\ m_0$, which is appropriate to the InAs-based semiconductors. The typical electron density is n ~ 10^{12} cm^{-2}. Accordingly, the length unit is $L^* = 5.0$ nm, the transverse width unit of the quantum channel is $W^* = \pi L^* = 15.7$ nm, the energy unit is $E^* = 66$ meV, the corresponding Fermi wave vector $k_F = 2 \times 10^6$ cm^{-1}, the Rashba spin-orbit coupling parameter is in units of $\alpha^* = \frac{E_F}{k_F} = \frac{\hbar^2 k_F}{m^*} = 3.317\times10^{-10}$ eV m and the Dresselhaus spin-orbit interaction parameter $\beta^* = \frac{E_F}{k_F} = \frac{\hbar^2 k_F}{m^*} = 3.317\times10^{-10}$ eV m [30]. All the physical units are shown in Appendix.

4.3.1 Ideal conductance with tunable the Dresselhaus effects

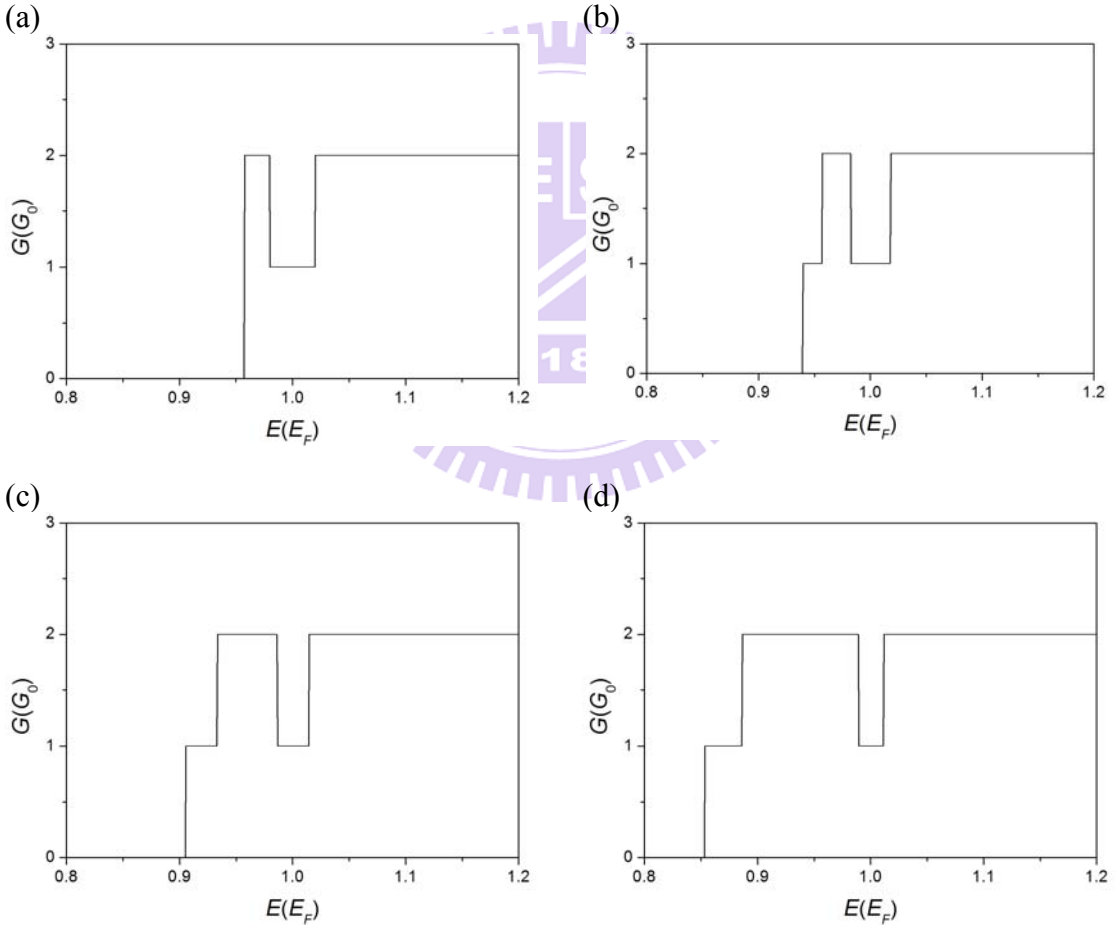

Fig. 4.3.1.1. Conductance (in units of $G_0 = e^2/h$) versus kinetic energy without the scattering potential in the presence of the Rashba spin-orbit interaction and in-plane magnetic field with different Dresselhaus coefficients: (a) $\alpha = 0.2$, $\beta = 0.0$, $gB = 0.02$; (b) $\alpha = 0.2$, $\beta = 0.1$, $gB = 0.02$; (c) $\alpha = 0.2$, $\beta = 0.2$, $gB = 0.02$; (d) $\alpha = 0.2$, $\beta = 0.3$, $gB = 0.02$. The Fermi energy $E_F = 66$ meV. The magnetic field strength is approximately 3T when $gB = 0.02$ ($g_s = -15$ for InAs).

In Fig. 4.3.1.1, we investigate the ideal conductance in the presence of the Rashba spin-orbit interaction and in-plane magnetic field with different Dresselhaus coefficients. Since there is no scattering potential, the electron can be totally transmitted in the quantum channel without scattering. It is shown in Fig. 4.3.1.1(a) when we only consider the Rashba spin-orbit interaction and an in-plane magnetic field in the system, the conductance will be identical to $2G_0$ with $G_0 = e^2/h$ above the subband bottom of the energy. In low energy regime, there are two inner modes (left and right going modes with low momentum) and two outer modes (left and right going modes with high momentum), and hence the transported electrons contribute to conductance $2G_0$. In mediate energy regime, that is the magneto-spin-orbit pseudo-gap energy regime, there are two outer propagating modes (left and right going modes), and the two inner modes belong to evanescent modes. The conductance reduces to G_0. In the high energy regime, namely the electron energy is higher than the bottom of the upper subband, there are four propagating modes (two left and two right going modes) and the conductance is increasing to $2G_0$.

As the Dresselhaus effect is 0.1 (Fig. 4.3.1.1(b)), above the subband bottom of the energy the conductance will not be identical to $2G_0$ anymore. Since in sufficient low energy regime there are only two propagating modes (one left and one right going modes with low momentum and high momentum, respectively), the transported electrons contribute to conductance G_0. In low energy regime there are two right-going modes hence the conductance is equal to $2G_0$. In magneto-spin-orbit pseudo-gap energy regime, the conductance reduces to G_0 since there are two outer modes (left and right going modes), and the two inner modes belong to evanescent modes. When the electron energy is higher than the bottom of the upper subband, the conductance is increasing to $2G_0$ because of two right-going modes in the high energy regime.

As we mentioned before in Fig. 4.1.2.1, the pseudo-gap decreases when the Dresselhaus effect increases. Therefore, we can see the pseudo-gap energy regime reduce in ideal conductance G_0 reduces when the Dresselhaus coefficients increases from 0.1 to 0.3 (Fig. 4.3.1.1(b), (c) and (d)).

4.3.2 Ideal conductance with the tunable Rashba-Dresselhaus effects

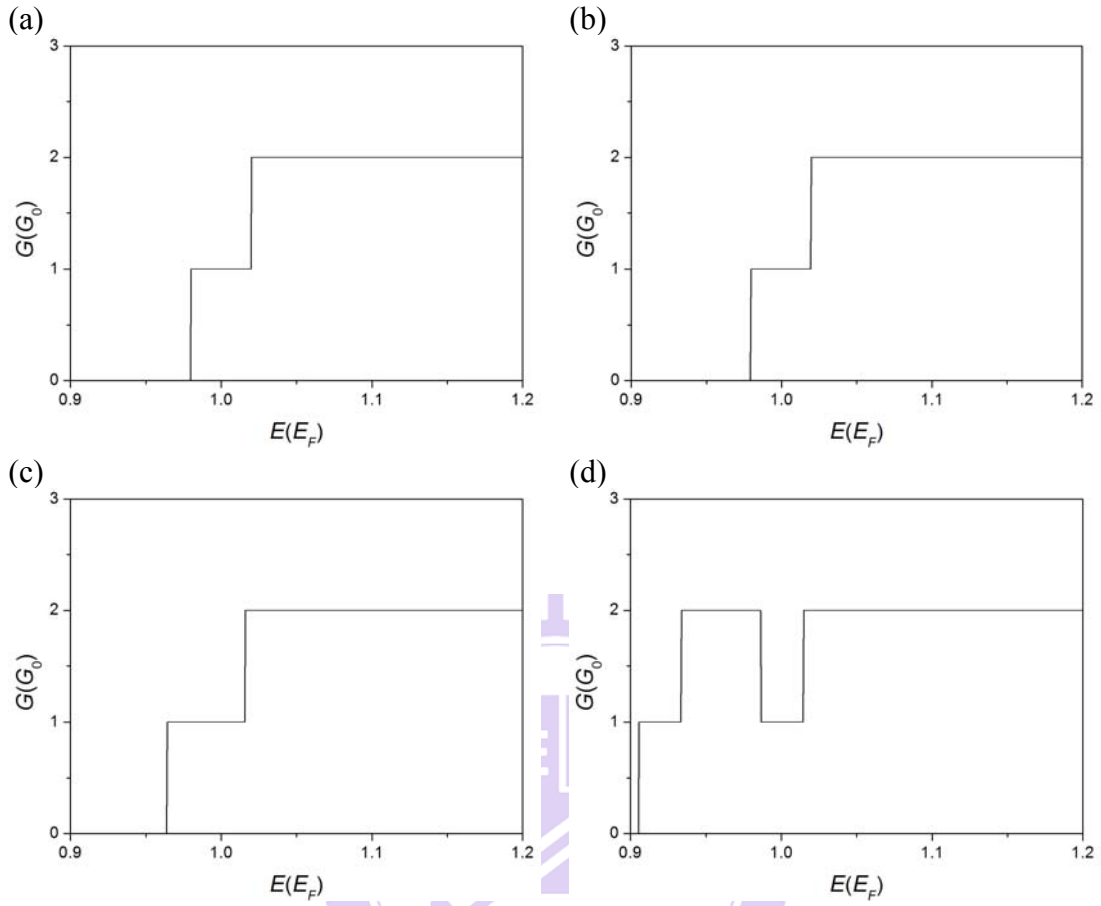

Fig. 4.3.2.1. Conductance (in units of $G_0 = e^2/h$) versus kinetic energy without the scattering potential in the presence of in-plane magnetic field with different Rashba and Dresselhaus coefficients: (a) $\alpha = \beta = 0.01$, $gB = 0.02$ (b) $\alpha = \beta = gB = 0.02$ (c) $\alpha = \beta = 0.1$, $gB = 0.02$ (d) $\alpha = \beta = 0.2$, $gB = 0.02$. The Fermi energy $E_F = 66$ meV. The magnetic field strength is approximately 3T when $gB = 0.02$ ($g_s = -15$ for InAs)

In this section, we consider the ideal conductance in the presence of in-plane magnetic field with different Rashba and Dresselhaus coefficients. As the Rashba and the Dresselhaus effects are less than the Zeeman effect, the ideal conductance is identical to G_0 above the subband bottom in low energy regime (Fig. 4.3.2.1(a)) since there is only a right-going mode in this energy regime (see Fig. 4.1.3.1(a)). When the energy is higher than the band bottom of the upper branch, the conductance will increase to $2G_0$ because of two right-going modes in this energy regime.

If the Rashba and the Dresselhaus coefficients are identical to the Zeeman coefficient, the corresponding energy spectrum (Fig. 4.1.3.1(b)) is also vertically splitting. Accordingly, in low energy regime the ideal conductance is identical to G_0 above the subband bottom and in higher energy regime the ideal conductance

increases to $2G_0$.

In Fig. 4.3.2.1(c) we show the ideal conductance for the Rashba and the Dresselhaus effects ($\alpha = \beta = 0.1$) larger than the Zeeman effect ($gB = 0.02$). The corresponding energy spectrum is in Fig. 4.1.3.1(c). Under the applying magnetic field, the Rashba and the Dresselhaus effects is not strong enough to form a pseudo-gap in mediate energy regime and therefore in low energy regime the ideal conductance is G_0 above the subband bottom and in higher energy regime the ideal conductance is increasing to $2G_0$. As the Rashba and the Dresselhaus effects ($\alpha = \beta = 0.2$) is significantly large enough to form a pseudo-gap in mediate energy regime, there are two propagating modes (a right-going mode and a left-going mode) and two evanescent modes in mediate regime. The ideal conductance will reduce from $2G_0$ to G_0 in the pseudo-gap regime (Fig. 4.3.2.1(d)).

4.3.3 The Dresselhaus effects in the presence of the Rashba spin-orbit interaction and in-plane magnetic field

(I) The attractive scattering potentials

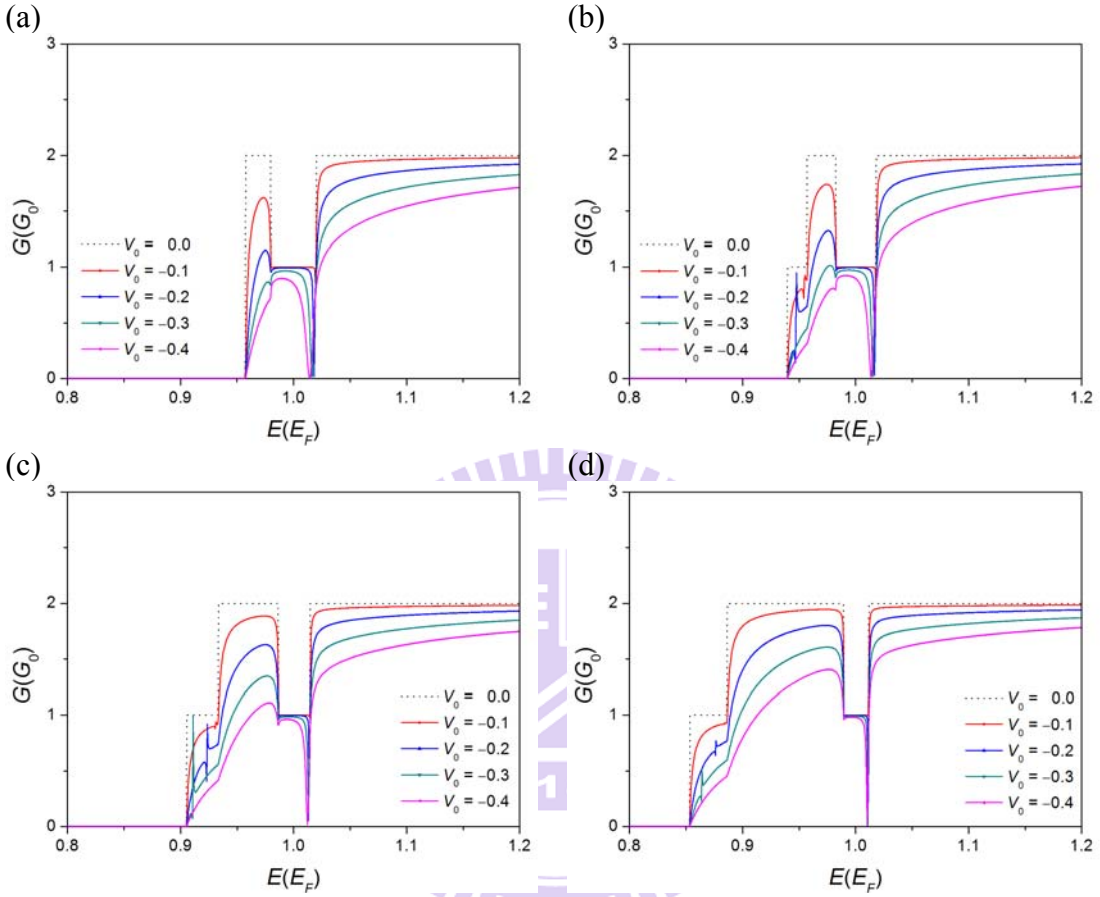

Fig. 4.3.3.1. Conductance (in units of $G_0 = e^2/h$) versus kinetic energy with the attractive scattering potential in the presence of the Rashba spin-orbit interaction and in-plane magnetic field with different Dresselhaus coefficients: (a) $\alpha = 0.2$, $\beta = 0.0$, $gB = 0.02$ (b) $\alpha = 0.2$, $\beta = 0.1$, $gB = 0.02$ (c) $\alpha = 0.2$, $\beta = 0.2$, $gB = 0.02$ (d) $\alpha = 0.2$, $\beta = 0.3$, $gB = 0.02$. The Fermi energy $E_F = 66$ meV. The magnetic field strength is approximately 3T when $gB = 0.02$ ($g_s = -15$ for InAs)

In the presence of the scattering potential, the conductance is not ideally quantized anymore since the electron is in the scattering process. The increasing strength of the attractive scattering potential causes the more suppressive conductance (Fig. 4.3.3.1). In the above picture we will show the transport properties in the presence of the Rashba spin-orbit interaction and in-plane magnetic field with different Dresselhaus coefficients. In Fig. 4.3.3.1(a), we show the conductance in the presence of the Rashba spin-orbit interaction and in-plane magnetic field but without the Dresselhaus effect which we already mentioned in Ch3. We can see under the

applying attractive scattering potential there is a dip structure appears at the energy corresponding to the electron-like quasi-bound state at the bottom of the upper branch (Fig. 4.3.3.1(a), (b), (c) and (d)). Since the attractive scattering potential will enhance the electron-like quasi-bound state.

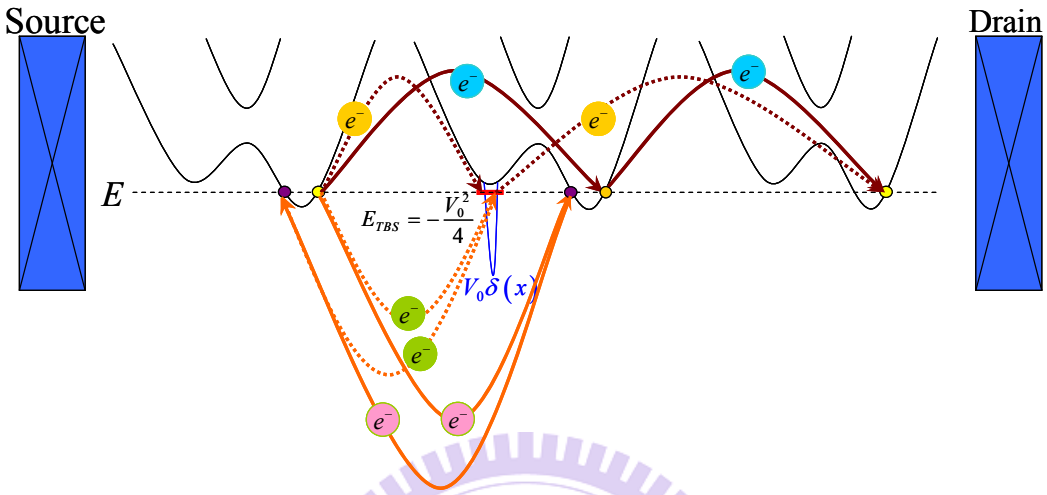

Fig. 4.3.3.2. Scattering process in the presence of the true bound state.

When the Dresselhaus coefficient is identical to 0.1, there is a Fano effect in sufficient low energy regime (Fig. 4.3.3.1(b)). When we apply a negative delta potential, below the band bottom of the lower branch there is a true bound state (TBS) $E_{TBS} = -V_0^2 / 4$ (Fig. 4.3.3.2). For the given energy of the electrons corresponding to the energy which is the binding energy E_{TBS} plus the band bottom energy of the lower branch, the electrons with this given energy at the right-going mode may be scattered into the bound state and then forward scattered into the right-going mode. These electrons will interference with the electrons directly transmitted at the right-going mode and result in the Fano peak. On the other hand, the electrons at the right-going mode may be scattered into the bound state and then back scattered into the left-going mode or scattered into the left-going mode. These electrons will interference and result in the Fano dip [34].

For the case of scattering potential $V_0 = -0.1$, shown in Fig. 4.3.3.1(b), the corresponding binding energy is $E_{TBS} = -0.0025$. The Fano effect occurs at 0.9552 which is less than the band bottom energy 0.9572 of the lower branch approximately 0.002. Under this applying potential strength the Fano effect is not apparent. When the scattering potential $V_0 = -0.2$, the corresponding binding energy is $E_{TBS} = -0.01$. Since the Fano effect is at 0.9479 less than the band bottom energy approximately

0.0095. The corresponding conductance of the Fano peak is approximately $0.95G_0$ and the conductance of the Fano dip is $0.14G_0$, the Fano effect under this applying potential strength is apparent. When the scattering potential is identical to –0.3 and –0.4, the energy (the binding energy subtracting from the band bottom energy) is 0.9347 and 0.9172, respectively. These energies are less than the band bottom energy 0.9056 of the lower branch, and therefore there are no propagating modes to transport.

When the Dresselhaus coefficient is identical to 0.2, there is a Fano effect in sufficient low energy regime as the attractive scattering potential is –0.1, –0.2 and –0.3 (Fig. 4.3.3.1(c)). As the Dresselhaus coefficient is 0.2, the energy range in low energy regime, $E_{b-,1}-E_{b-,2}=0.0282$, is larger than the energy range 0.0176 in low energy regime as the Dresselhaus coefficient is 0.1. Therefore, when the scattering potential is identical to –0.3, the Fano effect is at 0.911 which is above the subband bottom.

As the Dresselhaus coefficient is 0.3 (Fig. 4.3.3.1(d)), the Fano effect occurs when the attractive scattering potential is –0.1, –0.2 and –0.3. The Fano effect is not obvious when the attractive scattering potential is –0.1. When the scattering potential is –0.2 and –0.3, the Fano effect is also indistinct. In conclusion, we deduce that under the same Rashba spin-orbit interaction and the same in-plane magnetic field the Fano effect will be affected by the Dresselhaus effect.

(II) The repulsive scattering potentials]

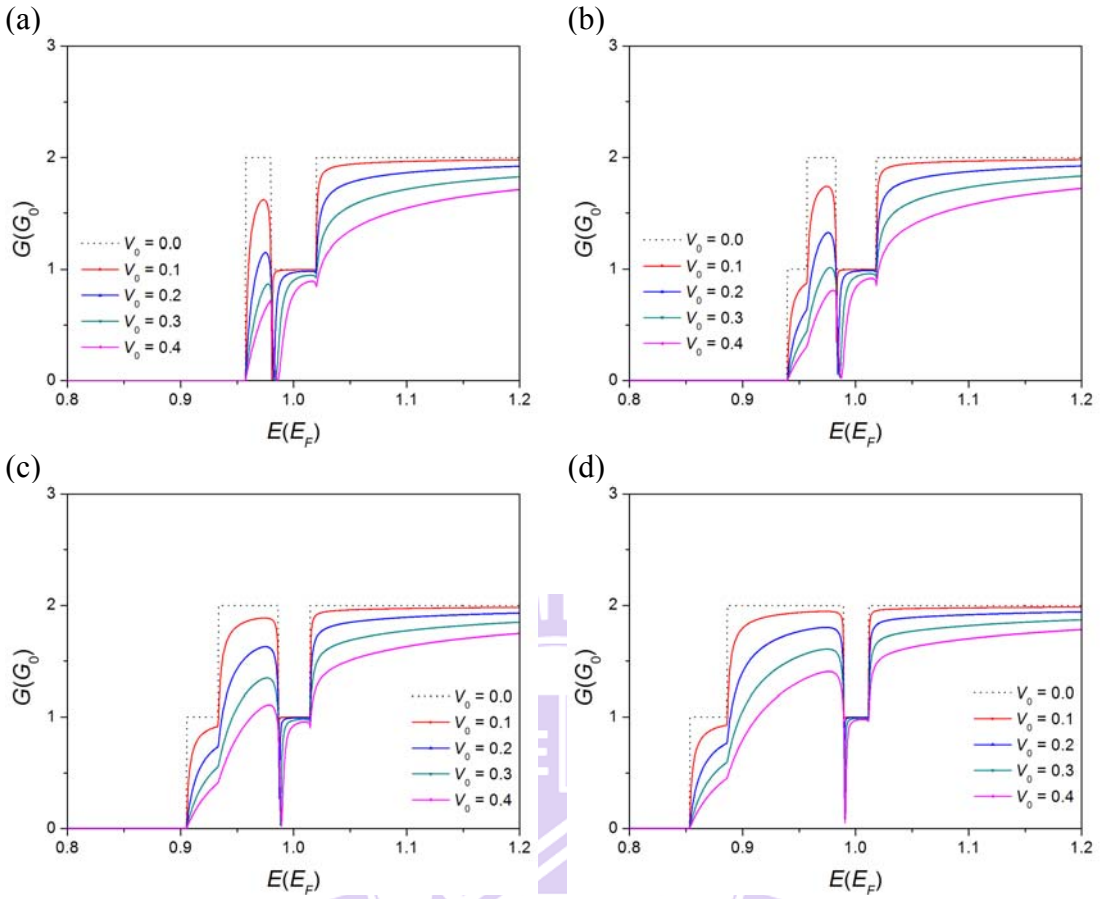

Fig. 4.3.3.3. Conductance (in units of $G_0 = e^2/h$) versus kinetic energy with the repulsive scattering potential in the presence of the Rashba spin-orbit interaction and in-plane magnetic field with different Dresselhaus coefficients: (a) $\alpha = 0.2$, $\beta = 0.0$, $gB = 0.02$ (b) $\alpha = 0.2$, $\beta = 0.1$, $gB = 0.02$ (c) $\alpha = 0.2$, $\beta = 0.2$, $gB = 0.02$ (d) $\alpha = 0.2$, $\beta = 0.3$, $gB = 0.02$. The Fermi energy $E_F = 66$ meV. The magnetic field strength is approximately 3T when $gB = 0.02$ ($g_s = -15$ for InAs)

In the presence of the repulsive scattering potential, the increasing strength of the attractive scattering potential also results in the more suppressive conductance. In Fig. 4.3.3.3(a), we show the conductance in the presence of the Rashba spin-orbit interaction and in-plane magnetic field but without the Dresselhaus effect which we already mentioned in Ch3. When the Dresselhaus coefficient is not identical to 0.1, there is a dip structure appears at the hole-like quasi-bound state. The corresponding energy of the hole-like quasi-bound state is at the top of the lower branch. Since when the scattering potential is repulsive, it will enhance the hole-like quasi-bound state. Additionally, we find that the width of the suppressed plateau is broadening with the increasing Dresselhaus coefficient.

4.3.4 Transport properties with the Rashba-Dresselhaus effects in the presence of an in-plane magnetic field

(I) The attractive scattering potentials

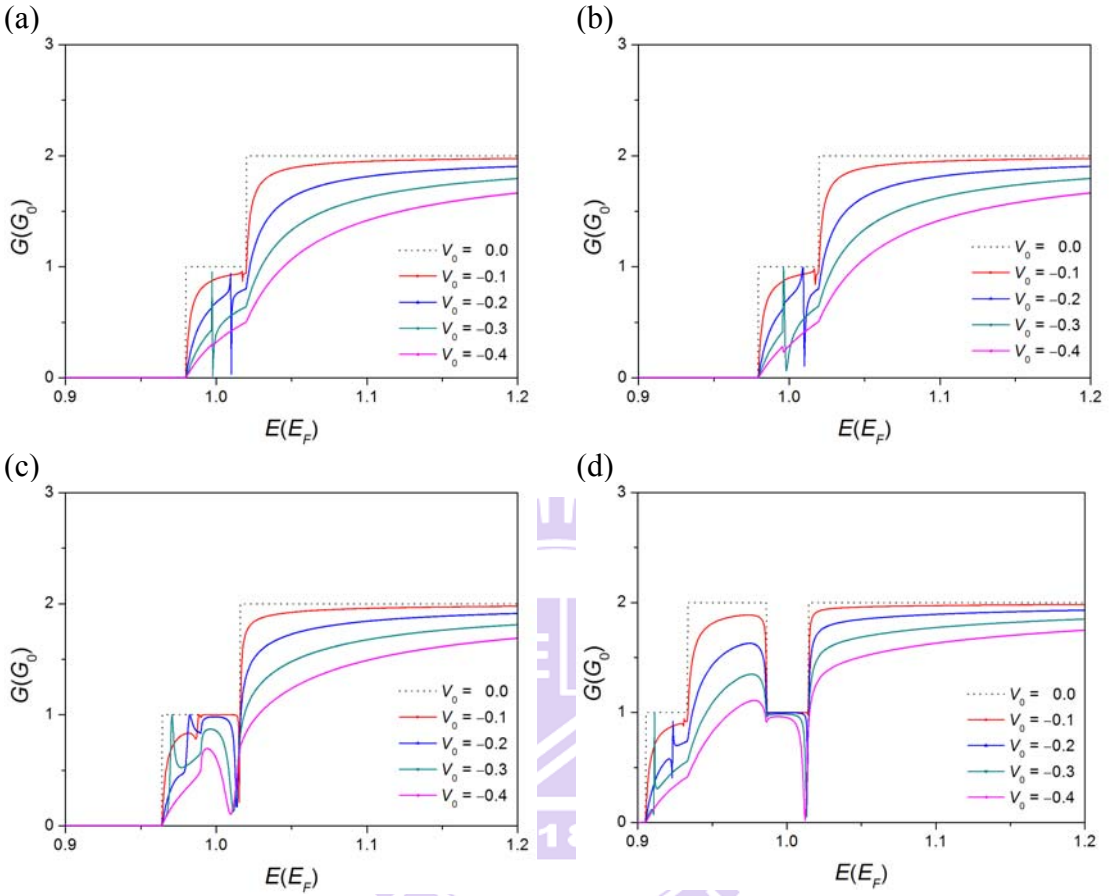

Fig. 4.3.4.1. Conductance (in units of $G_0 = e^2/h$) versus kinetic energy with the attractive scattering potential in the presence of in-plane magnetic field with different Rashba and Dresselhaus coefficients: (a) $\alpha = \beta = 0.01$, $gB = 0.02$ (b) $\alpha = \beta = gB = 0.02$ (c) $\alpha = \beta = 0.1$, $gB = 0.02$ (d) $\alpha = \beta = 0.2$, $gB = 0.02$. The Fermi energy $E_F = 66$ meV. The magnetic field strength is approximately 3T when $gB = 0.02$ ($g_s = -15$ for InAs).

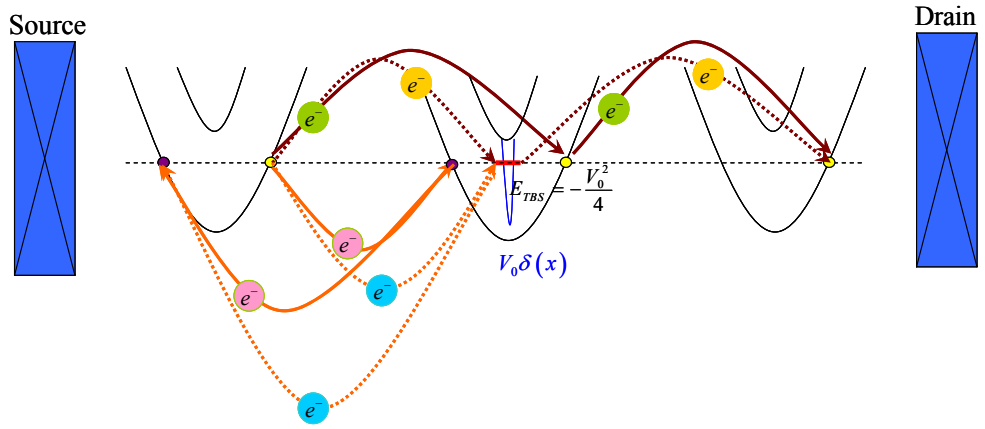

Fig. 4.3.4.2. Scattering process in the presence of the true bound state.

In Fig. 4.3.4.1 we show the transport properties with the Rashba and the Dresselhaus effects in the presence of an in-plane magnetic field. The corresponding energy spectrum is vertical splitting (Fig. 4.1.3.1(a) and (b)). Under the applying attractive scattering potential, there is a Fano effect in low energy regime. Below the band bottom of the upper branch there is a true bound state in binding energy $-\frac{V_0^2}{4}$ (Fig. 4.3.4.2). For the given energy of the electrons corresponding to the energy which is the binding energy E_{TBS} plus from the band bottom energy of the upper branch, the electrons at this given energy at the right-going mode may be scattered into the bound state and then forward scattered or back scattered. The forward scattering will result in the Fano peak. Otherwise, the back scattering will result in the Fano dip.

In Fig. 4.3.4.1(a), as the scattering potential is –0.1, the corresponding binding energy is –0.0025. The Fano effect occurs at 1.0175 which is less than the band bottom energy 1.02 of the upper branch approximately 0.0025. When the scattering potential is –0.2, the binding energy is –0.01. The corresponding Fano effect is at 1.01 less than the band bottom energy of the upper branch 1.02 approximately 0.01. Under this applying potential, the Fano peak is at $0.939G_0$ and the Fano dip is at $0.035G_0$, hence the Fano effect is apparent. Moreover, when the scattering potential is -0.3, the Fano effect occurring at 0.997 is also apparent since the Fano peak occurs at $0.95G_0$ and the Fano dip occurs at $0.017G_0$. As the scattering potential is -0.4 if there is a Fano effect, it is approximately at 0.98. However this corresponding energy, 0.98, is at the band bottom of the lower branch (Fig. 4.1.3.1(a)). Therefore, there is without any propagating mode to transport. In Fig. 4.3.4.1(b), the corresponding energy spectrum is also vertical splitting. Therefore, the transport properties in Fig. 4.3.4.1(b) are similar to the conductance in Fig. 4.3.4.1(a).

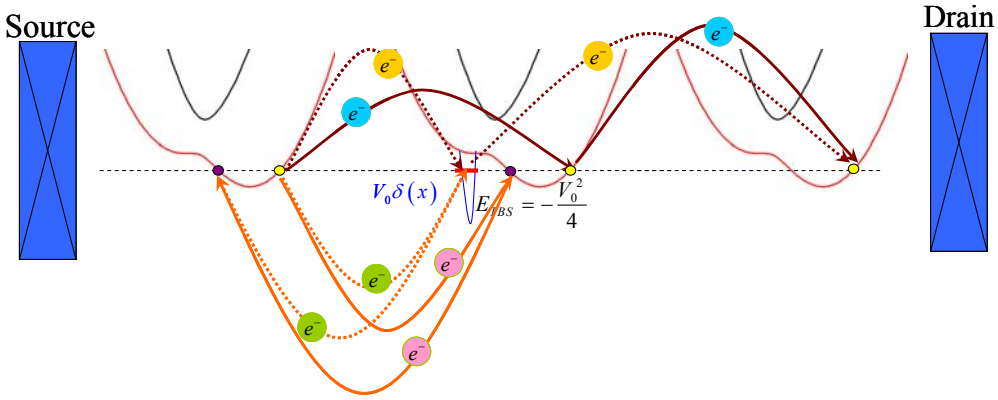

Fig. 4.3.4.3. Scattering process in the presence of the true bound state.

In Fig. 4.3.4.1(c), the Fano effect occurs at the binding energy E_{TBS} below subband (see Fig. 4.3.4.3). The corresponding energy spectrum is Fig. 4.1.3.1 (c). As the potential $V_0 = 0.1$, the Fano effect is not apparent. When $V_0 = 0.2$ and 0.3, there is a Fano effect and the width between the Fano peak and the Fano dip are larger than the Fano effect in other cases (Fig. 4.3.4.3 (a), (b) and (d)). That is, when the Rashba and Dresselhaus coefficients $\alpha = \beta = 0.1$ and the Zeeman coefficient $gB = 0.02$, the life time for the electron staying in the true bound state is shorter. When $V_0 = 0.4$, there is no propagating modes at the corresponding energy of the bound state. Hence, under this applying potential $V_0 = 0.4$, there is no Fano effect.

In Fig. 4.3.4.1(d), the Fano effect appears at the bound state below the band bottom of the lower branch. This picture we have mentioned before in section 4.3.3.1(c).

(II) The repulsive scattering potentials

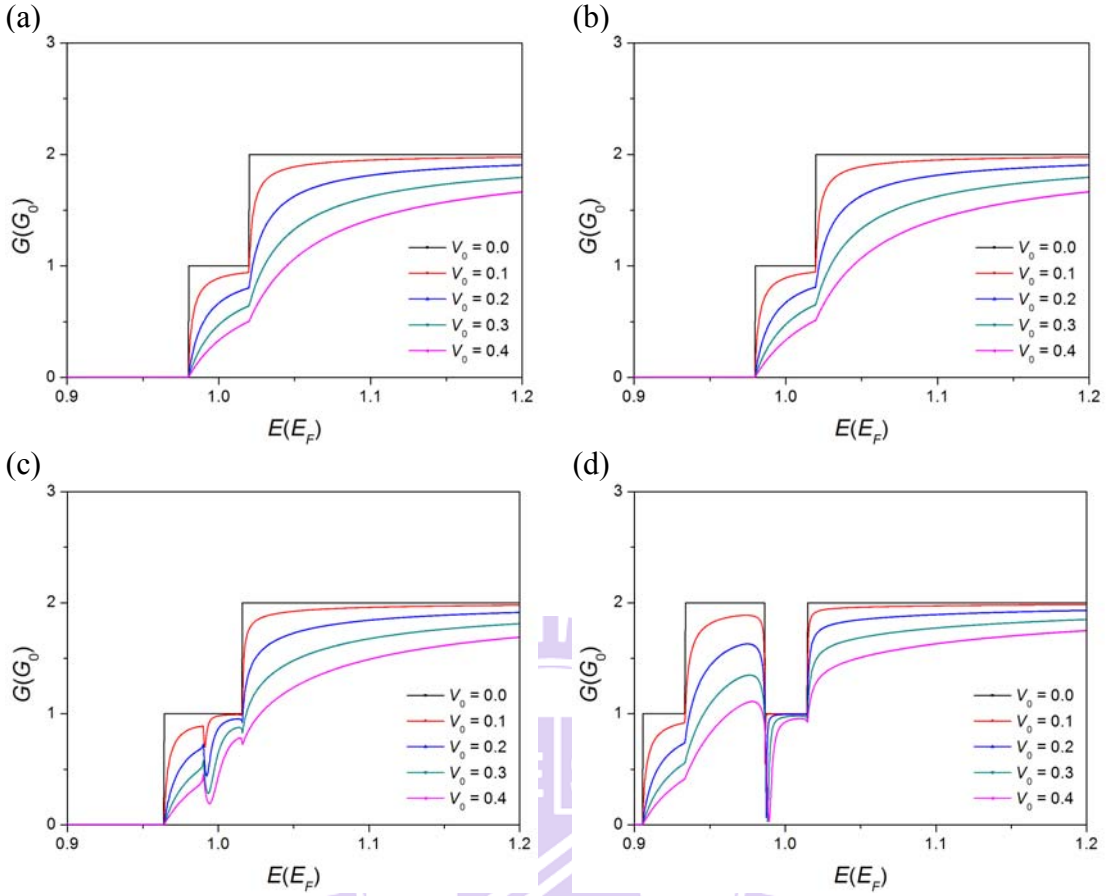

Fig. 4.3.4.4. Conductance (in units of $G_0 = e^2/h$) versus kinetic energy with the repulsive scattering potential in the presence of in-plane magnetic field with different Rashba and Dresselhaus coefficients: (a) $\alpha = \beta = 0.01$, $gB = 0.02$ (b) $\alpha = \beta = gB = 0.02$ (c) $\alpha = \beta = 0.1$, $gB = 0.02$ (d) $\alpha = \beta = 0.2$, $gB = 0.02$. The Fermi energy $E_F = 66$ meV. The magnetic field strength is approximately 3T when $gB = 0.02$ ($g_s = -15$ for InAs).

In the presence of the repulsive scattering potential, the increasing strength of the attractive scattering potential causes the more suppressive conductance. In Fig. 4.3.4.4 (a) and (b) under the applying repulsive scattering potential, the conductance is suppressed. As the Rashba and the Dresselhaus identical to 0.1 are stronger than the Zeeman effects, there are two local extreme values, 0.99 and 0.964 at the lower branch (Fig. 4.1.3.1(c)). Above subband bottom whose energy value is 0.99, there is a hole-like quasi-bound state. Therefore, as the energy is identical to the corresponding energy of the hole-like quasi-bound state, there is a dip structure. When the scattering potential is 0.1, 0.2, 0.3 and 0.4, the dip structure is at 0.99124, 0.99237, 0.99349 and 0.99429, respectively. Accordingly, the corresponding energy of the quasi-bound state will be affected by the potential strength.

In Fig. 4.3.4.4(d), the Rashba and the Dresselhaus identical to 0.2 are stronger than the Zeeman effects. There is a pseudo-gap in the corresponding energy spectrum (Fig. 4.1.3.1(d)). The repulsive applying potential will enhance the hole-like quasi-bound state hence the dip structure is obvious.

Chapter 5 Conclusion and future work

In Ch1, we start from the simple case and we investigate the transport properties in the presence of the static delta potential in the quantum wire. In Ch2, we introduce the spintronics. In recent years, there are a lot of researches about the spintronics. We expect that we can use the spin to carry some information. We realize that for spintronics the spin-orbit interactions are an efficient way to couple the electron spin and the momentum. Hence, in Ch3 we consider the Rashba spin-orbit interaction in our system. In addition, we apply the in-plane magnetic field along ***x*** direction. We use the analytical approach to calculate the conductance. Because of the in-plane magnetic field, in some specific cases, there is a pseudo-gap in the energy dispersion. We can see the electron-like dip structure and hole-like dip structure in the conductance pictures. Chapter 4 investigates the quantum wire in the presence of the Rashba and the Dresselhaus spin-orbit interactions and the in-plane magnetic field. The additional Dresselhaus term breaks the symmetry of the energy spectrum. In this chapter, we use the numerical approach to calculate the transport properties. Under the asymmetry of the energy spectrum, we can see the Fano effect in the transport properties.

In the future, we are going to change the direction of the magnetic field. We expect to see the variation about the energy spectrum and investigate how the different orientations of the magnetic field could affect the transport properties.

Bibliography

[1] S. Datta. "*Electronic Transport in Mesoscopic Systems*", Cambridge University Press, 1995).

[2] Y. Imry and R. Landauer, Rev. Mod. Phys. **71**, S306 (1999).

[3] C. S. Tang and C. S. Chu, Phys. Rev. B **53**, 4838 (1996).

[4] T. Kontos, Physics **4**, 28 (2011).

[5] D. Awschalom and N. Samarth, Physics **2**, 50 (2009).

[6] I. Žutić, J. Fabian, and S. Das Sarma, Rev. Mod. Phys. **76**, 323 (2004).

[7] J. E. Birkholz and V. Meden, Phys. Rev. B **79**, 085420 (2009).

[8] J. Linder and T. Yokoyama, Phys. Rev. Lett. **106**, 237201 (2011).

[9] K. Hosono, A. Yamaguchi, Y. Nozaki, and G. Tatara, Phys. Rev. B **83**, 144428 (2011).

[10] J. Schliemann, J. Carlos Egues, and D. Loss, Phys. Rev. Lett. **90**, 146801 (2003)

[11] N. Atodiresei, J. Brede, P. Lazić, V. Caciuc, G. Hoffmann, R. Wiesendanger, and S. Blügel, Phys. Rev. Lett. **105**, 066601 (2010).

[12] W. L. Wang, O. V. Yazyev, S. Meng, and E. Kaxiras, Phys. Rev. Lett. **102**, 157201 (2009).

[13] C. Flindt, A. S. Sørensen, and K. Flensberg, Phys. Rev. Lett. **97**, 240501 (2006).

[14] B. Das, S. Datta, and R. Reifenberger, Phys. Rev. B **41**, 8278 (1990).

[15] G. Burkard, D. Loss, and E. V. Sukhorukov, Phys. Rev. B **61**, R16303 (2000).

[16] W. D. Oliver, F. Yamaguchi, and Y. Yamamoto, Phys. Rev. Lett. **88**, 037901 (2002).

[17] G. Dresselhaus, Phys. Rev. **100**, 580 (1955).

[18] E. I. Rashba, Physica E. **34**, Issues 1-2 (2006).

[19] Y. V. Pershin and C. Piermarocchi, Phys. Rev. B **72**, 195340 (2005).

[20] Yu-Xian Li, Yong Guo, and Bo-Zang Li, Phys. Rev. B **72**, 075321 (2005).

[21] Y. X. Li, Phys. Lett. A **358**, 70 (2006).

[22] L.M. Roth, B. Lax, S. Zwerdling, Phys. Rev. **114**, 90 (1959).

[23] E.L. Ivchenko, A.A. Kiselev, **Sov. Phys. Semicond**. **26**, 827 (1992).

[24] H.W. van Kesteren, E.C. Cosman, W.A.J.A. van der Poel, Phys. Rev. B **41**, 5283–5292 (1990).

[25] G. Goldoni, A. Fasolino, Phys. Rev. B **48**, 4948 (1993).

[26] P. Peyla, A. Wasiela, and Y. Merle d'Aubigné, D.E. Ashenford, B. Lunn, Phys.Rev. B **47**, 3783 – 3789 (1993).

[27] G. Feve, W. D. Oliver, M. Aranzana, and Y. Yamamoto, Phys. Rev. B **66**, 155328 (2002).

[28] P. Středa and P. Šeba, Phys. Rev. Lett. **90**, 256601 (2003).

[29] P. F. Bagwell, Phys. Rev. B **41**, 10354–10371 (1990).

[30] D. Grundler, Phys. Rev. Lett. **84**, 6074–6077 (2000).

[31] C. H. L. Quay, T. L. Hughes, J. A. Sulpizio, L. N. Pfeiffer, K. W. Baldwin, K. W. West, D. Goldhaber-Gordon and R. de Picciotto, Nature Physics 6, 336 – 339 (2010).

[32] H. C. Lee and S.-R. E. Yang, Phys. Rev. B **72**, 245338 (2005).

[33] S. Giglberger, et al., Phys. Rev. B **75**, 035327 (2007).

[34] U. Fano, Phys. Rev. **124**, 1866 (1961).

Appendix:

The physical units for GaAs-based semiconductors

The effective mass m^*	The energy unit E^*	The length unit L^*	The frequency unit ω^*
$0.067m_0$	$9meV$	$7.96nm$	13.6THz

The physical units for InAs-based semiconductors

The effective mass m^*	The energy unit E^*	The length unit L^*
$0.023m_0$	$66meV$	$5nm$
width of the channel	Rashba parameter α^*	Dresselhaus parameter β^*
15.7nm	3.317×10^{-10} eV m	3.317×10^{-10} eV m